# ON THE EVOLUTION AND FATE OF INTERACTING MASSIVE BINARY STARS

by

## ALEJANDRO VIGNA GÓMEZ

A thesis submitted to the University of Birmingham for the degree of
DOCTOR OF PHILOSOPHY

Institute for Gravitational Wave Astronomy

School of Physics and Astronomy

College of Engineering and Physical Sciences

University of Birmingham

July 2019

# Abstract

Massive binary stars have been associated with X-ray binaries, Galactic double neutron stars, short gamma-ray bursts, luminous red novae, gravitational waves and other energetic astronomical phenomena. In this thesis we study their evolution and fate.

Rapid population synthesis is used to study double neutron stars and binary black holes. Synthesised populations are compared with observations of double compact objects. Our method reproduces the observed Galactic double neutron star period and eccentricity distributions as well as the binary black hole mass distribution. Intermediate phases in the evolution of binaries leading to double neutron stars are also studied. We focus on mass transfer leading to common-envelope events. It is found that most double neutron stars come from two formation channels with very distinctive common-envelope events. It is also found that a significant fraction of binaries will not be circular by the time the common-envelope phase begins.

Finally, detailed stellar evolution is used to model massive stellar mergers. Merger products evolve differently than their single star counterparts. A novel formation scenario involving stellar mergers is proposed as a progenitor of (pulsational) pair-instability supernovae. This scenario is suggested in the context of hydrogen-rich long-lasting multi-peaked transients like iPTF14hls.

# Dedication

Para mi tío Héctor, Whiskey, Mary y Angie, a quienes la travesía me impidió despedir.

# Acknowledgements

> CUSTOMS OFFICIAL: Anything to declare?
>
> AVI: Yeah. Don't go to England.
>
> (Guy Ritchie, "Snatch", 2000)

A mis padres por su apoyo y amor incondicional. A mi hermano, mi persona favorita en la historia del tiempo. A Luis, por acompañar a mi hermano. A mis amigos cercanos y familia. A Kat, por el tiempo que pasamos juntos.

Dedico un espacio a agradecer a toda la gente que fue parte de mi ingreso al doctorado. Gracias a mis profesores y mentores: Juan-Manuel Campos, Enrico Ramirez-Ruiz, Gabriela Montes, Fabio de Colle, Jürgen Engelfried, Mariana Kirchbach, Eduardo Gómez, Ricardo Guirado, Jesús Dorantes, Juan Martín Montejano, Alberto Molgado, Manuel Mirabal, Antonio Morelos, Enrique González Tovar y Jesús Urías.

Thanks to everyone at the University of Birmingham who was part of my life during my time there. Thanks to Alberto Vecchio and Andreas Freise for their great work running the group. Thanks to everyone at G26 and G27, with particular praise to my office mates of G27 for their patience. Many thanks to David J. Stops, Jo Cox and Sara Lawrence for their hard work and assistance.

Thanks to all the institutions which hosted me during a significant amount of time. To the Anton Pannekoek Institute at the University of Amsterdam for hosting me on several occasions. To the Niels Bohr Institute and DARK Cosmology Centre. To the Center for Astrophysics at Harvard University. To the Monash Centre for Astrophysics at Monash University. To the School of Physics and Astronomy and the Institute for Gravitational Wave Astronomy at the University of Birmingham.

Thanks to all of the COMPAS gang. To the old-school: James William Make-peace Barrett III, Coen "Junior" Neijssel and Simon "Mr. Anderson" Stevenson. I have great memories with you guys. To all of the summer and master students for your enthusiasm, work and help. To Floor Broekgaarden, George "G-boy" Howitt, Jeff Riley, Serena Vinciguerra and Reinhold Wilcox.

To all of my collaborators: Jim W. Barrett, Krzysztof Belczynski, Stephen Justham, Morgan MacLeod, Selma E. de Mink, Bernhard Müller, Coenraad J. Neijssel, Philipp Podsiadlowski, Mathieu Renzo, Simon Stevenson and Dorottya Szécsi.

To Dave, Coen, Reinhold, Jeff, Simon and Kendall for helping me proof read my thesis. To David and Kat for helping me to hand in my thesis.

Special thanks to Stephen Justham. You are an outstanding physicist and have been a great mentor. Your patience and encouragement played a great part in improving my understanding and knowledge of astrophysics, which remains astronomically far from yours.

To Herr Professor Doktor Doctor Ilya Mandel, current Councillor, former Mace-bearer and Senator. Ilya, it has been my pleasure to interact with you in the last years. I'm grateful to have learned from you and proud to call you my supervisor. You have many gifts, including the rare ability of making people around you become better physicists and scientists than they are. I respect and admire you, even when my narrative might suggest the opposite. Thank you also for opening the doors of your home. Thanks to Chef Claudia for all the great dinners and to Maxim and Victoria for the laughs.

Tecnología (CONACYT) and the University of Birmingham.

# Contents

3 **Common–Envelope Episodes en route to double neutron star formation** **83**

# List of Figures

# List of Tables

# Chapter 1

# Introduction

Gravitationally-bound interacting binary systems are some of the most common astrophysical configurations. Other configurations include not only interacting binaries, but systems with higher order multiplicity which contain numerous and complicated combinations of objects, e.g. stars, planets, moons, in both gravitationally bound and unbound orbits. Our Solar System itself contains a vast set of different astrophysical multiple systems. The Earth-Moon binary is arguably the most well known astrophysical binary. Additionally, the Sun and the planets create a complex multiple-body gravitationally-bound system. This line of reasoning, with astrophysical parts creating astrophysical wholes, escalates rapidly thanks to the long-range effect of gravity. We then can think about our Solar System interacting with the Milky Way, galaxies interacting with each other and galaxy clusters interacting throughout time.

Nevertheless, we will focus our attention in the stellar mass regime of two-star gravitationally-bound systems which we hereafter refer to as binary stars or binaries.

The adoption of the scientific method[1] and development of the telescope[2], both around the 17th Century and likely correlated, provided the stepping stones in what is now our understanding of binary stars. The term "binary", in the context of a binary star, is attributed to William Herschel [117] in the early 19th Century. The 19th Century hosted some of the scientists who developed the foundations of modern binary evolution theory, such as Édouard Roche and George Howard Darwin. All of the observational evidence for binaries before the 19th Century came from the optical spectrum. Infrared astronomy widened the observing spectrum during the 19th Century. The 20th Century saw the emergence of technologies that gave rise to radio [273], X-ray [141] and gamma-ray [151] astronomy, as well as enhanced optical and infrared astronomy. Different evolutionary phases of binaries have been associated to transients all over the electromagnetic spectrum. Additionally, in 2015, the Laser Interferometer Gravitational-Wave Observatory detected gravitational waves from a binary black-hole merger for the first time [2], further expanding the reach of astronomy. Two years later, the first detection of gravitational waves from a binary Neutron Star (NS) merger [8] prompted the largest electromagnetic follow up campaign to date [10]. There are great expectations for the current and future observations of astronomical events associated to binary stars, as well as potential prospects from archival data of previous surveys that have not yet been analysed or published.

The structure of this chapter is the following. In section 1.1 we briefly introduce the field of stellar evolution, with particular attention to the remnants of single stars. In section 1.2 we qualitatively discuss the distinguishing features of binaries as well as some of the proposed formation channels. In section 1.3 we present the rapid binary population synthesis method, as well as some basic physical parameterisations we use in our approach to this method. Finally, in section 1.4 we present an overview

---

[1]By Francis Bacon and René Descartes, among others.
[2]Notably by Galileo Galilei.

of the structure of this thesis.

## 1.1   Single massive stars: a brief overview

Before engaging in the details of massive binary evolution, we give an overview on the evolution of single massive stars. We follow Duchêne and Kraus [84] and broadly define a massive star as one with mass $M \gtrsim 8$ $M_\odot$ (but see also section 1.1.1). Our current understanding on their life and evolution can be summarised among the following lines. If a molecular cloud is dense enough, it might become unstable and collapse into a proto-star. The proto-star, which now has approximately the mass of the future star, will continue contracting and getting hotter. Once it is hot and dense enough to begin hydrogen nuclear fusion, the Main Sequence (MS) begins. During the MS the star burns hydrogen into helium in the core. The MS is the longer lived phase from the life of a star. For the most massive stars it lasts up to a few times $10^6$ years; for the lowest mass stars it can last up to $10^{12}$ years. Once hydrogen is depleted in the core the MS comes to an end. The end of the MS leads to a drop in radiation pressure, which is then followed by a contraction of the core at somewhat constant luminosity and on shorter (thermal) timescales. The rapid core contraction leads to radial expansion of the envelope. This part of the evolution of the star is associated with the crossing of the Hertzsprung Gap (HG) in the Hertzsprung-Russell (HR) diagram, and is usually referred to simply as the "Hertzsprung Gap". The core contraction stops shortly after helium is ignited. At that point, helium burning in the core is enough to for the whole star to regain gravo-thermal equilibrium. Different nuclear reactions are ignited or enhanced at different temperatures, and fusing stars keep producing heavier elements in their cores. Once an iron core has been formed and nuclear burning has effectively ended, the star dies.
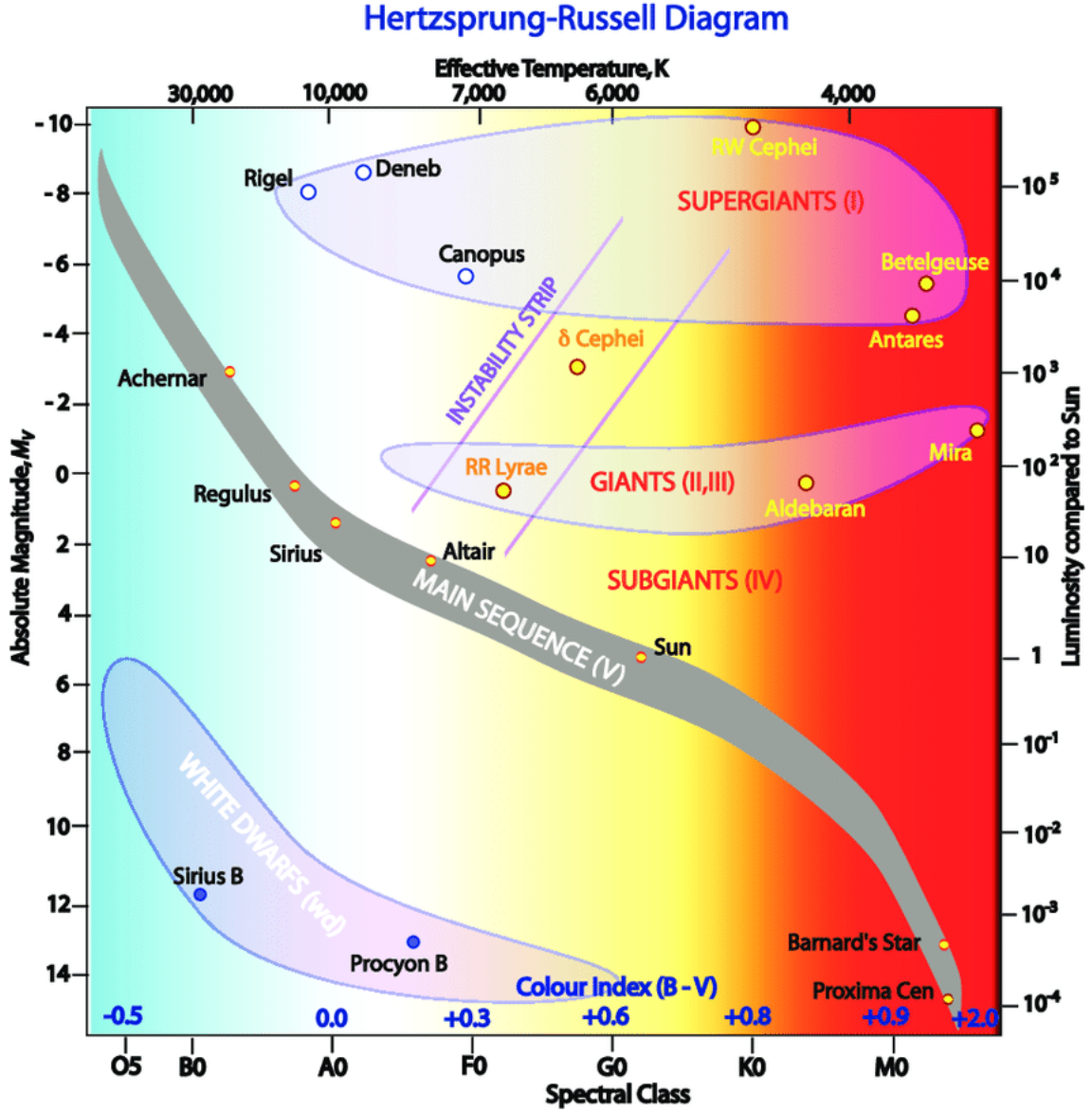
Figure 1.1: HR diagram as shown in figure 1 of Althaus et al. [13].

Some of the evolutionary phases of single massive stars can be seen in figure 1.1 and 1.2. Figure 1.1 [13] shows MS stars in a grey stripe and post-MS stars as giants and supergiants in blue-shaded regions. Figure 1.2 shows stellar tracks from Ekström et al. [92], where they model stars with masses between $0.8 \leq M/\mathrm{M}_\odot \leq 120$ at metallicity $Z = 0.014$. According to these stellar models, massive stars have luminosities $L > 10^3$ $\mathrm{L}_\odot$. For reference, these tracks can be visually compared with the regions and observations from figure 1.1.

4
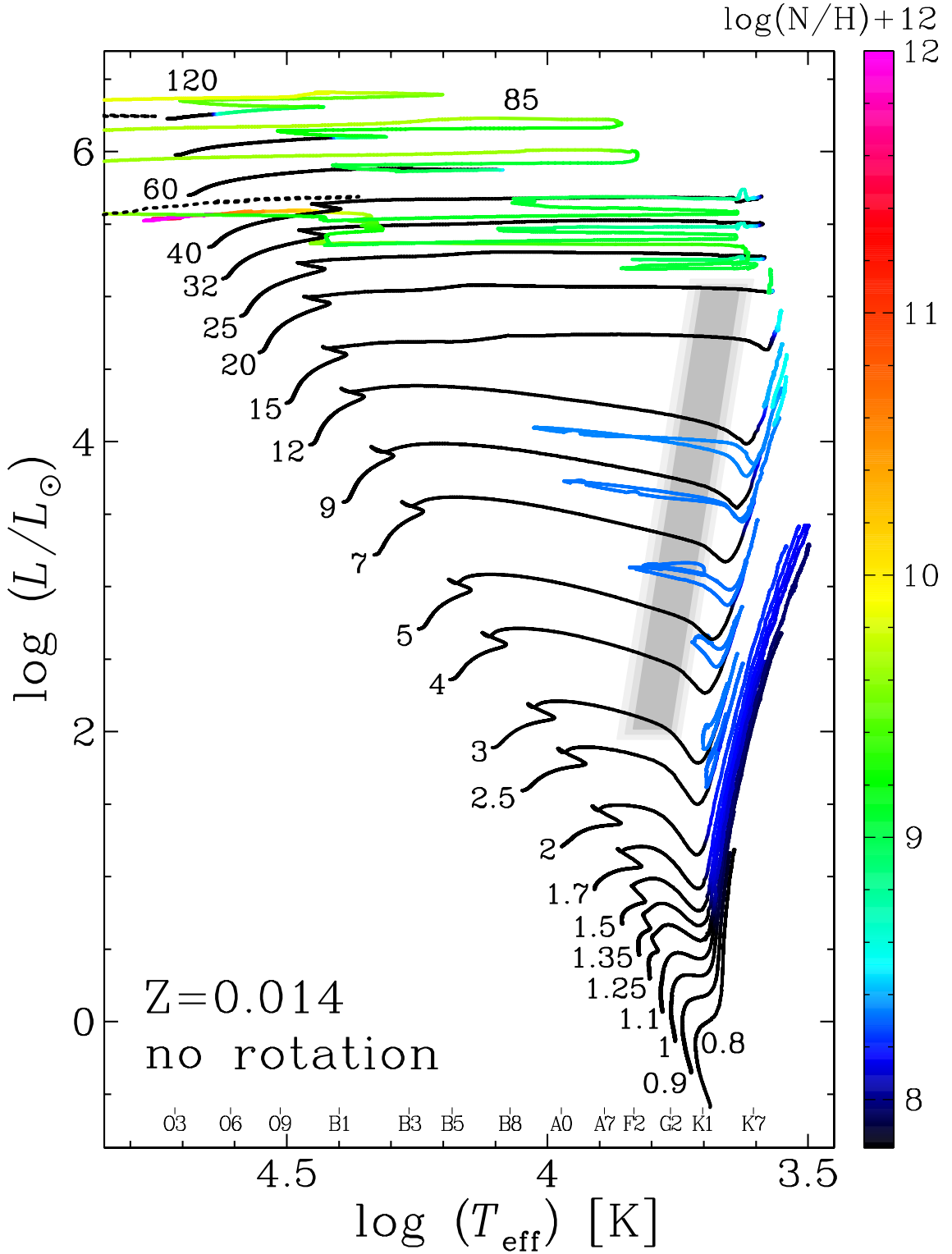
Figure 1.2: Figure 4 of Ekström et al. [92]: "Hertzsprung-Russell diagram for the non-rotating models. The colour scale indicates the surface number abundance of nitrogen on a log scale where the abundance of hydrogen is 12. Once the star has become a WNE type Wolf-Rayet star, the tracks are drawn with black dotted lines. The grey shaded area represents the Cepheid instability strip Tammann et al. 276".

The theory of stellar evolution from a mainstream and modern science perspective is quite recent. Some of the early efforts on a quantitative theory of stellar structure go back to Emden [95] and his study "Gaskugeln", or "gas balls". The 20th Century witnessed some major breakthroughs in our physical understanding of stars (e.g., [51, 65, 145] and references therein). The invention of digital computers, and their rapid ongoing development, has been instrumental in the study of stellar systems. From the computational point of view, one-dimensional parameterisations of stellar evolution have been the dominant tool of stellar structure studies in recent decades, including, but not limited to, software such as STARS [88, 86, 89], KEPLER [304, 114], BEC [112, 44, 314, etc.], Geneva [85] and MESA [216, 217, 218, 219]. More recently, three-dimensional studies of stellar structure have begun to arise (e.g., [184, 135]). The results of these type of efforts have shown that they are inherent to further development in our understanding of stellar evolution, but they remain scarce given their high complexity and computational expense.

While the study of single stellar evolution has improved significantly in recent decades, there are still uncertainties in key aspects of the physics. A significant amount of work has been devoted to understand nuclear reaction rates, atomic and molecular opacities, neutrino losses and the effect of metallicity and composition (see section 1 of Pols et al. [234] and references therein), among others. All of the aforementioned are considered minor uncertainties. On the other hand, the effect of magnetic fields (for a review see Maeder and Meynet [174]), rotation [114, 92, 44], mass loss rates [240, 246], convection [37, 61, 65] and semi-convection (see Langer et al. [158] and references therein) are all considered major uncertainties. Their parameterisations are usually oversimplified and give unrealistic results; the approach of Mixing Length Theory and its wide use is the canonical example of this. Throughout this work we will neither study nor focus on the variation of parameters

6

and parameterisations of single stellar evolution.

## 1.1.1   Remnants

The fate of single massive stars has been explicitly studied in the literature from a theoretical perspective [115] and, while our understanding has improved [199, 192], it is not yet a solved problem [272, 190]. This is understandable given how uncertainties in stellar evolution affect the late time structure of stellar models, which are often used to infer the plausible type of remnant object [104]. Predicting the properties of a stellar remnant has been an active topic of research in recent decades [287, 103]. For single stars these properties depend largely on the initial mass and metallicity [25, 267]. One illustrative example is mass loss through stellar winds, which is a strong function of both mass and metallicity [301]. Without considering the effect of binarity in stars, we briefly describe and present some of the remnants of stars at the end of their nuclear fusing lifetimes. For a visual summary of this section, see figure 1.3.

**White Dwarfs**

If a single star is not massive enough to collapse after nuclear burning has finished, it will form a White Dwarf. This roughly corresponds to the limit $M < 8$ M$_\odot$ as specified in section 1.1. However, the actual limit can be model dependant. White Dwarfs form when fusion has stopped and the star is supported solely by electron degeneracy pressure. Different compositions exist such as helium, carbon-oxygen or oxygen-neon White Dwarfs. The composition is believed to mostly depend on the initial mass of the progenitor. Most White Dwarfs have a carbon-oxygen composition. Oxygen-neon White Dwarfs have more massive progenitors and are less common.

Helium White Dwarfs are the product of binary interactions. White Dwarfs have mass limits of approximately $0.1 \lesssim m_{\mathrm{WD}}/\mathrm{M}_\odot < 1.4$ and Earth-like radius [259]. The upper mass limit of a White Dwarf is associated to the Chandrasekhar limit [50]. An usual convention for the low/high mass star bifurcation is given depending on whether the star becomes a White Dwarf (low-mass star) or a NS (high-mass star). Given that we follow the convention of low mass stars leading to White Dwarfs, they will not be discussed in detail at any point in this work, which is focussed on massive stars.

**Neutron Stars**

NSs are compact objects supported by neutron degeneracy pressure [288, 203, 306]. They have masses of approximately $1 \lesssim m_{\mathrm{NS}}/\mathrm{M}_\odot \lesssim 2$, and radii of $\sim 10$ km [208]. Hewish et al. [118] reported the discovery of rapidly pulsating radio sources and correctly suggested that some of them might have a NS progenitor. Since the first discovery of radio pulsars, thousands more detections have been made [175]. Core-collapse Supernovae (CCSNe) are the canonical formation path to NS formation. CCSN progenitors are stars massive enough to fuse elements with products as heavy as iron and develop an onion-like structure of decreasing mean atomic mass, going from the core to the surface. NSs form as a result of the nickel-iron core of the progenitor reaching the Chandrasekhar mass, which leads to the collapse. An alternative proposed scenario for NS formation is as an Electron-Capture Supernova (ECSN). In this alternative scenario, an oxygen-neon-magnesium core collapses due to electron captures into $^{24}\mathrm{Mg}$ and $^{20}\mathrm{Ne}$ before neon ignition, which eventually leads to collapse and NS formation [188].

**Stellar-mass Black Holes**

Stellar-mass Black Holes (BHs) are formed when even neutron degeneracy pressure is insufficient to prevent the collapse of the core [257]. Bowyer et al. [40] reported the detection of eight X-ray sources, one of them the notorious Cygnus X-1, arguably the first indirect detection of a BH. We will refer to stellar-mass BHs simply as BHs; we will not discuss micro BHs, primordial BHs, intermediate-mass BHs or super-massive BHs. There have been claims in the literature of an observational gap between the more massive NS and the least massive BH observed to date [19]. There is currently no clear consensus regarding the existence of the so-called first black-hole mass gap [209, 97, 152, 311].

**Transients without remnants**

An alternative outcome from the death of a star is to leave no remnant. Pair-instability Supernovae (PISNe) are a theoretical candidate of massive stars leaving no remnant. PISNe are believed to occur in stars with oxygen-carbon (O/C) cores that reach high temperatures and densities which lead to pair formation [101]. In this scenario, electron-positron pair formation leads to a significant decrease in radiation pressure support and posterior explosive oxygen burning. The energy released in this process can be enough to fully disrupt the star. Heger and Woosley [113] predict PISNe in stars with helium cores between $64 - 133$ M$_\odot$. The explosion of massive stars with O/C cores slightly less massive than $\approx 64$ M$_\odot$, referred to as pulsational PISNe, will not be enough to fully disrupt the star. Pulsational PISNe are predicted to experience episodic explosions initiated by the pair instability, but leading to BH formation. The explosion of massive stars with O/C cores more massive than $\approx 133$ M$_\odot$ will not be energetic enough to counterbalance the gravitational binding energy of the O/C core and will lead to direct collapse into a BH. Single stellar

9

## Remnants of massive single stars
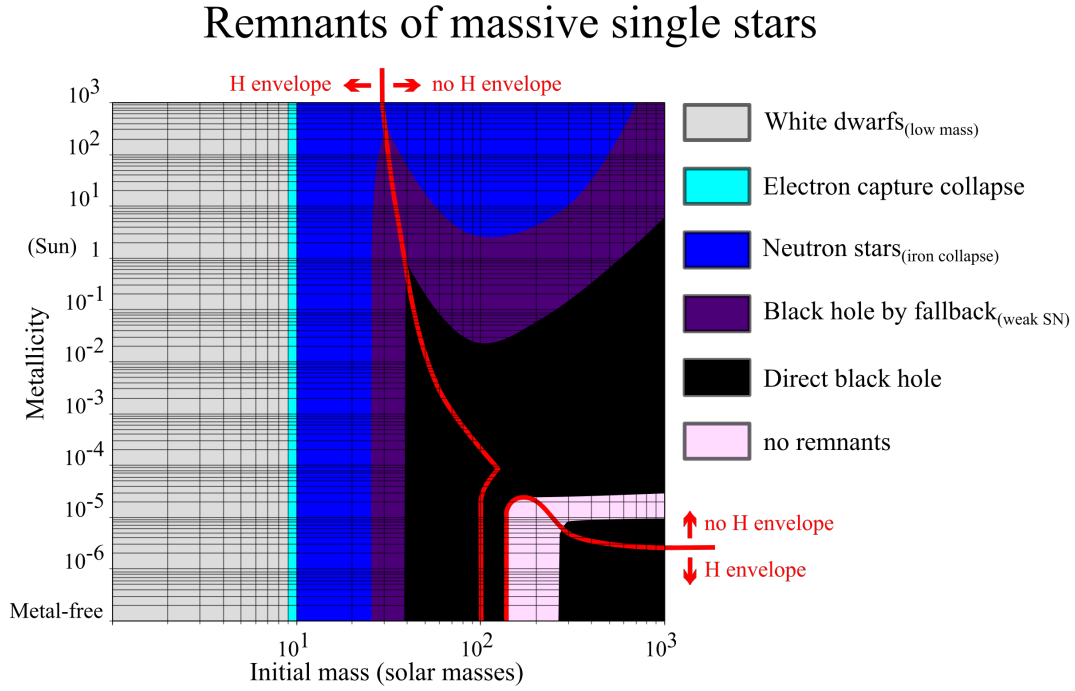


Figure 1.3: Visual summary of the possible remnant type from single stellar models as a function of initial mass and metallicity. Supernovae as initial mass-metallicity by fulvio314 is licensed under CC BY-SA 3.0 and adapted from figure 1 of Heger et al. [115].

evolution, particularly via PISNe, predicts a second BH mass gap along this regime [115]. To date, there has been no confirmed observational candidate of a PISN. More detections, likely gravitational-wave observations, are needed in order to make statements about the properties around the predicted second BH mass-gap regime [113].

## 1.1.2   Single massive stars: aftermath

The exact physics of single stellar evolution remains uncertain; early predictions, such as PISNe [20, 241], have not yet been confirmed. Even full understanding of the Sun, our most famous and studied star, has not been achieved. Single stellar evolution is a vast field itself and stellar multiplicity adds to the complexity.

## 1.2  Binary evolution

For massive stars, multiple-star systems are more common than single stars (for a review see Duchêne and Kraus [84]). Binaries, the lowest order multiple-star system possible, are a frequent configuration [11]. Most stars with masses larger than 15 M$_\odot$ (spectral type O) are expected to be part of a binary; more than 70% of them will experience mass transfer during their lifetimes [251]. The role of massive binary evolution has become a recurring research theme in the past decades [e.g., 54, 292, 55, 294, 33, 228, 23, 229, 136, 73, 281]. Following the detections of gravitational waves from Double Compact Objects (DCOs) [2, 4], there has been an enhanced and renewed interest in their progenitors, i.e. massive binaries. Hereafter, we will further constrain our interest to the study of interacting massive binaries.

### 1.2.1  Interacting binaries

The behaviour of the constituent stars of a long-period non-interactive binary can be approximated to that of single stars. While the orbit is gravitationally bound and might be altered by the evolution of each star, e.g. due to mass and angular momentum loss from stellar winds, the fate of the binary can be predicted based on single stellar models. The evolution and properties of short-period interacting binaries are harder to model and predict. We define an interactive binary as any binary which experiences at least one mass transfer episode. Some binaries are believed to be in contact early in the main sequence; they are referred to as massive overcontact binaries [179]. For simplicity, we assume that binaries are born detached, unless stated otherwise.

**Mass transfer**

Mass transfer is arguably the most important feature of binary evolution. The effect of a mass transfer episode on the binary depends on the orbital configuration and evolutionary phase of the stars at the onset of the episode. Slightly different configurations can lead to, e.g., an early MS stellar merger compared to the formation of a DCO. Our broad description and treatment on the mass transfer phase follows the classic approach as described in Eggleton [87] and Podsiadlowski [227], among others.

A mass transfer episode begins when a star expands beyond the Roche lobe (see figure 1.4). The Roche lobe, an equipotential solution of the Roche potential, is the region within which material is gravitationally bound to that star. The Roche lobe is delimited by the first Lagrangian point, which lies between both stars.

During a mass transfer episode we refer to the star which fills its Roche lobe as the donor star and to the companion as the accretor. Given that more massive stars evolve, and therefore expand, more rapidly than less massive ones, we expect that the more massive star will be the donor in the first mass transfer episode. What happens to the mass lost from the donor and how it affects the orbit depends on the configuration of the binary. A full, general solution to the mass transfer problem is still an active topic of research in the literature.

The most simple type of mass transfer episode is when the mass is transferred in a stable manner and is fully accreted by the companion. A stable episode occurs when mass transferring leads to the cessation of further transfer of mass; this may happen, for example, if the orbit widens or the donor star has a radiative envelope. If the amount of mass lost by the donor is fully accreted by the companion then total mass and angular momentum are conserved. If not all of the mass transferred

by the donor is accreted by the companion, then the episode is non-conservative. The amount of non-accreted mass will leave the system and remove some orbital angular momentum with it. Depending on the amount of non-accreted mass and where is it lost from, the orbital separation will evolve differently.

The alternative to a stable mass transfer episode is, unsurprisingly, an unstable mass transfer episode. An unstable episode is a runaway process which occurs when mass transferring leads to further transfer of mass; this may happen, for example, if the orbit shrinks or the donor star has a deep convective envelope. Unstable mass transfer is rapid and (highly) non-conservative. The non-accreted mass can pile up around the accretor before leaving the system. If this piling up leads to expansion and posterior Roche lobe filling of the accretor, the system engages in a Common-envelope Episode (CEE).

**Common Envelope Episodes**

CEEs may be the most intricate and complex phase of binary evolution [211, 128]. They begin as a result of dynamically unstable mass transfer, when the envelope of the donor star engulfs the orbit formed by the core of the primary star and the companion. This engulfment occurs when the mass that is rapidly transferred to the accretor is not able to thermally adjust and expands up to the outer Lagrangian point ($L_2$ in figure 1.4). The loss of corotation between the envelope and the inner binary generates drag forces between them. This drag can transport orbital angular momentum and energy out of the system, reducing the orbital period quite significantly. If the radiated frictional energy is enough to unbind the common envelope, the CEE terminates with a significant shrinkage of the orbit. If, on the other hand, the energy budget is not enough to unbind the common envelope, the phase leads to a merger.
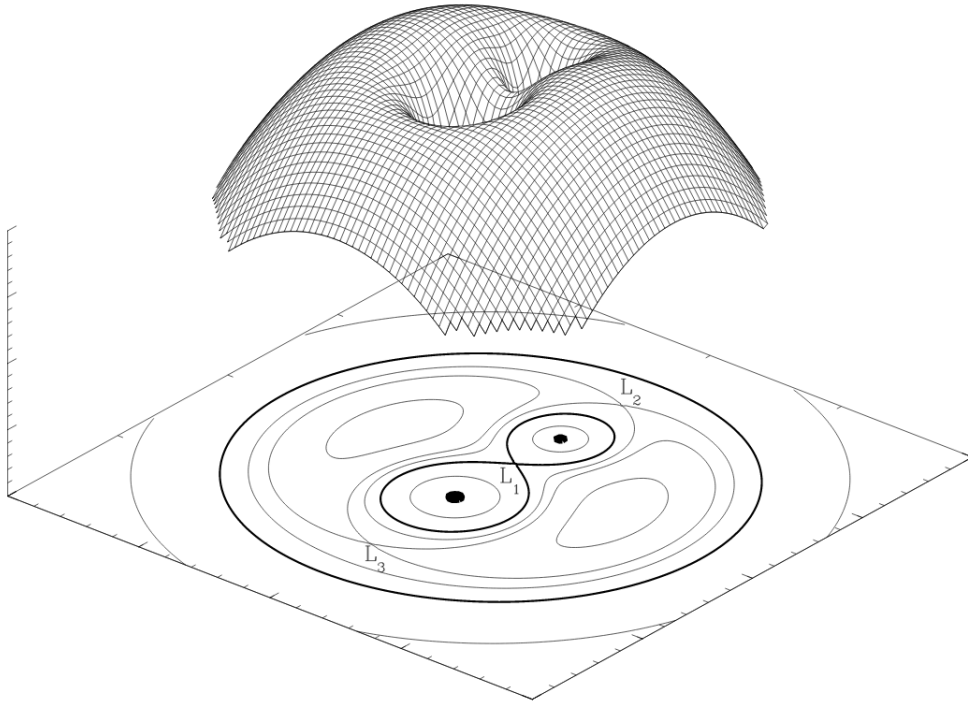
Figure 1.4: Roche potential. Three-dimensional (mesh) and orbital-plane projection (contours) of a binary with $M_{\mathrm{donor}} = 2M_{\mathrm{accretor}}$. The more massive donor lies within the first ($L_1$) and third ($L_3$) Lagrangian points, while the less massive accretor lies within $L_1$ and the second ($L_2$) Lagrangian point. The orbital plane projection shows the Roche lobe in a solid black line with the geometrical shape of a lemniscate. This region delimits whether the material is gravitationally bounded to that star. This is figure 6.3 from Sluijs [262].

CEEs have been suggested as a solution to creating short orbital period binaries at late evolutionary phases. Observations of short gamma-ray bursts and gravitational waves, both the end points of binary evolution, require binaries to have small separations at the moment of DCO formation in order for them to merge within the age of the universe [220]. Progenitors of short gamma-ray bursts and current gravitational-wave observations are believed to be the remnants of massive binaries [9]. The caveat lies in the fact that massive binaries are expected to have separations of at least tens of solar radii at birth in order to avoid Zero-age Main Sequence (ZAMS) contact. They are also expected to expand tens to hundreds of solar radii during their lifetimes. Nevertheless, the separation needed at DCO formation for these systems to merge via gravitational-wave radiation is a few solar radii at most. This requires an initially wide binary to become a close DCO within a few million years.

Additionally, CEEs, both succesful ejection and mergers, have been linked to planetary nebulae [39], luminous red novae (see, e.g., [127]) and other type of astronomical events, such as, Thorne-Żytkow objects [286].

**Tides**

Binary components experience tidal deformations from the presence of their companions. This deformation of the tidal bulge leads to an effective torque on the distorted star, which in tight binaries tends to synchronise the star with the orbit (see Zahn [317] for a summary). Further dissipation of energy leads to the state of minumum kinetic energy: a coplanar synchronised circular orbit [64, 123]. Efficient tidal interactions are expected to synchronise and circularise the orbit. The efficiency of the interactions is dependant on the orbital separation and the structure of the distorted star.

There is a particular case of tidally interacting binaries leading to a CEE: the Darwin instability [66]. This instability arises if one of the component stars, synchronously spinning with the orbit, has a significant spin angular momentum ($J_{\text{star}}$) compared to the orbital angular momentum ($J_{\text{orb}}$). In the case of a system where the structure of the stars remains fixed throughout the spin-up leading to the instability, and where the synchronisation timescale is smaller than the rest of the orbital evolution timescales, the instability will occur if $J_{\text{star}} > \frac{1}{3}J_{\text{orb}}$. In that case, the spin-up of the star will extract angular momentum from the orbit, leading to orbital spin-up, which will lead to higher synchronisation frequencies, and so on. This instability is particularly, but not exclusively, important for systems during the ZAMS, as it can lead to early stellar mergers.

## 1.2.2  Isolated Binary Evolution

A binary is considered to be isolated if it does not experience any interaction with other astrophysical objects. Any isolated binary would be in an environment where the nearest neighbouring object would not perturb its orbital properties. An example of this is a binary that is born from a single gas cloud in the field.

Isolated and interactive massive binaries have been thoroughly studied in the literature in the context of different astronomical phenomena (see De Marco and Izzard [69] for a review). Some examples of these phenomena are: X-ray binaries [e.g., 293], colliding-wind binaries [e.g., 91], Galactic Double Neutron Stars (DNSs) (see Bhattacharya and van den Heuvel [33] for a review), short gamma-ray bursts [e.g. 36] and gravitational-wave sources [e.g., 283].

Some of the previously mentioned transients have also been studied and proposed in alternative scenarios. These scenarios may compel completely different fields of

active research. In the next section, we mention them for completion and not in an effort to make any detailed review nor summary of their respective fields.

### 1.2.3  Other formation scenarios

Interactive binaries may arise in astrophysical scenarios that are not the classical isolated binary evolution channel. Here we present some alternative formation scenarios that could give similar outcomes. Among other things, one of the active research goals of binary evolution is to predict observables which would distinguish, and even rule out, different formation scenarios.

**Chemically Homogeneous Evolution**

Chemically homogeneous evolution can occur in isolated binaries. Nevertheless, chemically homogenous evolution has very peculiar properties and therefore we segregate it for clarity purposes. Rapidly spinning stars are assumed to experience enhanced mixing; if the rotational rates are high enough, the mixing leads to chemical structure which is homogeneous (hence the name). These stars experience fully or quasi-chemically homogeneous evolution [313].

Close binaries experience tidal interactions which tend to synchronise the orbital and stellar spin frequencies [315, 316, 123]. Stars in short orbital period binaries are expected to evolve chemically homogeneously, particularly if they don't experience significant angular momentum losses. These stars remain quite compact through evolution, therefore likely avoiding any mass transfer episode. Chemically homogeneously evolving binaries have been proposed as a plausible evolutionary pathway to LIGO sources, particularly binary black-hole mergers [179, 70, 176, 93]. Chemically

homogeneously evolving stars won't significantly expand. They could be born close enough to become DCOs without having to interact. This would avoid the need of a CEE to explain merging DCOs.

Alternatively, a mass transfer episode can lead to quasi-chemically homogeneous evolution, which can be very similar to chemically homogeneous evolution from a single rapidly-rotating star [47]. In this scenario, the donor transfers mass and angular momentum to the companion. This increases the rotational rate of the companion and leads to quasi-chemically homogeneous evolution.

**Dynamical Formation**

Highly dense stellar environments, such as globular or nuclear clusters, lead to chaotic binary-single and binary-binary interactions [116]. These interactions have significant effects on the evolution of these environments. Some of the initially bound binaries might disrupt, swap companions, merge or become ejected. Even if few-body interactions don't alter the fate of the binaries so abruptly, the interaction with an object may alter the evolution of the binary in different ways with respect to isolated binary evolution. Some Galactic DNSs have been detected in globular clusters and therefore are likely to have been formed there (see Tauris et al. [282] and references therein). Gravitational-wave sources have also been suggested to form in the dynamical formation scenario [e.g., 224, 235, etc.].

**Triples and higher order multiple systems**

Ternary stellar systems, colloquially referred to as triples, are gravitationally stable three-star configurations. While triples are a subset, and the lowest order systems,

of the dynamical formation scenario, we consider them here as a different channel. Stable triple systems composed of a close binary perturbed by a distant companion, a hierarchical triple, have become a more active topic of research in recent years. An example is the dynamical interaction of the outer companion with the inner binary, leading to changes in eccentricity and inclination, in the "eccentric Kozai-Lidov" mechanism [163, 149]. Hierarchical triples have been evoked in the context of X-ray binaries (see Naoz et al. [193] and references therein) and gravitational-wave sources [249]. High order multiple systems are also frequent in nature, with massive stars mostly forming in multiple systems [252].

## 1.3  Rapid Binary Population Synthesis

Population synthesis is a method to study large astrophysical populations. Given the nature of these studies, populations are usually studied within a statistical framework. While larger populations are not always imperatively preferred over smaller populations, a representative sample of the population of interest must be generated in order to make significant qualitative and quantitative statements. Binary population synthesis focuses on the uncertain and non-trivial evolution of binaries, as well as their possibles outcomes. The purpose of most binary population synthesis methods is to rapidly evolve binaries with as much detail as possible; depending on the respective interests and approach, detail is prioritised over speed, or vice versa. In rapid population synthesis models, a single binary is expected to evolve in fractions of a second using a single processor.

Some population studies prioritise the details of the methods rather than the speed of simulation time. Detailed models using a single processor can take hours or days to be simulated. Other detailed and thorough methods, e.g. general relativistic

magnetohydrodynamics studies, may require millions of CPU hours in supercomputers, making those sorts of population studies presently impossible on reasonable timescales. While future developments may help us overcome some of these problems, more rapid methods will always have the advantage of creating vast populations in shorter timescales. This rapid approach is particularly handy if you are interested in the effect of physical assumptions and parameterisations on populations.

## 1.3.1 Compact Object Mergers: Population Astrophysics and Statistics (COMPAS)

In order to model and study populations of DCOs we use the Compact Object Mergers: Population Astrophysics and Statistics (COMPAS) suite [270, 21, 299, 194]. COMPAS contains a rapid binary population synthesis module which evolves a binary from ZAMS until merger, disruption or DCO formation. Chapters 2 and 3 use this module to do population studies of DCOs, particularly DNSs. In this section we elaborate on some of the physical parameterisations used in COMPAS. We leave the intricate details of COMPAS to the method sections of chapters 2 and 3.

The COMPAS rapid population synthesis module follows closely the BSE algorithm [122] and the `StarTrack` code [23, 24, etc.]. Other codes developed for rapid population synthesis studies are the Scenario Machine [164, 165, etc.], SeBa [237, 238, 289, etc.], binary_c [129, 130, 131], Mobse [107], SEVN [267, 268, 269] and ComBinE [155], to name a few.

## 1.3.2 Physical parameterisations

In order to model the evolution of populations of binaries, we choose different parameterisations of the different physical interactions. For single stellar evolution, we follow Hurley et al. [121] polynomial fitting formulae to Pols et al. [234] detailed stellar models.

If the stars are part of a binary, the physical parameterisation of interest could describe the effect on the star, the companion and the orbit. For our description of COMPAS, we focus on the most basic interactions: mass transfer, common envelopes, stellar winds, supernovae and gravitational-wave emission. Next we describe our approach to each of them. We follow closely Hurley et al. [122], Benacquista [30] and Postnov and Yungelson [239], among others. While tidal dissipation mechanisms are not currently fully implemented within the COMPAS framework, some of the theoretical background and parameterisations are presented and discussed in section 3.3.3.

**The two-body problem**

The most simplified parameterisation of the orbital solution of a binary is the two-body problem, which solves for the motion of two point particles given a central force. In this case, we particularly want to solve for the angular momentum $J$. Given that we assume stars to be point-like particles, $J = J_{\mathrm{orb}}$, where the subscript $J_{\mathrm{orb}}$ is the orbital angular momentum. The Lagrangian of the system is

$$\mathcal{L} = \frac{1}{2}m_1 v_1^2 + \frac{1}{2}m_2 v_2^2 + \frac{Gm_1 m_2}{|\mathbf{r}_2 - \mathbf{r}_1|},$$ (1.1)
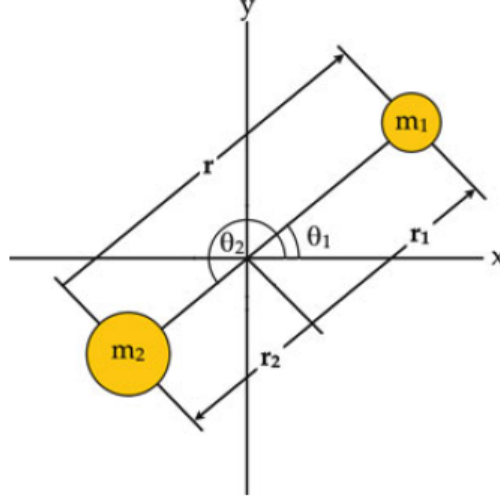
Figure 1.5: Barycentric coordinate system for a binary, as shown in figure 2.1 of Benacquista [30].

Where $m_i$, $\boldsymbol{r}_i$ and $v_i$ are the mass, position and velocity of the star of interest, with $i = 1, 2$, and $G$ is the gravitational constant. We consider the two point particles to be in a barycentric coordinate system (see figure 1.5) with $m_1\mathbf{r}_1 + m_2\mathbf{r}_2 = 0$ and $r = r_1 + r_2$ so that $r_i = m_j r/M$, where $M = m_1 + m_2$ is the total mass. Also, following figure 1.5 we show $\theta_1 = \theta_2 - \pi = \theta$. Assuming the orbit lies in a plane, given the polar-coordinate nature of the problem, we can express

$$v_i^2 = \dot{r}_i^2 + r_i^2\dot{\theta}_i^2 = \left(\frac{\mu}{m_i}\right)^2 \left(\dot{r}^2 + r^2\dot{\theta}^2\right), \tag{1.2}$$

where $\mu = m_1 m_2/M$. We rewrite Equation 1.1 as

$$\mathcal{L} = \frac{1}{2}\mu\dot{r}^2 + \frac{1}{2}\mu r^2\dot{\theta}^2 + \frac{G\mu M}{r}. \tag{1.3}$$

Given the Euler-Lagrange equation

$$\frac{\mathrm{d}}{\mathrm{dt}} \frac{\partial \mathcal{L}}{\partial \dot{\theta}} - \frac{\partial \mathcal{L}}{\partial \theta} = 0, \tag{1.4}$$

and the fact that $\mathcal{L}$ is independent of $\theta$, we have $\partial \mathcal{L}/\partial \dot{\theta}$ is a constant, and we can rewrite to

$$J = \frac{\partial \mathcal{L}}{\partial \dot{\theta}} = \mu r^2 \dot{\theta}. \tag{1.5}$$

For a circular orbit, we can equate the centripetal force $F_{\mathrm{c,i}} = m_i r_i \dot{\theta}^2$ to the gravitational force $F_{\mathrm{g}} = Gm_1 m_2/r^2$, and solve for $\dot{\theta}^2$ in order to derive Kepler's Third Law in the form

$$\dot{\theta}^2 = \frac{GM}{r^3}. \tag{1.6}$$

In the case of the circular binary $r = a$, where $a$ is the semi-major axis, we can express the angular momentum of the system as

$$J = \mu \sqrt{GMa}. \tag{1.7}$$
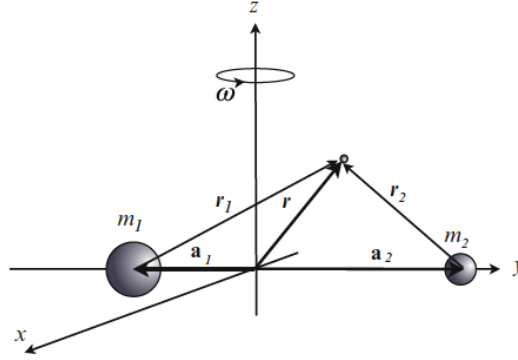
Figure 1.6: Corotating coordinate system for the three-body problem, composed of the binary with $m_1$ and $m_2$ components, as well as a test mass, as shown in figure 13.1 of Benacquista [30].

## Roche potential, Roche lobe and Roche-lobe radius

Roche-lobe overflow (RLOF) determines the beginning of a mass transfer episode. In COMPAS, and generally in rapid binary population synthesis, there are several assumptions and simplifications to determine if mass transfer occurs.

A Roche potential is calculated for a circular corotating binary system. The volume of the Roche lobe can then be numerically integrated [189]. This volume can be compared to that of a sphere to get a volume equivalent Roche-lobe radius [210]. If the radius of the star is larger than this Roche-lobe radius, we assume there is RLOF leading to mass transfer.

The solution of the Roche potential is given by solving for the motion of a test particle under the influence of the binary. We choose a corotating coordinate system which keeps the stars at fixed positions (see figure 1.6 for coordinate system and defined quantities). We write the Lagrangian for the third body in the $x - y$

plane as it rotates through the $z$-axis as

$$\mathcal{L} = \frac{1}{2}m(\dot{x}^2 + \dot{y}^2 + \dot{z}^2) + \frac{1}{2}m\omega^2(x^2 + y^2) + \frac{Gm_1 m}{r_1} + \frac{Gm_2 m}{r_2}, \tag{1.8}$$

where $r_i = |\mathbf{r} - \mathbf{a}_i|$. We can do the classic old trick of grouping the last three terms of the Lagrangian into a single (pseudo)potential:

$$\Phi_0 = \frac{1}{2}m\omega^2(x^2 + y^2) + \frac{Gm_1 m}{r_1} + \frac{Gm_2 m}{r_2}. \tag{1.9}$$

In order to plot equipotential surfaces of the pseudopotential we change the coordinate system so that $a = 1$, $a_i = m_j/M$, $r_1 = \sqrt{x^2 + y^2}$ and $r_2 = \sqrt{x^2 + (y-1)^2}$. In this new coordinate system, the pseudopotential can be rewritten as

$$\Phi_0' = -\frac{Gm_1}{r_1} - \frac{Gm_2}{r_2} - \frac{\omega^2}{2}\left[x^2 + \left(y - \frac{m_2}{M}\right)^2\right]. \tag{1.10}$$

We define a normalised potential $\Phi = -2\Phi_0'/(GM)$ and mass ratio $q = m_2/m_1$ (with $m_2 < m_1$) so we finally rewrite the normalised potential as

$$\Phi = \frac{2}{(1+q)\sqrt{(x^2 + y^2)}} + \frac{2q}{(1+q)\sqrt{(x^2 + (y-1)^2)}} + x^2 + \left(y - \frac{q}{1+q}\right)^2 \tag{1.11}$$
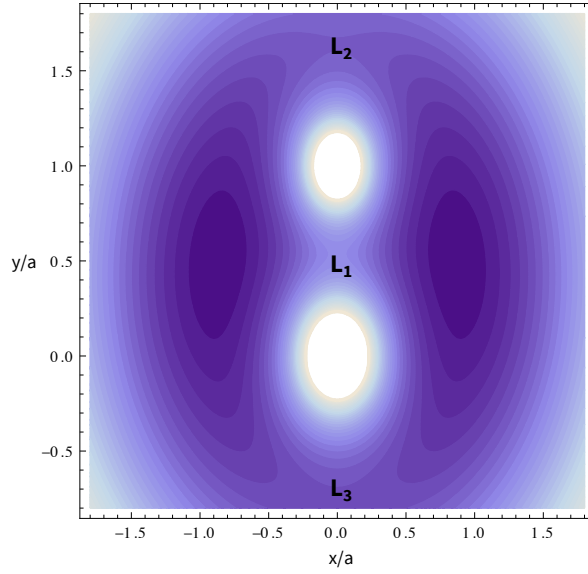
Figure 1.7: Roche potential orbital-plane projection of a $q = m_2/m_1 = 0.7$, with the more massive primary at $(x, y) = (0, 0)$ and the secondary at $(x, y) = (0, 1)$. $L_1$ lies at $(x, y) = (0, 0.46)$.

so that $m_1$ and $m_2$ align in the normalised $x - y$ axis (see figure 1.7).

Kopal [148] was the first to tabulate the Roche-lobe radius as a measure of the size of a Roche lobe. Paczyński [210] gave a fitting formulae as a function of mass ratio that could approximate those values to within 2%, later improved by Eggleton [90] with a smooth approximation, to better than 1%, in the form:

$$\frac{r_{\mathrm{RL}}}{a} = \frac{0.49q^{2/3}}{0.6q^{2/3} + \ln(1 + q^{1/3})}, \ 0 < q < \infty, \tag{1.12}$$

where $r_{\mathrm{RL}}$ is the effective Roche-lobe radius, that we use to approximate the Roche-lobe radius. The effective Roche-lobe radius corresponds to the radius of a sphere with the same volume as the Roche lobe in a binary.

**Mass Transfer**

Mass transfer begins when $R_{\mathrm{star}} \geq r_{\mathrm{RL}}$. If a mass transfer episode begins, we need to determine if it will be either stable or unstable and on which timescale will it occur. In order to determine stability, we use the mass-radius exponents:

$$\zeta = \frac{d \log R}{d \log m}. \tag{1.13}$$

For dynamical stability, we compare the adiabatic mass-radius exponent of the donor ($\zeta_{\mathrm{ad}}$) to the Roche-lobe mass-radius exponent ($\zeta_{\mathrm{RL}}$) as seen from the donor. The adiabatic mass-radius exponent determines the response of the radius to mass loss on an adiabatic timescale. Given that the denominator for $\zeta_{\mathrm{star}}$ during mass loss is negative, $\zeta_{\mathrm{star}} > 0$ implies that the star contracts, while $\zeta_{\mathrm{star}} < 0$ means it expands. Stars with radiative envelopes have $\zeta_{\mathrm{star}} > 0$ and thus contract as a response to mass loss, while stars with convective envelopes have $\zeta_{\mathrm{star}} < 0$ and thus expand. If $\zeta_{\mathrm{star}} \geq \zeta_{\mathrm{RL}}$, we assume the mass transfer episode is dynamically stable.

In COMPAS, stable mass transfer can occur on the thermal or nuclear timescale of the donor star. We approximate the thermal timescale as the Kelvin-Helmholtz timescale

$$\tau_{\mathrm{KH}} = \frac{Gmm_{\mathrm{env}}}{RL}, \tag{1.14}$$

where $m$ is the mass, $m_{\mathrm{env}}$ is the envelope mass, $R$ is the radius and $L$ is the luminosity (all of the donor star).

If the mass transfer episode occurs during the MS of the donor, when the star has a radiative envelope, the star is stripped on a thermal timescale until it fits within its Roche lobe; this is referred to as fast phase "case A" mass transfer [144, 233]. After the star stops RLOF, the natural expansion of the star occurs on a nuclear timescale. This leads to mass transfer episodes on longer (nuclear) timescales with smaller mass transfer rates. For more evolved stars the envelope is assumed to be lost within a thermal timescale.

Once we know the timescale of the mass transfer episode, there are three main things that we need to know in order to solve the evolution of a binary: how much mass is donated ($\Delta m_{\mathrm{donor}}$), how much mass is accreted ($\Delta m_{\mathrm{accretor}}$), and how the non-accreted mass is lost from the binary.

Similarly to what defines the relevant timescale, the amount of mass donated has to do with the stellar phase. For MS stars $\Delta m_{\mathrm{donor}}$ will be the amount of mass required to stop filling the Roche lobe. For more evolved stars $\Delta m_{\mathrm{donor}} = m_{\mathrm{env,donor}}$. Given that we are interested in massive binaries, we do not account for mass transfer from White Dwarf donors.

The amount of mass accreted by the companion will be determined by its evolutionary phase and parameterised by a multiplying factor $0 \leq \beta \leq 1$, so that $\Delta m_{\mathrm{accretor}} = \beta \times \Delta m_{\mathrm{donor}}$. For non-compact accretors, i.e. regular stars, we determine the efficiency as $\beta = \min(1, \mathrm{C} \times \tau_{\mathrm{KH,donor}}/\tau_{\mathrm{KH,accretor}})$, with $C = 10$ following Hurley et al. [122]. For compact object accretors, $\beta = \min(1, \dot{m}_{\mathrm{Edd}}/\dot{m}_{\mathrm{donor}})$, where $\dot{m}_{\mathrm{Edd}}$ is the Eddington accretion limit. We define $\dot{m}_{\mathrm{Edd}} = 4\pi G m_{\mathrm{accretor}} m_{\mathrm{p}}/\epsilon c \sigma_{\mathrm{t}}$, where $m_{\mathrm{p}}$ is the mass of the proton, $\epsilon$ is the fraction of energy released in radiation, $c$ is the speed of light and $\sigma_{\mathrm{t}}$ is the Thomson cross section.

The non-accreted mass is lost from the binary and it carries away angular mo-

mentum with it. We parameterise this rate of change of angular momentum in terms of the angular momentum of the binary as $\dot{J}/\dot{m} = \gamma J/M$, where $\gamma$ is a constant multiplicative factor.

In order to solve for the orbital separation after the mass transfer episode we take the time derivative of Equation 1.7 and parameterise it in terms of $\beta$ and $\gamma$ to get

$$\frac{\dot{a}}{a} = -2\frac{\dot{m}_{\mathrm{donor}}}{m_{\mathrm{donor}}}\left[1 - \beta\frac{m_{\mathrm{donor}}}{m_{\mathrm{accretor}}} - (1-\beta)(\gamma + \frac{1}{2})\frac{m_{\mathrm{donor}}}{M}\right]. \tag{1.15}$$

Alternatively, if $\zeta_{\mathrm{star}} < \zeta_{\mathrm{RL}}$, the mass transfer episode is dynamically unstable and leads to a CEE.

**Common Envelope Event**

In COMPAS, we use the $\alpha\lambda$-formalism to solve for the orbital evolution during a CEE [305, 68]. This approach compares the binding energy of the envelope of the donor star at the onset of RLOF to the gravitational energy radiated from the inspiral of the binary.

We parameterise the binding energy as

$$E_{\mathrm{bind,donor}} = -\frac{Gm_{\mathrm{donor}}m_{\mathrm{env,donor}}}{\lambda R_{\mathrm{donor}}}, \tag{1.16}$$

where $\lambda$ is a structure parameter which can be determined given a detailed stellar model.

We parameterise the change in the orbit as

$$\alpha \Delta E_{\rm orb} = \alpha \left( \frac{G m_{\rm core,donor} m_{\rm companion}}{2 a_{\rm final}} - \frac{G m_{\rm donor} m_{\rm companion}}{2 a_{\rm initial}} \right), \qquad (1.17)$$

where $\alpha$ is an efficiency factor which accounts for how much of the radiated gravitational energy is used to unbind the envelope. While $\alpha$ is also dependant on the structure of the binary, it is less well constrained and understood than $\lambda$; a fixed value, e.g. $\alpha = 1$, is very often used in population studies (and is the default in COMPAS). We then compare Equations 1.16 and 1.17 to solve for the final separation.

**Stellar winds**

We assume that stellar winds are rapid ($v_{\rm winds} \gg v_{\rm orb}$) and that they carry the specific angular momentum of their respective wind-emitting star. This type of mass loss can be described as a fully non-conservative mass transfer episode where mass is lost from the frame of reference of the donor star. If we do so, we can rewrite Equation 1.15 as

$$\frac{\dot{a}}{a} = -2 \frac{\dot{m}_{\rm donor}}{m_{\rm donor}} \left[ 1 - (\gamma + \frac{1}{2}) \frac{m_{\rm donor}}{M} \right]. \qquad (1.18)$$

In order to find the value for $\gamma$ when mass is lost from the donor (Fast or Jeans mode), we consider that the wind leaves with the specific angular momentum of the

donor star, $\dot{J}_{\mathrm{orb}} = (\dot{m}J/m)_{\mathrm{donor}}$ and $J_{\mathrm{donor}} = m_{\mathrm{accretor}}J_{\mathrm{orb}}/M$, so that

$$\gamma = \frac{\dot{J}_{\mathrm{orb}}}{\dot{m}}\frac{M}{J_{\mathrm{orb}}} = \frac{m_{\mathrm{accretor}}}{m_{\mathrm{donor}}}. \tag{1.19}$$

If we substitute Equation 1.19 in 1.18, we can now approximate the evolution of the orbit due to fast stellar winds as

$$\frac{\dot{a}}{a} = -\frac{\dot{m}}{M}. \tag{1.20}$$

**Supernovae**

A generic Supernova (SN) explosion can be parameterised as an extremely rapid asymmetric ejecta of mass from the frame of reference of the exploding star; this parameterisation can be solved analytically [34, 41, 278, 122]. We follow Postnov and Yungelson [239] to illustrate the effect of the explosion on the separation, eccentricity and orbital plane of the pre/post-SN binary.

The pre-SN binary moves in a circular orbit with separation $a_{\mathrm{pre}}$ and relative velocity $\mathbf{v}_{\mathrm{pre}}$. We choose a cartesian instantaneous reference frame centered on the non-exploding star, with the orbital plane on the $x-y$ axis and perpendicular to the $z$ plane. The $x$ axis is the line formed between the center-of-mass of the stars, and the $y$ axis points in the direction of $\mathbf{v}_{\mathrm{pre}} = (0, v_{\mathrm{pre}}, 0)$. The pre-SN relative velocity and angular momentum are $v_{\mathrm{pre}} = \sqrt{GM_{\mathrm{pre}}/a_{\mathrm{pre}}}$ and $\mathbf{J}_{\mathrm{pre}} = \mu_{\mathrm{pre}}\mathbf{r}_{\mathrm{pre}} \times \mathbf{v}_{\mathrm{pre}}$ respectively, with $\mathbf{r}_{\mathrm{pre}} = (a_{\mathrm{pre}}, 0, 0)$ and $\mu_{\mathrm{pre}} = m_1 m_2/M_{\mathrm{pre}}$.

If the explosion is instantaneous, as we expect from a SN, the position vector will remain unchanged so that $\mathbf{r}_{\mathrm{post}} = \mathbf{r}_{\mathrm{pre}}$. The post-SN relative velocity and angular momentum, on the other hand, will change to $\mathbf{v}_{\mathrm{post}} = (\omega_{\mathrm{x}}, v_{\mathrm{pre}} + \omega_{\mathrm{y}}, \omega_{\mathrm{z}})$ and $\mathbf{J}_{\mathrm{post}} = \mu_{\mathrm{post}}\mathbf{r}_{\mathrm{post}} \times \mathbf{v}_{\mathrm{post}} = \mu_{\mathrm{post}}a(0, \omega_{\mathrm{z}}, v_{\mathrm{pre}} + \omega_{\mathrm{y}})$, where $\boldsymbol{\omega} = (\omega_{\mathrm{x}}, \omega_{\mathrm{y}}, \omega_{\mathrm{z}})$ is the kick velocity and $\mu_{\mathrm{post}} = m_{\mathrm{rem}}m_2/M_{\mathrm{post}}$, with $M_{\mathrm{post}} = m_2 + m_{\mathrm{rem}}$ and $m_{\mathrm{rem}}$ being the mass of the remnant compact object.

We compare the orbital energy and angular momentum of an initially circular orbit after the SN with a the resulting final elliptical orbit with separation $a_{\mathrm{e}}$ and eccentricity $e$:

$$\mu_{\mathrm{post}}\frac{v_{\mathrm{post}}^2}{2} - \frac{Gm_{\mathrm{rem}}m_2}{a} = -\frac{Gm_{\mathrm{rem}}m_2}{2a_{\mathrm{e}}}, \tag{1.21}$$

$$\mu_{\mathrm{post}}a\sqrt{\omega_{\mathrm{z}} + (v_{\mathrm{pre}} + \omega_{\mathrm{y}})^2} = \mu_{\mathrm{post}}\sqrt{GM_{\mathrm{post}}a_{\mathrm{e}}(1 - e^2)}. \tag{1.22}$$

We can then solve and simplify Equations 1.21 and 1.22 for $a_{\mathrm{e}}$ and $e$, respectively:

$$a_{\mathrm{e}} = \left[2 - \frac{M_{\mathrm{pre}}}{M_{\mathrm{post}}}\left(\frac{\omega_{\mathrm{x}}^2 + (v_{\mathrm{pre}} + \omega_{\mathrm{y}})^2 + \omega_{\mathrm{z}}^2}{v_{\mathrm{pre}}^2}\right)\right]^{-1} a, \tag{1.23}$$

and

$$1 - e^2 = \frac{M_{\text{pre}}}{M_{\text{post}}} \frac{a}{a_{\text{e}}} \left[ \frac{\omega_{\text{z}} + (v_{\text{pre}} + \omega_y)^2}{v_{\text{pre}}^2} \right]. \tag{1.24}$$

We define $\theta$, the angle between the pre-SN and post-SN orbital planes, as

$$\cos \theta = \frac{\boldsymbol{J}_{\text{post}} \cdot \boldsymbol{J}_{\text{pre}}}{|\boldsymbol{J}_{\text{post}}||\boldsymbol{J}_{\text{pre}}|} = \frac{v_{\text{pre}} + \omega_y}{\sqrt{\omega_z^2 + (v_{\text{pre}} + \omega_y)^2}}. \tag{1.25}$$

**Gravitational-wave emission**

The emission of gravitational waves removes orbital energy and orbital angular momentum from the binary. Peters and Mathews [221] and Peters [220] derive the gravitational-wave evolution of a two-point mass binary. The loss of orbital energy and orbital angular momentum leads to circularisation and inspiral of the binary. Peters [220] provides an analytical solution to the average inspiral and circularisation timescales

$$\left\langle \frac{da}{dt} \right\rangle = -\frac{64}{5} \frac{G^3 m_1 m_2 M}{c^5 a^3 (1 - e^2)^{7/2}} \left( 1 + \frac{73}{24} e^2 + \frac{37}{96} e^4 \right), \tag{1.26}$$

and

$$\left\langle \frac{de}{dt} \right\rangle = -\frac{304}{15} e \frac{G^3 m_1 m_2 M}{c^5 a^4 (1-e^2)^{5/2}} \left( 1 + \frac{121}{304} e^2 \right),$$

(1.27)

respectively. Given a binary with an initial separation ($a_0$) and eccentricity ($e_0$), we can use equations 1.26 and 1.27 to solve for the decay time ($T$) of the orbit

$$T(a_0, e_0) = \frac{15}{304} \frac{c^5}{G^3 m_1 m_2 M} \left[ \frac{a_0(1-e_0^2)}{e_0^{12/19}} \left( 1 + \frac{121}{304} e_0^2 \right)^{-870/2299} \right]^4$$
$$\times \int_0^{e_0} \frac{e^{29/19}[1 + (121/304)e^2]^{1181/2299}}{(1-e^2)^{3/2}} de.$$

(1.28)

## 1.4   Overview of the Thesis

The aim of this thesis is to study some plausible outcomes the classic isolated binary evolution channel and make predictions about the fate of the binaries at the end of their stellar lifetimes. We present results of population studies and detailed stellar evolution calculations.

The structure is the following. In chapter 2 we present a population synthesis study of Galactic-like DNSs, which we compare to the observed population. In chapter 3 we present a catalogue of binary properties at the onset of a CEE for a population of binaries which eventually form DNSs. In chapter 4 we study the role that stellar mergers play as PISN progenitors, and propose that they are plausible progenitors of hydrogen-rich pulsational PISNe. Finally, in chapter 5 we present the

conclusions.                                    35

# Chapter 2

# On the formation history of Galactic double neutron stars

Alejandro Vigna-Gómez[1,2], Coenraad J. Neijssel[1], Simon Stevenson[1,3], Jim W. Barrett[1], Krzysztof Belczynski[4], Stephen Justham[5,6,2], Selma E. de Mink[7], Bernhard Müller[8], Philipp Podsiadlowski[9,2], Mathieu Renzo[7], Dorottya Szécsi[1], Ilya Mandel[1,8,2]

[1] Birmingham Institute for Gravitational Wave Astronomy and School of Physics and Astronomy, University of Birmingham, Birmingham, B15 2TT, United Kingdom

[2] DARK, Niels Bohr Institute, University of Copenhagen, Blegdamsvej 17, 2100, Copenhagen, Denmark

[3] OzGrav, Swinburne University of Technology, Hawthorn VIC 3122, Australia

[4] Nicolaus Copernicus Astronomical Center, Polish Academy of Sciences, ul. Bartycka 18, 00-716 Warsaw, Poland

[5] School of Astronomy & Space Science, University of the Chinese Academy of Sciences, Beijing 100012, China

[6] National Astronomical Observatories, Chinese Academy of Sciences, Beijing 100012, China

[7] Anton Pannekoek Institute for Astronomy, University of Amsterdam, 1090 GE Amsterdam, The Netherlands

[8] Monash Centre for Astrophysics, School of Physics and Astronomy, Monash University, Clayton, Victoria 3800, Australia

[9] Department of Astronomy, Oxford University, Oxford OX1 3RH, UK

This chapter is a reformatted copy of Vigna-Gómez et al. [299], published in MNRAS and with arXiv number 1805.07974. My contribution to this work was to (i) write the code to simulate mass transfer and CEEs, (ii) generate all the simulated populations, (iii) do the population analysis (except the model comparison, Section 2.3.3, done by Simon Stevenson), (iv) interpret the results, (v) make all the Figures (except Figure 2.9, made by Coenraad J. Neijssel), and (vi) write and edit the text.

## 2.1    Abstract

Double neutron stars (DNS) have been observed as Galactic radio pulsars, and the recent discovery of gravitational waves from the DNS merger GW170817 adds to the known DNS population. We perform rapid population synthesis of massive binary stars and discuss model predictions, including formation rates, mass distributions, and delay time distributions. We vary assumptions and parameters of physical processes such as mass transfer stability criteria, supernova kick distributions, remnant mass distributions and common–envelope energetics. We compute the likelihood of observing the orbital period–eccentricity distribution of the Galactic DNS population under each of our population synthesis models, allowing us to quantitatively compare the models. We find that mass transfer from a stripped post-helium-burning sec-

ondary (case BB) onto a neutron star is most likely dynamically stable. We also find that a natal kick distribution composed of both low (Maxwellian $\sigma = 30$ km s$^{-1}$) and high ($\sigma = 265$ km s$^{-1}$) components is preferred over a high-kick component alone. We find that the observed DNS mass distribution can place strong constraints on model assumptions.

## 2.2   Introduction

Since the first detection of a Galactic DNS [120], the growing observed population continues to provide constraints on the orbital parameters of DNSs. Precise measurements of Keplerian and post-Keplerian parameters [150] contain valuable information about the progenitors and formation history of NSs and DNSs. Additionally, GW170817 [8] became the first gravitational wave signal detected from a binary neutron star merger. These precise measurements allow us to test our understanding on the massive binary progenitor populations and their formation history [e.g., 33].

Tutukov and Yungel'son [290] carried out an early rapid population synthesis study of Galactic NSs. The formation and fate of DNSs has been studied with a similar approach by Portegies Zwart and Yungelson [238], who made an analysis of the observed systems and predictions of the merger rates of gamma ray bursts, and Belczyński and Bulik [22], who emphasised gravitational–wave merger rates. Voss and Tauris [302] studied both gamma ray–bursts and gravitational–wave merger rates for Galactic DNSs (and binary black holes). O'Shaughnessy et al. [205] used six DNSs observed in the Galactic disk to constrain population synthesis models. Several binary population synthesis studies have focussed on kick distributions [e.g., 41, 229, 42], short gamma ray bursts locations [e.g., 59], evolutionary channels [e.g.,

15] and merger rates [e.g., 58]. More recently, Kruckow et al. [155] used their population synthesis model, calibrated to match the observed Galactic DNS population, to predict merger rates in the local Universe.

Using the rapid population synthesis element of the COMPAS suite [270], we use the Galactic DNS population as an observational constraint on massive binary evolution, from two ZAMS stars to a pair of neutron stars. COMPAS binary evolution simulates isolated binaries; the majority of the confirmed Galactic DNSs (14 confirmed systems, for details, see Table 2.1, Tauris et al. [282] and references therein) come from isolated binaries which lie in the Galactic disk. We do not address the two Galactic globular cluster binaries in this work, $B2127+11C$ [14] and $J1807-2500B$ [169, not a confirmed DNS], since dynamical interactions likely played a key role in their formation [225].

Our paper explores the role of model comparison of multiple observable variables, i.e. orbital parameters of Galactic DNSs and inferred mass distributions of gravitational wave events, as a way of quantifying how relevant physical interactions and parameterisations of binary evolution may be. For each model, we provide predicted DNS formation rates and orbital parameters as observed in the present time. We compare the DNS masses $(m_1, m_2)$ and orbital parameters (period P, eccentricity e) to those of the observed Galactic DNSs to differentiate between our models. We find that the natal kicks received by neutron stars during formation in a supernova and mass transfer stability criteria play a fundamental role in recreating the Galactic DNS population.

The paper is structured as follows. Section 2.3 describes population synthesis and presents our `Fiducial` model. Changes made to binary evolution in COMPAS since Stevenson et al. [270] are specified. Section 2.4 presents the results of the `Fiducial` population, with particular emphasis on the formation history of Galactic DNSs.

Table 2.1: Measured parameters of the Galactic DNSs used as a diagnosis in this study. Notes: [†]Systems which will merge via gravitational-wave emission in less than 3000 Myrs. [‡]Double pulsar. [⋆]Measurements used only for diagnosis in the $P - e$ space. The masses of the DNSs are presented as $M_{\mathrm{plsr}}$ and $M_{\mathrm{cmpn}}$, the mass of the pulsar and the companion respectively. References: [a]Martinez et al. [182]. [b]Kramer et al. [150]. [c]Fonseca et al. [100]. [d][98]. [e]Hulse and Taylor [120]. [f]Lazarus et al. [160]. [g] Cameron et al. [46]. [h]Janssen et al. [133]. [i]Corongiu et al. [63]. [j]Champion et al. [49]. [k]Swiggum et al. [275]. [l]Keith et al. [140]. [m]Martinez et al. [183]. [n]Stovall et al. [271].

| Pulsar | $P$ [days] | $e$ | $M_{\mathrm{plsr}}$ [M$_\odot$] | $M_{\mathrm{cmpn}}$ [M$_\odot$] | Ref |
|---|---|---|---|---|---|
| J0453 + 1559 | 4.072 | 0.113 | 1.559 | 1.174 | a |
| J0737 − 3039[†,‡] | 0.102 | 0.088 | 1.338 | 1.249 | b |
| B1534 + 12[†] | 0.421 | 0.274 | 1.333 | 1.346 | c |
| J1756 − 2251[†] | 0.320 | 0.181 | 1.341 | 1.230 | d |
| B1913 + 16[†] | 0.323 | 0.617 | 1.440 | 1.389 | e |
| J1913 + 1102[†] | 0.206 | 0.090 | 1.580 | 1.300 | f |
| J1757 − 1854[†] | 0.184 | 0.606 | 1.338 | 1.395 | g |
| J1518 + 4904[⋆] | 8.634 | 0.249 | - | - | h |
| J1811 − 1736[⋆] | 18.779 | 0.828 | - | - | i |
| J1829 + 2456[⋆] | 1.176 | 0.139 | - | - | j |
| J1930 − 1852[⋆] | 45.060 | 0.399 | - | - | k |
| J1753 − 2240[⋆] | 13.638 | 0.304 | - | - | l |
| J1411 + 2551[⋆] | 2.616 | 0.169 | - | - | m |
| J1946 + 2052[⋆] | 0.078 | 0.064 | - | - | n |

The effect of variations, such as mass transfer during the post-helium-burning phase and the comparison between different kick distributions is mentioned. We conclude with a summary and discussion in section 2.5.

## 2.3   Methods

### 2.3.1   Population Synthesis

The COMPAS suite includes a rapid population synthesis code designed to simulate isolated binary evolution. Rapid population synthesis aims to simulate a binary in

sub-second computing time; this makes it possible to simulate millions of binaries in a few days using a single processor. In order to generate a population, initial distributions of masses, separation and eccentricity are sampled using Monte Carlo methods. Given a mass and metallicity at ZAMS, we define the initial conditions and evolution of a star following the fitting formulae of single-star evolution (SSE) as given in Hurley et al. [121] to the detailed models calculated in Pols et al. [234]. We use the same nomenclature as Hurley et al. [121] to define stellar phases. For every binary we follow the centre of mass evolution of the system, computing the masses, separation and eccentricity at every time step. We use parameterisations to quantify the effect on the orbit of the physics involving mass loss through stellar winds, mass transfer, supernovae and common envelope events. For supernovae, we also use remnant mass distributions which will determine the ultimate fate of our stars. Each binary is evolved until the system either merges, becomes unbound, or forms a double compact object (DCO). The population generates a set of DCOs, where DNS are sub-selected into our final distribution of interest. COMPAS population synthesis is similar to the general approach of SeBa [237, 238, 289], BSE [122], `StarTrack` [23, 24] and binary_c [129, 130, 131], all of which use the SSE fits from Hurley et al. [121].

Our current approach to the study of populations by proposing an initial model and studying the variations is similar to the one described in Dominik et al. [81]. That study used `StarTrack` to simulate populations from ZAMS to DCO formation and predict merger rates for all compact objects. Their "Standard" model overlaps with some of our `Fiducial` model assumptions.

## 2.3.2 Fiducial model

**Changes since Stevenson et al. [270]**

The main changes to binary evolution modelling in COMPAS relative to the default assumptions in Stevenson et al. [270], hereafter referred to as COMPAS_$\alpha$, are:

(i) incorporation of the fitting formulae of the binding energy parameter $\lambda_{\mathrm{Nanjing}}$ instead of a fixed $\lambda = 0.1$, as described in section 2.3.2.

(ii) a bimodal kick distribution, where CCSN contribute to the high mode ($\sigma_{\mathrm{high}}$ = 265 km s$^{-1}$) while USSN and ECSN constitute the low mode ($\sigma_{\mathrm{low}} = 30$ km s$^{-1}$), as described in section 2.3.2.

(iii) mass transfer stability criteria, allowing for always stable case BB mass transfer, as described in section 2.3.2.

(iv) the "optimistic" common envelope (CE) assumption, which allows donors classified as Hertzsprung Gap (HG) stars in the SSE models [121] to engage and survive a CE phase, as described in section 2.3.2.

**Initial distributions**

To initialise a binary, our initial distributions sample mass, separation and eccentricity of the binary at ZAMS. For the mass distribution, we draw the primary mass $5 \leq m_1/\mathrm{M}_\odot \leq 100$ from the Kroupa initial mass function [153] in the form $dN/dm_1 \propto m_1^{-2.3}$. The secondary is drawn from a flat distribution in mass ratio $0.1 < q_{\mathrm{ZAMS}} \equiv m_2/m_1 \leq 1$ [251]. The initial separation follows the flat-in-the-log distribution in the range $0.1 < a_{\mathrm{ZAMS}}/\mathrm{AU} < 1000.0$ [202, 251]. We assume that all of our binaries are circular at ZAMS, with $e_{\mathrm{ZAMS}} = 0$.

**Supernovae**

We differentiate between three supernova scenarios: Core-collapse Supernovae (CCSN), Ultra-stripped Supernova (USSN) and Electron-capture Supernova (ECSN).

For the CCSN treatment, we use the "rapid" explosion scenario, as presented in Fryer et al. [104], to determine the compact object remnant mass according to the total and O/C core mass of the progenitor, with a maximum allowed NS mass of $m_{\mathrm{NS,max}} = 2.0$ M$_\odot$. In this scenario, the collapse does not allow for accretion onto the proto-NS, and is able to reproduce the proposed mass gap between neutron stars and black holes [209, 97]. There is no consensus yet whether the mass gap is due to observational selection effects or if it is intrinsic to the explosion mechanism [152, 311].

Another explosion scenario comes from USSN [280, 281]. A star becomes stripped when it loses its hydrogen envelope during its evolution; if, during later stages, it manages to lose its helium envelope, it becomes ultra-stripped. In COMPAS, any star which engages in a stable case BB mass transfer episode with a NS as an accretor is considered to be ultra-stripped. We define case BB as a mass transfer episode which involves a Helium donor star which has stopped burning helium in the core (naked helium star Hertzprung Gap, HeHG). Ultra-stripped stars are left with an ONeMg core with a thin carbon and helium layer [280]. The compact object remnant mass of an USSN is determined in the same way as for CCSN.

A single star with $8 \lesssim m_{\mathrm{ZAMS}}/\mathrm{M}_\odot \lesssim 10$ (binary stars spread the initial mass range) may collapse in an ECSN [195]. We assume the baryonic mass of the degenerate ONeMg core leading to an ECSN is 1.38 M$_\odot$ [196]. We approximate the ECSN remnant mass as $m_{\mathrm{ECSN}} = 1.26$ M$_\odot$ using the quadratic approximation $m_{\mathrm{bar}} - m_{\mathrm{grav}} = 0.075 m_{\mathrm{grav}}^2$ [287].

For the natal kicks of the supernovae, we assume a bimodal distribution [e.g., 139, 256, 31, 295]. For CCSN, we draw kick magnitudes from a Maxwellian velocity distribution with a one-dimensional standard deviation of $\sigma_{\mathrm{high}} = 265$ km s$^{-1}$ following the isolated pulsar distribution from Hobbs et al. [119]. USSN and ECSN kick magnitudes are drawn from a Maxwellian velocity distribution with a one-dimensional standard deviation of $\sigma_{\mathrm{low}} = 30$ km s$^{-1}$, following Pfahl et al. [222] and Podsiadlowski et al. [229]. All natal kicks from supernovae are assumed to be isotropic in the frame of reference of the exploding star, i.e. the direction is defined by randomly drawing the angles $\theta$ and $\phi$ from a spherical coordinate system.

**Mass transfer**

A crucial part of binary evolution is mass transfer, which begins when one or both stars fill their Roche lobe [90]. In our population synthesis approach, mass transfer is treated by determining stability, timescales and conservativeness. Rapid population synthesis oversimplifies the complex hydrodynamics involved in a mass transfer episode. There have been some efforts to provide generalised models [e.g., 71, 60, 281]. In particular, determining whether mass transfer is dynamically stable is challenging [e.g., 215].

To determine dynamical stability during mass transfer episodes, we compare the response of the donor star's radius to adiabatic mass loss $\zeta_{\mathrm{ad}} = (d\mathrm{log}\mathrm{R}/d\mathrm{log}\mathrm{M})_{\mathrm{ad}}$, to the response of the Roche lobe radius of the donor $\zeta_{\mathrm{RL}}$, under the same mass exchange conditions. Mass transfer is defined as dynamically stable if $\zeta_{\mathrm{ad}} \geq \zeta_{\mathrm{RL}}$. We use fixed values of $\zeta_{\mathrm{ad,MS}} = 2.0$ for hydrogen (MS) and $\zeta_{\mathrm{ad,HG}} = 6.5$ for hydrogen shell burning (HG) stars which are typical for these phases, following models by Ge et al. [106]. For later phases which still possess hydrogen envelopes we use a fit to $\zeta_{\mathrm{ad}} = \zeta_{\mathrm{SPH}}$ for condensed polytrope models of a red giant as provided in Soberman

et al. [265]. Case BB mass transfer is always stable in the `Fiducial` model, broadly in agreement with Tauris et al. [281].

The timescale of a mass transfer episode from a main-sequence donor is estimated as follows [144, 233]. The analytic formulae we use to describe stellar evolution are unable to accurately represent the donor stars during thermal-timescale mass transfer. We take advantage of the equilibrium mass-radius relations provided by these analytic formulae to determine when stable mass transfer is driven by thermal readjustment. If the calculated donor-star radius cannot stay within its Roche lobe during thermally stable mass transfer then we remove the mass on a thermal timescale. Once the donor's calculated equilibrium radius can again fit within its Roche lobe, we assume that the mass transfer occurs on a nuclear timescale [60].

Dynamically stable mass transfer from evolved stars is assumed to always proceed on the thermal timescale until the entire envelope is removed (but see, e.g. [110]). We approximate the thermal timescale as the Kelvin-Helmholtz timescale of the donor's envelope $\tau_{\mathrm{KH}} = GMM_{\mathrm{env}}/RL$, where $G$ is the gravitational constant, $M$ is the total mass, $M_{\mathrm{env}}$ is the mass of the envelope, $R$ is the radius and $L$ is the luminosity of the star.

Conservativeness is defined as the fraction of transferred mass from the donor that the accretor will accept and retain. When mass is lost from the system during non-conservative mass transfer, the fraction of mass lost and the specific angular momentum it carries away determine the orbital parameters and subsequent evolution of the system. In the `Fiducial` model, if mass transfer is non-conservative, the non-accreted mass is lost from the vicinity of the accreting star via isotropic re-emission, carrying away the specific orbital angular momentum of the accretor. The conservativeness of our mass transfer episode is limited by the accretor. For non-degenerate accretors we assume a star can accrete at a maximum rate $\dot{M}_{\mathrm{acc}} = CM_{\mathrm{acc}}/\tau_{\mathrm{KH}}$ [122].

We use $C = 10$ following Hurley et al. [122]. For degenerate accretors, we assume the compact object accretion is limited by the Eddington accretion limit.

**Common Envelope**

If one or both stars begin dynamically unstable mass transfer, the binary may become engulfed in a common envelope (CE) phase. The loss of corotation between the binary system and the envelope generates drag forces, which allow the binary to inspiral. The gravitational energy lost from the orbit can be deposited in the envelope and may be enough to eject it from the binary. The whole process allows the system to decrease its separation by several orders of magnitude.

The classical isolated binary evolutionary scenario for the formation of DCOs often involves a CE phase [211, 128, 27]. We use the $\alpha\lambda$-formalism, as proposed by Webbink [305] and de Kool [68], to estimate the effect of the CE phase on the orbit of the binary.

The value of $\lambda$, which parametrises the envelope's binding energy, is calculated from detailed models of the stellar structure. For our `Fiducial` model, we adopt $\lambda_{\mathrm{Nanjing}}$ (originally referred to as $\lambda_{\mathrm{b}}$, which includes internal energy) as calculated by Xu and Li [312] and implemented in `StarTrack` [81].

The value of $\alpha$, which parametrises the efficiency of converting orbital energy into unbinding the envelope, depends on the orbital parameters, energy sources and energy exchange during the CE phase, and is difficult to constrain even with detailed hydrodynamical models [128]. We use $\alpha = 1$. We assume that the orbit is always circularised during a CE phase. We allow donor stars which engage into a CE phase during hydrogen shell burning (HG) to survive the event and expel the common

envelope if allowed by the energy condition. This assumption is labeled "optimistic" CE in the literature [81], while the alternative, "pessimistic" CE, always leads to a merger for HG donors.

### 2.3.3  Model comparison

In order to quantify how well our models match the observed Galactic DNS period–eccentricity distribution, we calculate the likelihood $\mathcal{L}_i$ that observations could have come from the synthesised DNS population for each model $i$. We use the period–eccentricity distribution because of the 14 observed Galactic DNSs used in this study, all have precise measurements of the period and the eccentricity, but only half of them have precise measurements of their individual masses (see table 2.1). We do not use any of the mass measurements in the likelihood calculation. We also do not attempt to account for selection biases in the observed period–eccentricity distribution.

The details of how the likelihoods $\mathcal{L}_i$ are computed are given in Appendix A.1. We quote our results as the ratio of the likelihood for a given model to the likelihood of the `Fiducial` model $i$, i.e., the Bayes factor:

$$\log \mathcal{K}_i = \log \mathcal{L}_i - \log \mathcal{L}_{01} \,, \tag{2.1}$$

where $\mathcal{L}_{01}$ is the likelihood of the `Fiducial` model. All logarithms in this study are base $e$ unless stated otherwise. A positive log Bayes factor $\log \mathcal{K} > 0$ means that the given model is preferred over the `Fiducial` model. On the other hand, a negative log Bayes factor means that the `Fiducial` model is preferred over the given model. If all models have equal a priori probability, the odds ratio is equal to the Bayes factor. The odds ratio determines how significantly favoured or unfavored the

Table 2.2: We list all simulations computed for this study; for simulations 02 through 19, we state the physical interaction or assumption varied relative to the `Fidicual` model and the actual parameter varied. For each simulation, we give the formation rate $\mathcal{R}$ of DNS which will merge in a Hubble time in the Galaxy and its log Bayes factor relative to the `Fidicual` model model (see Appendix A.1) given the observed Galactic DNS period-eccentricity distribution. See figure A.1 for the predicted period–eccentricity distributions for all models.

| Number | Physics | Variation | $\mathcal{R}$ [Myr$^{-1}$] | $\log(\mathcal{K})$ |
|---|---|---|---|---|
| 00 | COMPAS_$\alpha$ | | 16.35 | -16.78 |
| 01 | COMPAS `Fiducial` | | 34.64 | 0 |
| 02 | Stability | Case BB: unstable | 35.37 | -3.12 |
| 03 | SNe | Fryer Delayed | 40.43 | 3.03 |
| 04 | SNe | Müller | 44.61 | -2.50 |
| 05 | SNe | Single Mode | 13.20 | -3.08 |
| 06 | SNe | $\sigma_{\mathrm{ECSN}} = \sigma_{\mathrm{high}}$ | 21.77 | -1.05 |
| 07 | SNe | $\sigma_{\mathrm{USSN}} = \sigma_{\mathrm{high}}$ | 19.50 | -3.19 |
| 08 | CE | $\lambda = 0.1$ | 23.49 | -0.07 |
| 09 | CE | $\lambda_{\mathrm{Kruckow}} \propto R^{-5/6}$ | 13.09 | 0.02 |
| 10 | CE | $\alpha = 0.1$ | 7.59 | 1.76 |
| 11 | CE | $\alpha = 10.0$ | 13.74 | -1.97 |
| 12 | Circularisation | $a_{\mathrm{p}} = a(1-e)$ | 20.38 | 2.54 |
| 13 | Circularisation | $a_{\mathrm{SR}} = a(1-e^2)$ | 22.06 | 0.27 |
| 14 | Mass Loss Mode | Jeans | 9.64 | -3.34 |
| 15 | Mass Loss Mode | Circumbinary | 40.43 | -2.67 |
| 16 | Distribution | $f_e(e) =$ Thermal | 14.73 | -0.07 |
| 17 | Metallicity | Z=0.002 | 28.96 | -3.23 |
| 18 | Metallicity | Z=0.001 | 34.67 | -2.22 |
| 19 | CE | Pessimistic | 20.60 | -0.16 |

model is with respect to the `Fiducial` model. For readers unfamiliar with Bayes factors, we indicate when odds ratios for these model comparisons exceed $20:1$ (or $1:20$ for disfavoured models), corresponding to the common significance threshold with a p–value of $p < 0.05$. Limited sampling of the synthetic distributions leads to uncertainties of order unity on $\log \mathcal{K}_i$, corresponding to a factor of 2–3 uncertainty in the Bayes factor; this statistical uncertainty can be improved with more simulations. The calculated Bayes factors are plotted in figure 2.1 and presented in table 2.2.
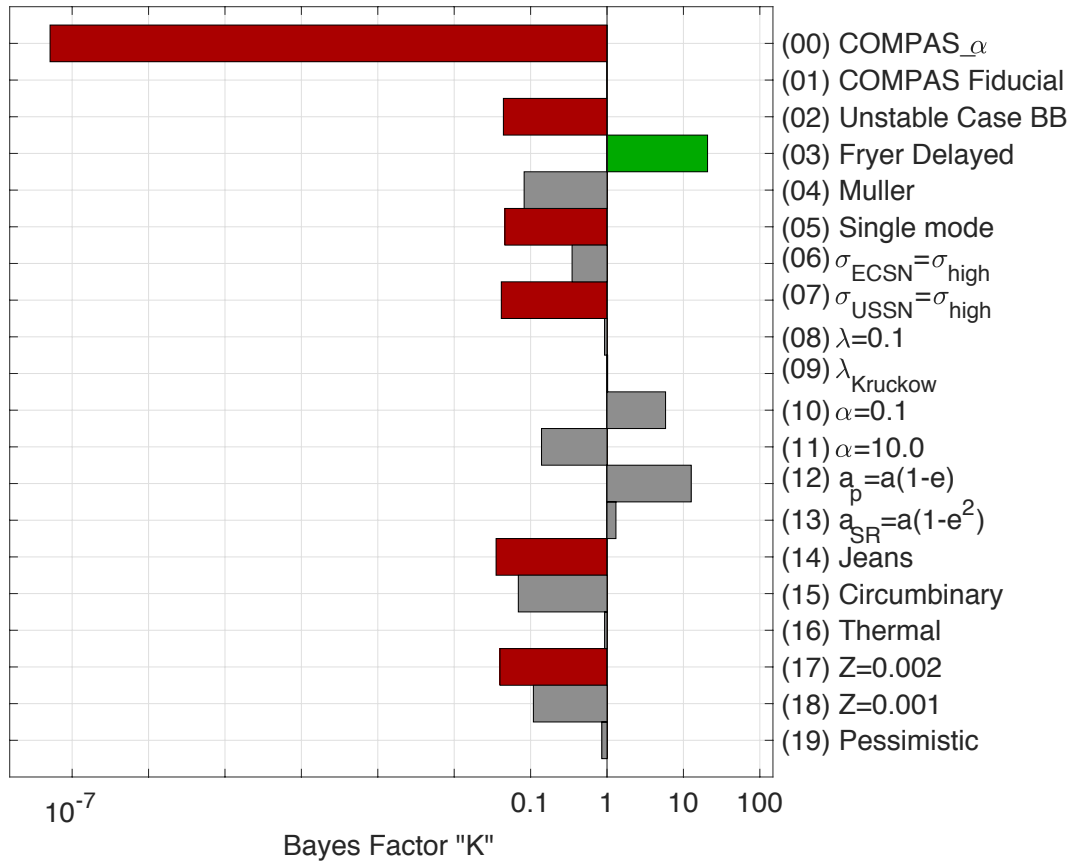
Figure 2.1: The ratio of the likelihood of each model to the likelihood of the `Fiducial` model (01). Green (red) bars denote models significantly favoured (disfavoured) by an odds ratio of greater than $20 : 1$ relative to the `Fiducial` model.

## 2.4  Results

We evolve $1,000,000$ binaries with a total evolved mass of 20,250,000 $M_\odot$ for each simulation; this represents 54,568,000 $M_\odot$ of total star forming mass under the assumed initial mass distribution. All binaries have an initial metallicity $Z_\odot = 0.0142$ [18] as a proxy for Galactic metallicity.

We present the detailed results of our `Fiducial` model $(01)^1$ and some variations to it, all with identical initial parameters (unless stated otherwise). The diagnostic tools we use to analyse all of our variations are the period and eccentricity $(P - e)$ distribution (see figure 2.2, section 2.3.3 and Appendix A.1 for details), remnant NS mass distribution (see figure 2.7) and formation rate estimates (see Table 2.2). We report the number of significant figures based on statistical simulation uncertainty, i.e., the Monte Carlo uncertainty.

We illustrate the plausible distribution of simulated Galactic DNS (see figure 2.2 for `Fiducial` model and figure A.1 for all models), which shows, in $P - e$ space, how systems may evolve from DNS formation to a typical observable distribution. To illustrate this, we assign each binary a random probability of being born at any given point in the last 10 Gyr (a proxy for the age of the Galactic thin disk, see [74]), and then follow their gravitational-wave driven orbital evolution until present time.

Our models predict the mass ratio (see figure 2.5) and time distributions (see figure 2.6). The mass ratio distribution depends on the explosion mechanism of the supernovae. The time distributions we provide are the formation time ($t_{\mathrm{form}}$), coalescence time ($t_{\mathrm{c}}$) and time delay ($t_{\mathrm{delay}}$). The formation time is the time it takes a

---

[1]We will label the variations by their number (see Table 2.2) in parentheses; e.g.: `Fiducial` model (01) or `COMPAS`$_\alpha$ (00). The simulations used in this chapter can be found in `http://doi.org/10.5281/zenodo.3358304` [297]

binary to evolve from ZAMS to DCO formation. The coalescence time is the time it takes the DCO to inspiral until coalescence due to gravitational radiation, following the post-Newtonian approximation as given by Peters [220]. The time delay is the sum of the formation time and the coalescence time.

Given the orbital properties of the population and the estimated time distributions we are able to predict the formation rate $\mathcal{R}$ of DNS which will merge in a Hubble time (assuming $H_0^{-1} = 14.03$ Gyr flat $\Lambda$CDM cosmology [226]). If a system has a time delay of less than a Hubble time we include it in the formation rate $\mathcal{R}$.

Formation rates are calculated for a galaxy with a continuous star formation rate of $f_{\mathrm{SFR}} = 2.0$ M$_\odot$/yr [57], with all systems in our simulated universe born in binaries. The star formation rate is chosen to mimic the Milky Way value of $f_{\mathrm{SFR}} = 1.9 \pm 0.4$ M$_\odot$/yr [57]; any shifts in the chosen value would proportionately shift the quoted DNS formation rate.

A summary of all the formation rates and Bayes factors for the different variations is given in table 2.2.

### 2.4.1 On the `Fiducial` model

**Formation Channels**

There are two dominant formation channels in our `Fiducial` model. Below we will explain some of the crucial steps in the formation channels and the fraction $f$ of systems that went through different stages of binary evolution. The dominant *Channel I*, illustrated in figure 2.3, is responsible for the formation of roughly 70% of all DNSs. This formation channel is consistent with the canonical channel described
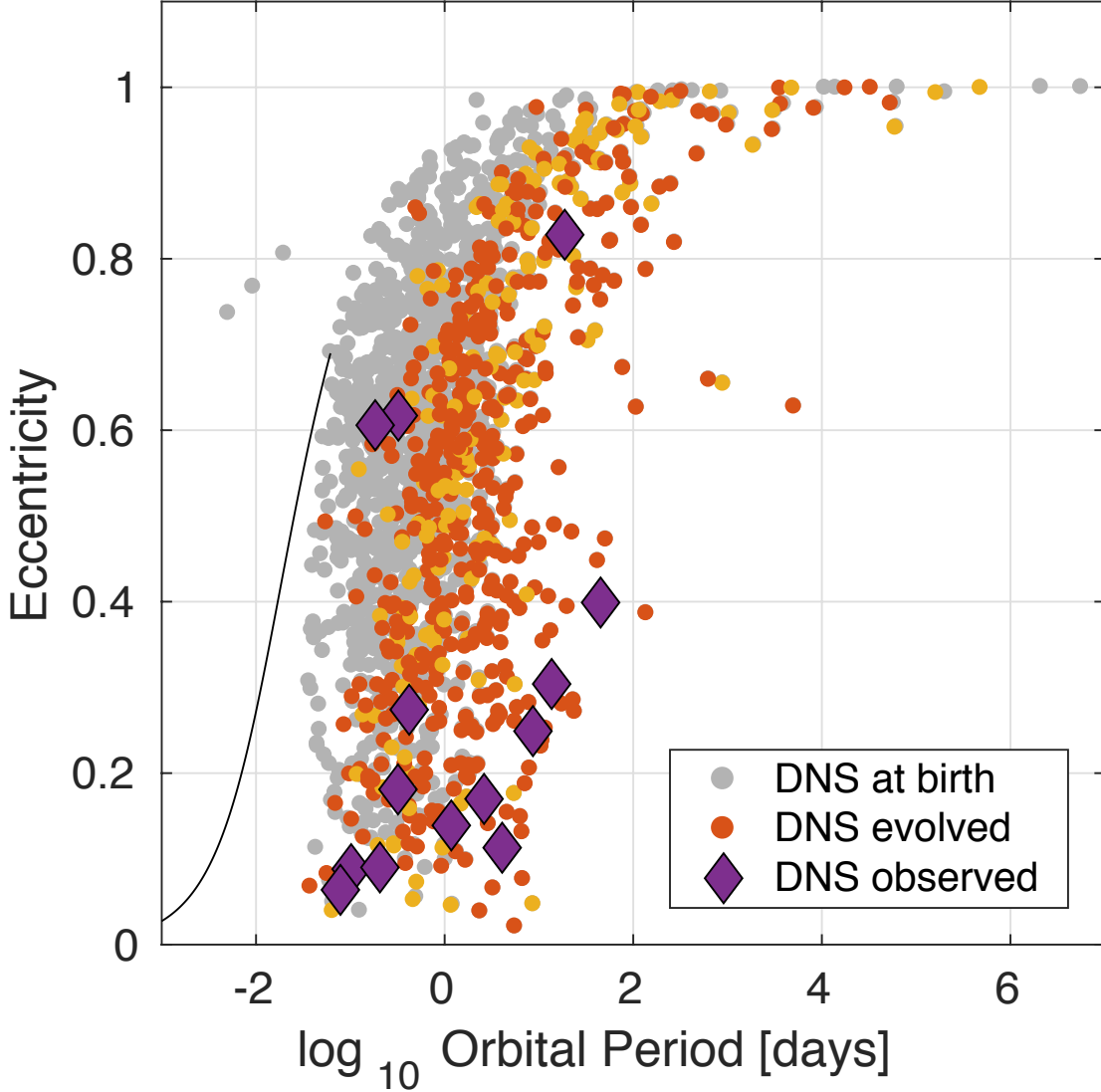
Figure 2.2: Predicted period-eccentricity distribution of Galactic DNSs under the `Fiducial` model. Gray dots in the back are all DNSs at DCO formation. DCO period and eccentricity are evolved forward from birth until present age given gravitational-wave radiation emission, removing a fraction of the short-lived short-period binaries from the observable population. Coloured dots represent the DNS distribution at present age. Colour denotes the type of common envelope phase: red for a single-core and yellow for a double-core common envelope phase. The single-core and double-core can be, in most cases, associated with *Channel I* and *Channel II* respectively (see Section 2.4.1). Purple diamonds represent the observed Galactic DNS; all observed systems have precise period–eccentricity measurements with error bars within the thickness of the symbol. The black curve illustrates a gravitational-wave driven period–eccentricity evolution from DCO formation to merger; this system, with initial $P = 1.5$ hours, $e = 0.69$ and characteristic NS masses $m_1 = m_2 = 1.2$ M$_\odot$, would merge in $\approx 3$ Myr through gravitational-wave emission.

by, e.g., Bhattacharya and van den Heuvel [33] and Tauris and van den Heuvel [279]. *Channel I* involves a single-core CE phase in which the primary has already collapsed into a NS. A single-core CE phase occurs when only one of the stars has a clear core–envelope separation; all compact objects are assumed not to have a clear core–envelope separation, as well as main sequence (MS) stars and stripped helium stars (HeMS). This channel proceeds as follows:

*Channel I*:

(i) The stars in the binary begin their evolution with the more massive primary evolving faster than its companion.

(ii) *≈22% of the all the initial systems experience stable mass transfer from the primary during the hydrogen shell burning phase onto a main sequence secondary.* This is because 52 per cent of the primaries never expand enough to start the mass transfer, and of the ones that do 47 per cent of them are stable during this phase.

(iii) *≈4% of those ≈22% systems are able to have a primary go supernova producing a NS and remaining in a bound orbit.* In the previous mass transfer episode the primary becomes a stripped helium main sequence (HeMS) star. The majority of the HeMS stars are either too light to become NSs or heavy enough to become BHs. Only 30% of them have the mass of a NS progenitor. In this first supernova, there are ten times more CCSN than there are ECSN but, given the higher kick magnitude, their survival rate is only 9% compared to 47% of the ECSN.

(iv) *≈25% of those ≈4% experience and survive a CE phase initiated by the post main sequence secondary (HG, CHeB, or EAGB in SSE notation).* Only 33% of the secondaries expand enough to engage in RLOF mass transfer. This mass transfer episode, with a primary NS accretor, is usually dynamically unstable and leads to a CE phase. 85% of these systems are able to successfully eject their envelope, hardening the binary by 2–3 orders of magnitude.

(v) *≈40% of those ≈25% begin mass transfer episode (case BB) of a helium shell*

*burning secondary onto a NS primary.* There the HeHG star recycles its NS companion while being (ultra-)stripped for a second time to a O/C core. Half of those cores are in the right mass range to become a NS (lighter cores may form a NS-WD binary while heavier cores yield a NS-BH binary).

(vi) *≈96% of those ≈40% systems will remain bound after the second supernova and form a DNS.* The tight post–CE orbit and the reduced kicks for USSN make it relatively easy for binaries to survive the kick and end up as a DNS system. The systems that are still disrupted either lost enough mass and/or had orbital velocities low enough that even the reduced USSN kick disrupted the system.

The secondary formation *Channel II*, illustrated in figure 2.4, is experienced by approximately 21% of the formed DNSs; it is prevalent for systems with initial mass ratio $q_{\text{ZAMS}} \approx 1$ and similar evolutionary timescales. This channel experiences a double-core CE phase [45, 80, 124], in which both of the stars have a clear core-envelope separation. *Channel II* proceeds as follows:

*Channel II*:

(i) *≈ 1% of the primaries start their first mass transfer episode as a Helium-burning star (CHeB or EAGB) with a slightly less evolved, but also post-main-sequence secondary (HG or CHeB).* Almost all of these systems (90%) initiate a double-core CE phase during this mass transfer episode.

(ii) *≈35% of those ≈ 1% binaries can eject their envelopes.* Only a tiny fraction (≈2%) lose enough mass to become white dwarfs whereas the majority become two naked helium stars (HeMS) evolving in a tighter orbit.

(iii) *≈87% of those ≈35% have primaries in binaries that can initiate a second mass transfer episode (case BB).* The primaries begin case BB donating their helium envelope to the secondary (HeMS). All these mass transfer episodes are dynamically stable.

(iv) *≈35% of those ≈87% systems are able to have a primary go supernova producing a NS and remaining in a bound orbit.* As in *Channel I*, the mass transfer episodes reduce the mass of the primary and only 63% will supernova. They are all CCSN and although the CE phase leaves them in a tight orbit the higher kick magnitude still disrupts 45% of the systems.

(v) *≈80% of those ≈35% begin a third mass transfer episode (case BB) from the secondary to a NS accretor.* This mass transfer episode onto the NS is defined to always be stable and the secondary now becomes an ultra-stripped O/C core.

(vi) *≈55% of those ≈80% have secondaries which experience and survive a supernova and become NSs.* 71% of the O/C cores are heavy enough to go SN, and given the previous episode of mass transfer they are all USSN. The lower kicks and tighter orbits helps to get a survival rate of 77%, resulting in a DNS system.

Most of the single-core systems come from *Channel I* and the double-core from *Channel II* (see $P - e$ distributions in figures 2.2, 2.8, and Appendix A.1). The rest of the DNSs, about 9% of the total, come from more exotic or fortuitous channels, including non–recycled DNSs ($\leq 1\%$ of all Galactic-like DNS). Non-recycled DNSs progenitors are systems which never had stable mass transfer onto a NS [29], which leads to spin up and recycling; they may have experienced common envelopes in our models, which we assume to be inefficient at spinning up the NS and suppressing its magnetic field [171].

We find that our `Fiducial` model has a formation rate of $\mathcal{R} = 34.64$ Myr$^{-1}$ per Galaxy. All of our DNSs experienced and survived at least one CE phase, 23% of them in a double-core scenario.
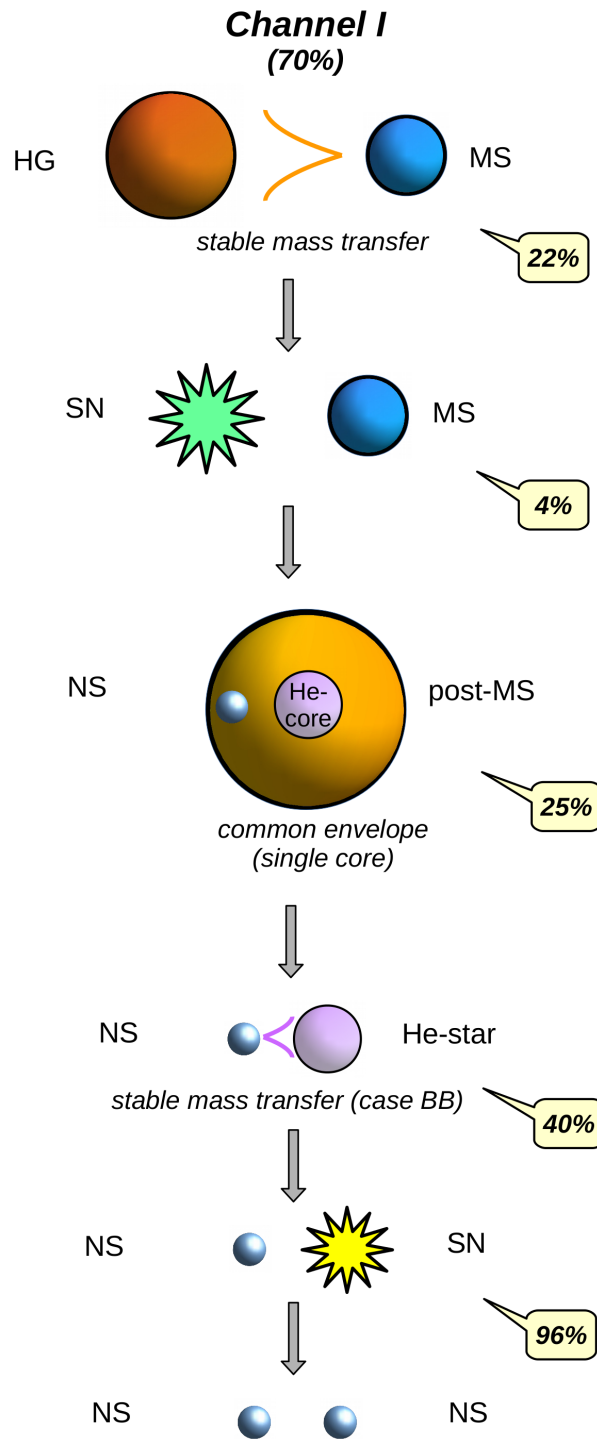
Figure 2.3: Evolutionary history of formation *Channel I* (top to bottom); 70% of all DNS in our `Fiducial` population were formed through this channel. The numbers in the callout symbols represent the percentage of simulated binaries that end up in that particular stage among those that follow the preceding evolutionary history. For example, 22% of all simulated binaries experience stable mass transfer from a hydrogen shell burning primary onto a main sequence secondary; among those 22%, 4% of systems will have a primary that undergoes a supernova producing a NS while remaining in a bound orbit; and so on.
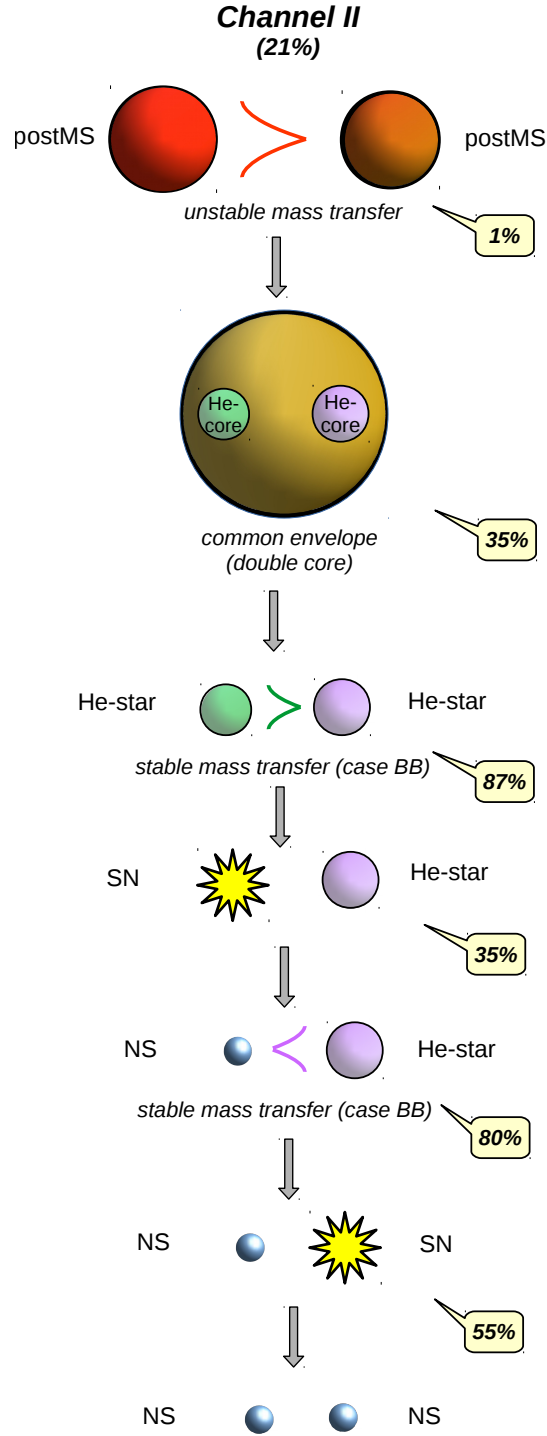
Figure 2.4: Evolutionary history of formation *Channel II* (top to bottom); 21% of all DNS in our `Fiducial` population were formed through this channel. The numbers in the callout symbols represent the percentage of simulated binaries that end up in that particular stage among those that follow the preceding evolutionary history. For example, 1% of all simulated binaries initiate mass transfer while both companions are post-MS stars; among those 1%, 35% enter and survive a double-core common envelope phase; and so on.

**Mass ratio distribution**

Figure 2.7 shows the mass distribution of all the Galactic DNSs at the moment of birth, while figure 2.5 shows the distribution of the predicted mass ratio $q_{\mathrm{DCO}}$ for the merging Galactic DNSs. We define $q_{\mathrm{DCO}} = m_{\mathrm{NS,lighter}}/m_{\mathrm{NS,heavier}}$; the heavier NS is not necessarily the more massive star at ZAMS. In the `Fiducial` model, the initially less massive star produces the more massive NS in 31% of the systems, due to the accretion of mass from the companion, and its core growth, during the early phases of evolution. The mass ratio lies between $0.58 \leq q_{\mathrm{DCO}} \leq 1$. Among the merging Galactic DNSs, 90% of the systems have $q_{\mathrm{DCO}} > 0.8$, 50% have $q_{\mathrm{DCO}} > 0.9$ and 30% have $q_{\mathrm{DCO}} > 0.95$. There are two significant peaks in this distribution: (i) $\approx 16\%$ of systems have $q_{\mathrm{DCO}} \approx 0.88$; most systems close to this mass ratio are formed through *Channel I*, with an ECSN forming the first NS (with gravitational mass of 1.26 $M_{\odot}$) and an USSN forming the second (with lower mass remnants of 1.1 $M_{\odot}$), and (ii) the second peak, with $\approx 14\%$ of the total DNSs, has a mass ratio $q_{\mathrm{DCO}} \approx 1$, from $q_{\mathrm{ZAMS}} \approx 1$ systems that evolved through the double-core CE, with a low mass CCSN and an USSN (*Channel II*). The mass range of neutron stars in our `Fiducial` population is $[m_{\mathrm{NS,min}}, m_{\mathrm{NS,max}}] = [1.1, 1.9]$ $M_{\odot}$.

**Time distributions**

Figure 2.6 shows the formation, coalescence and delay time distributions for our `Fiducial` model. Time distributions were made for DNSs which have a merger time of less than the Hubble time.

The simulated systems at the extreme ends of the time distributions are $8.5 \leq t_{\mathrm{form}}/\mathrm{Myr} \leq 41.6$ for the formation time (ZAMS to DNS formation), $900.0 \leq t_{\mathrm{c}}/\mathrm{yr}$ for the coalescence time (DNS formation to merger) and $12.6 \leq t_{\mathrm{delay}}/\mathrm{Myr}$ for the
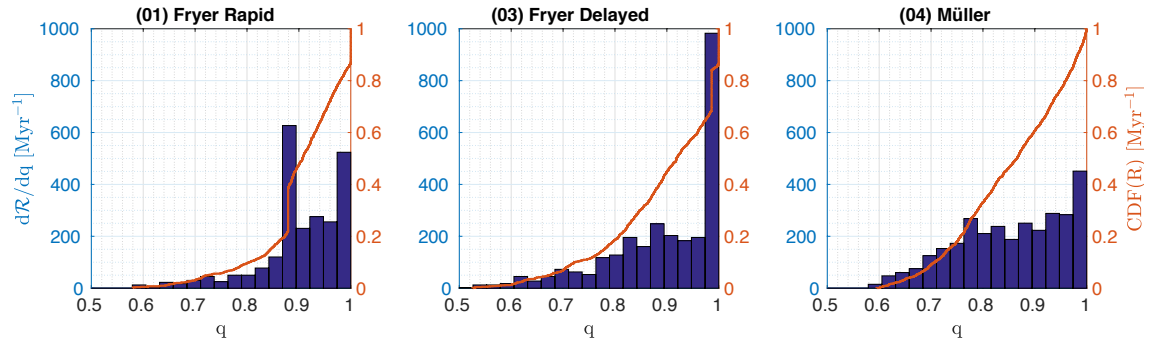
Figure 2.5: Mass ratio distribution of merging DNSs (blue histogram) and its cumulative distribution function (orange curve) for three supernova fallback and kick models: (01) Fryer Rapid [left], (03) Fryer Delayed [middle], (04) Müller [right]. See sections 2.4.1 and 2.4.3 for a discussion of the evolutionary channels leading to sharp features in the histograms.

total time delay.

Fewer than 0.5% of merging DNSs have very short coalescence times of less than 10 Myr (see middle panel of figure 2.6 and outliers in A.3 – note that the apparent gap in the middle panel is a sampling artefact, and does not represent an actual gap in the population). Those systems usually experience common envelopes, reduce their orbit during case BB mass transfer and have fortuitous kick directions which place them on a low-periapsis orbit at DCO formation. Systems with $t_{\mathrm{c}} > 10^{-3}$ Gyr represent the bulk of the population in figure 2.2; shorter coalescence times are exhibited by outliers with orbital periods of $\lesssim 10^{-2}$ days.

**Supernovae**

Of all NSs leading to a DNS 20% were formed via ECSN. From all secondaries leading to a DNS, 92% experienced ultra–stripping before exploding. Fewer than 0.1% were formed as double-ECSN. In 19% of the systems, the primary went ECSN, leading the secondary to being stripped in case B mass transfer with a NS companion; we asume this mass transfer episode recycles the NS. Then, the secondary ends up as
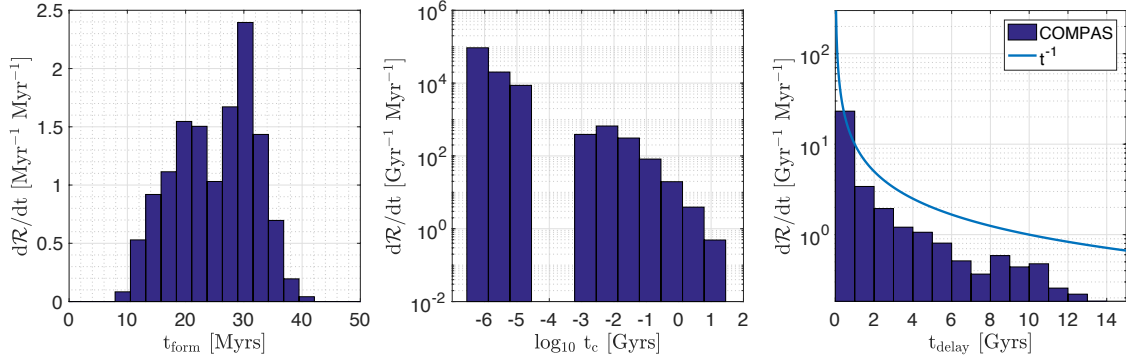
Figure 2.6: Time distributions of merging DNSs (blue histogram) for our `Fiducial` model (01): time from ZAMS to DNS formation [left], coalescence time from DNS formation to merger [middle] and total time delay from ZAMS to merger [right]. We show a $\mathrm{d}\mathcal{R}/\mathrm{d}t \propto t_{\mathrm{delay}}^{-1}$ curve for comparison with the delay time distribution in the right panel. The apparent gap in the middle panel is a sampling artefact.
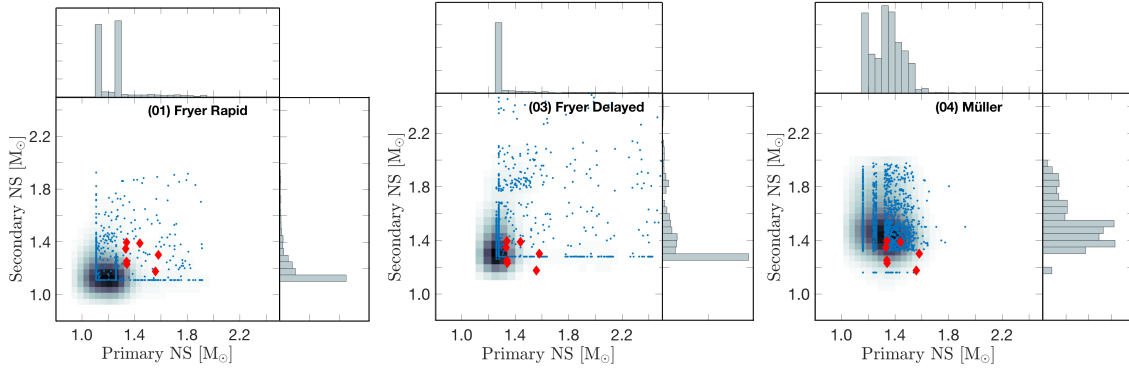


Figure 2.7: Predicted mass distribution of all DNSs under three different supernova fallback and natal kick models: (01) Fryer Rapid [left], (03) Fryer Delayed [center], (04) Müller [right]. Primary and secondary mass of the NSs are shown in the horizontal and vertical axes respectively. Red diamonds denote observed Galactic DNS with well-constrained masses (see Table 2.1), with pulsar and companion NS mass shown in the horizontal and vertical axes respectively. Blue dots correspond to the DNS masses at DCO formation. The density map shows the two-dimensional DNS mass probability distribution; the histograms show its one-dimensional linear projections. See sections 2.4.1 and 2.4.3 for a discussion of the evolutionary channels leading to sharp features in the histograms.

60

an USSN.

In our single stellar models, ECSN progenitors have masses at ZAMS of $7.8 \leq m/M_\odot \leq 8.1$; more recent detailed models find that the mass range of single star progenitors at metallicity Z=0.02 which become ECSN is $7.5 \leq m/M_\odot \leq 9.25$ [231]. Interaction during binary evolution increases this range to $7.8 \leq m_1/M_\odot \leq 28.4$ for the primary and $4.5 \leq m_2/M_\odot \leq 10.8$ for the secondary in our study. Detailed studies of ECSNe from interacting binary systems find that the mass range for an interacting primary at Z=0.02 is between $13.5 \leq m/M_\odot \leq 17.6$ [232], where 17.6 $M_\odot$ is the highest mass primary used in that study.

## 2.4.2   Variations

COMPAS is a modular code designed to explore the effects of different treatments of uncertain physical assumptions. Given the complexity of the formation channels we explore the uncertainties by changing one assumption per variation. This allows us to link all the changes in the population and its formation channels to a specific physical treatment and test the robustness of our `Fiducial` model. The parameters of the physical interactions may be correlated, and this approach does not account for this. However, computing these correlations is computationally expensive (see e.g., [21]), so we do not consider correlations here.

**On mass transfer stability criteria**

Stable case BB mass transfer leads to orbital periods similar to the observed Galactic DNS population. Meanwhile, unstable case BB, leading to a CE phase, typically results in sub-hour orbital periods (see right panel of figure 2.8); such orbital periods

yield coalescence times of $\lesssim 10$ Myr. About 90% of Galactic DNS progenitors in the `Fiducial` model experience case BB mass transfer. At the onset of the episode, 90% of systems have mass ratio $q \geq 0.2$ and 9% with $q \geq 0.4$. Claeys et al. [60] assume that mass transfer of HeHG donors with a degenerate accretor will be stable if $q > 0.21$ (see Table 2 of that paper), while Tauris et al. [281] propose to consider mass ratio and orbital period to define stability criteria in order to account for the evolutionary phase of the donor at the onset of Roche lobe overflow; in that study, orbital periods of $P \geq 0.07$ days at the onset of RLOF lead to stable case BB mass transfer. In our `Fiducial` model, all Galactic DNS progenitors have $P \geq 0.07$ days at the onset of case BB mass transfer.

In COMPAS, we probe the extreme cases of either stable or dynamically unstable case BB mass transfer for a whole population. The difference in formation rate $\mathcal{R}$ between the stable (01) and dynamically unstable case BB mass (02) transfer is comparable within a few percent, with $\{\mathcal{R}_{01}, \mathcal{R}_{02}\} = \{34.64, 35.37\}$ per Galaxy per $\text{Myr}^{-1}$. Nevertheless, the log Bayes factor of model 02 relative to model 01 is log $\mathcal{K} = -3.12$, which favours our `Fiducial` model, and ultimately, significantly favours stable against unstable mass transfer in a dichotomous scenario. In our `Fiducial` population, the assumption that case BB mass transfer is always stable is in broad agreement with mass ratio constraints from [60], which if enforced would define more than 90 per cent of these systems to experience stable mass transfer. If instead we used the the stability criteria presented in Tauris et al. [281] (as shown in Kruckow et al. [155]), all of the aforementioned systems remain stable.

**On the "Delayed" explosion scenario**

The "delayed" explosion scenario (03), proposed in Fryer et al. [104], allows for accretion onto the proto-NS before the standing-accretion shock instability (SASI)
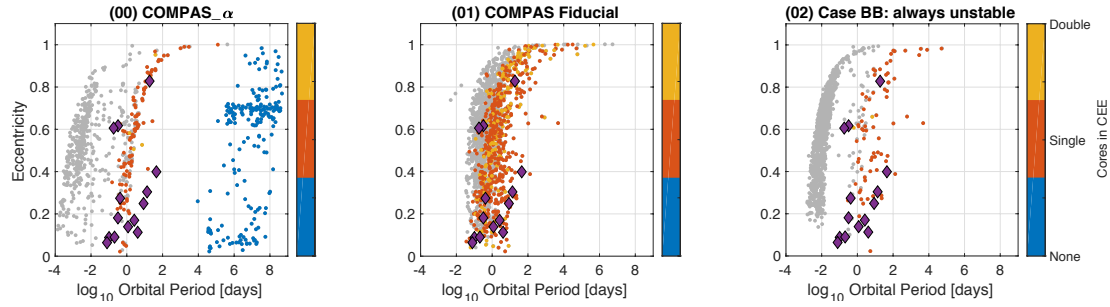
Figure 2.8: Predicted period-eccentricity distribution of Galactic double neutron stars at DCO formation: (00) Stevenson et al. [270] standard [left], (01) `Fiducial` [middle], (02) variation with unstable case BB mass transfer [right] (for more details see Table 2.1). Purple diamonds represent the Galactic DNS. Colour denotes the type of common envelope phase: blue for no CE phase, red for a single-core and yellow for a double-core common envelope phase. The single-core and double-core common-envelope formation are typically associated with *Channel I* and *Channel II*, respectively. Blue dots on the left panel correspond to double-ECSN with $\sigma_{\text{ECSN}} = 0$ km s$^{-1}$ in COMPAS_$\alpha$.

or convection become powerful enough to support a neutrino-driven explosion. This accretion removes the mass gap and creates a continuous remnant mass distribution from NS to BH; in the "delayed" explosion scenario we redefine 2.5 M$_\odot$ as the mass cut between NS and BH. The model 03 formation rate is $\mathcal{R} = 40.43$ per Galaxy per Myr$^{-1}$. The "delayed" explosion scenario (03), which changes the remnant mass given a O/C core at the moment of supernova, produces a slightly different period-eccentricity distribution than the `Fiducial` model because of the impact of mass loss at the moment of the explosion on the binary's orbit. The middle panel of figure 2.7 shows visually that the "delayed" explosion scenario lies close to the observed population and is preferred over the `Fiducial` model with a log $\mathcal{K} = 3.03$. The "delayed" explosion scenario (03), which does not have a mass gap between neutron stars and black holes, has the largest likelihood of all models.

**On the supernovae kick distribution and magnitude**

Both mass loss during the supernova and the natal kick magnitude and direction modify the orbital parameters and determine whether the binary is disrupted. Low-kick ECSN and USSN therefore play a prominent role in DNS formation and possible eventual merger, as would low-mass iron-core-collapse supernovae with a reduced kick. Our `Fiducial` model allows for a bimodal kick distribution, which distinguishes between CCSN (high mode, $\sigma_{\mathrm{high}} = 265$ km s$^{-1}$), ECSN (low mode, $\sigma_{\mathrm{low}} = 30$ km s$^{-1}$) and USSN (low mode). When allowing for a bimodal distribution, but with only either USSN (06) or ECSN (07) contributing to the low component of the Maxwellian distribution, the DNS formation rate $\mathcal{R}$ drops by a factor of $\approx 2$ relative to the `Fiducial` model. We also simulated a single high-mode distribution (05) with high kicks for both USSN and ECSN, which is also the assumption in COMPAS_$\alpha$ (00). In this case, $\mathcal{R}$ decreases by a factor of $\approx 3$; this single high-mode variation (05) also fails to create the observed longer period DNS with low eccentricities. The formation rates and log Bayes factors are $\{\mathcal{R}_{05}, \mathcal{R}_{06}, \mathcal{R}_{07}\} = \{13.20, 21.77, 19.50\}$ per Galaxy per Myr$^{-1}$ and log $\{\mathcal{K}_{05}, \mathcal{K}_{06}, \mathcal{K}_{07}\} = \{-3.08, -1.05, -3.19\}$ for variations with a single high mode (05), $\sigma_{\mathrm{ECSN}} = \sigma_{\mathrm{high}}$ (06) and $\sigma_{\mathrm{USSN}} = \sigma_{\mathrm{high}}$ (07), respectively. Given the log Bayes factors, the `Fiducial` model is significantly preferred over single high mode (05)) and $\sigma_{\mathrm{USSN}} = \sigma_{\mathrm{high}}$ (07) variations. It is preferred, but not significantly, over the $\sigma_{\mathrm{ECSN}} = \sigma_{\mathrm{high}}$ variation.

**On the "Müller" prescription**

We introduce the "Müller" supernovae prescription (04), a fit to the detailed models described by Müller et al. [190], useful for rapid population synthesis. The full description and fit is provided in Appendix A.2. The "Müller" prescription maps a O/C core mass to a NS remnant mass and a natal kick. The remnant and ejecta

mass and the explosion energy are obtained semi-analytically and calibrated to numerical models. We update the analytic supernova models of Müller et al. [190] by using a shock radius factor $\alpha_{\rm turb} = 1.18$ and a compression ratio at the shock $\beta = 3.2$, which fit constraints on the progenitor masses of Type IIP supernovae [263] slightly better than the original version. The kick velocity is obtained from these by assuming a uniform ejecta anisotropy [132]. The kick magnitude, with a dominant mode at $v_{\rm kick} \approx 100$ km s$^{-1}$ is therefore correlated with the NS remnant mass, unlike for the other models considered here. The mass range of neutron stars in our evolved population, using the "Müller" supernova mechanism, is $[m_{\rm NS,min}, m_{\rm NS,max}] = [1.2, 2.0]$ M$_\odot$. The formation rate and log Bayes factor of model 04 are $\mathcal{R} = 44.61$ per Galaxy per Myr$^{-1}$ and log $\mathcal{K} = -2.50$, respectively. This Bayes factor was calculated using only the period–eccentricity distribution. The mass distribution (figures 2.7 and 2.10) will play an important role in distinguishing the "rapid" (01), "delayed" (03) and "Müller" (04) explosion mechanism variations.

**On the comparison with** COMPAS_$\alpha$

We compare our `Fiducial` model to the one described by Stevenson et al. [270] (00, COMPAS_$\alpha$). The latter uses different parameterisations: both CCSN and USSN kicks are drawn from a high mode Maxwellian distribution and all ECSN have a $v_{\rm kick} = 0$ km s$^{-1}$; stability is determined using $\zeta_{\rm SPH}$ for all stellar phases, which often leads to dynamically unstable mass transfer, particularly during case BB RLOF; and the binding energy parameter is $\lambda_{\rm fixed} = 0.1$ for all stars in any evolutionary stage.

That study was successful in explaining all gravitational–wave events from the first Advanced LIGO observing run [GW150914, LVT151012 and GW151226, 2, 4, 3] via a single evolutionary scenario: isolated binary evolution. However, the
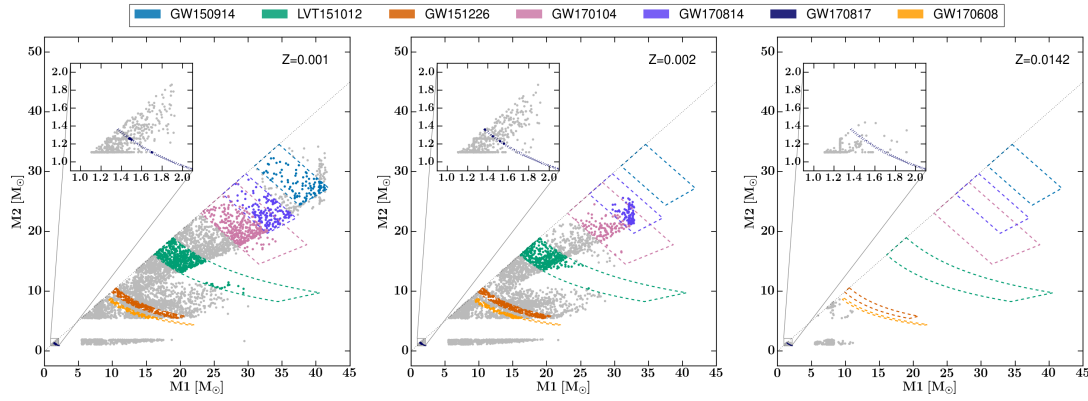
Figure 2.9: Masses of merging compact binaries predicted by the `Fiducial` model at three different metallicities: $Z = 0.001$ (left), $Z = 0.002$ (center) [cf. Stevenson et al. [270]] and solar metallicity $Z = 0.0142$ (right). Coloured regions correspond to masses matching LIGO detections within the reported 90 per cent credible intervals.

same assumptions fail to reproduce the observed Galactic DNS populations (see left panel of figure 2.8). Model 00, which yields a DNS formation rate of $\mathcal{R}_{00} = 16.35$ per Galaxy per Myr$^{-1}$, is the least preferred model from our variations, with a log Bayes factor of log $\mathcal{K} = -16.78$. In particular, the extreme hardening of case BB binaries through a second common envelope phase in COMPAS_$\alpha$ leads to a gap in the period-eccentricity distribution where systems such as J0737-3039 are observed. From the major changes, dynamical stability during case BB mass transfer and a bimodal natal kick distribution are preferred over the alternatives in the `Fiducial` model (see unstable case BB mass transfer (02) and single mode natal kick distribution (05) variations), which are ruled out in our model comparison.

On the other hand, the `Fiducial` model is able to explain, in a consistent form with Stevenson et al. [270], the gravitational wave events from the first LIGO observing run, as well as GW170104 [5], GW170608 [6], GW170814 [7] and the DNS merger GW170817 [8], all detected during the second observing run of Advanced LIGO and Advanced Virgo (see figure 2.9).

**On the circularisation during mass transfer**

Our `Fiducial` model does not circularise the orbit during a mass transfer episode, except as a consequence of dynamically unstable mass transfer (CE). As a variation, we consider circularisation at the onset of Roche lobe overflow (e.g., as a consequence of tidal dissipation prior to mass transfer or during the episode). We allow for two types of circularisation: (i) circularisation to periastron $a_p = a(1 - e)$, which dissipates both orbital energy and angular momentum (12), and (ii) circularisation to semilatus rectum $a_{SR} = a(1 - e^2)$, which conserves the angular momentum of the orbit (13). The DNS formation rates and log Bayes factors are $\{\mathcal{R}_{12}, \mathcal{R}_{13}\} = \{20.38, 22.06\}$ per Galaxy per Myr$^{-1}$ and log $\{\mathcal{K}_{12}, \mathcal{K}_{13}\} = \{2.54, 0.27\}$ respectively. Rates decrease by less than a factor of 2. Circularisation to periastron at the onset of mass transfer is slightly preferred than the alternatives, but not enough for us to consider it clearly preferred over the `Fiducial` model. Circularisation which conserves angular momentum is not favoured or disfavoured with respect to the `Fiducial` assumption (no circularisation at all).

**On the angular–momentum loss during non-conservative mass transfer**

During a non-conservative mass transfer episode, the specific angular momentum of the removed matter is determined by how mass leaves the system. In our `Fiducial` assumption, any non–accreted mass is removed isotropically in the reference frame of the accretor; this mass loss mode is usually referred to as "isotropic re–emission" (01). Another common parameterisation is the "Jeans" mode (14), which consists of ejecting the mass isotropically in the reference frame of the donor, similarly to fast winds. The last possibility we take into account is the formation of a circumbinary disk (15), with a radius of $a_{\rm disk} = 2a$ [17], from which the mass will be ejected. While isotropic re-emission (01) and the "Jeans" mode (14) tend

to effectively widen the orbit, that is not the case if mass is lost from a circumbinary disk (15). The formation rates of Galactic–like DNS and the log Bayes factor for these models are $\{\mathcal{R}_{14}, \mathcal{R}_{15}\} = \{9.64, 40.43\}$ per Galaxy per $\mathrm{Myr}^{-1}$ and log $\{\mathcal{K}_{14}, \mathcal{K}_{15}\} = \{-3.34, -2.67\}$ respectively. The `Fiducial` model is strongly preferred over the "Jeans" mode (14) variation; it is also mildy preferred over the circumbinary disk (15) variation. The mass loss mode also affects the future fate of the formed DNS. The fraction of all formed DNSs that will merge in a Hubble time is $\{f_{01}, f_{14}, f_{15}\} = \{0.73, 0.14, 0.94\}$ for the "isotropic re–emission", "Jeans" and "circumbinary disk" mode, respectively.

**On the Common Envelope parameters**

We consider several variations to the parameters that govern CE evolution: $\lambda$, which determines the envelope binding energy, and $\alpha$, which determines the amount of orbital energy needed to expel the envelope. In our `Fiducial` model all of the Galactic DNS experience a CE phase and therefore varying $\lambda$ and $\alpha$ from the `Fiducial` model choices $\lambda_{\mathrm{Nanjing}}$ and $\alpha = 1$ will affect the final distributions.

$\lambda_{\mathrm{Nanjing}}$ is a function of core mass, total mass and radius. We use a fixed value $\lambda_{\mathrm{fixed}} = 0.1$ (08) for comparison with previous population synthesis studies [e.g., 23]. Recently, Kruckow et al. [154] found for several models at different mass and metallicity that $\lambda$ depends on the radius in a roughly power-law form $\lambda \propto R^\beta$, with $-1 \leq \beta \leq -2/3$. We made a fit to figure 1 Kruckow et al. [154] in the form $\lambda_{\mathrm{Kruckow}} = 1600 \times 0.00125^{-\beta} R^\beta$, assuming a monotonically decreasing function. For our particular variation, we use an average value where $\beta = -5/6$ (09). The formation rates of DNS and the log Bayes factors for these variations in $\lambda$ are $\{\mathcal{R}_{08}, \mathcal{R}_{09}\} = \{23.49, 13.09\}$ per Galaxy per $\mathrm{Myr}^{-1}$ and log $\{\mathcal{K}_{08}, \mathcal{K}_{09}\} = \{-0.07, 0.02\}$ respectively, neither favouring nor disfavouring the $\lambda$ variations with respect to the `Fidu-`

`cial` model.

Higher values of $\alpha$ lead to wider post–common–envelope orbits than low values of $\alpha$. Without exploring the full and continuous parameter space, we vary $\alpha$ to extreme values of $\alpha_{min} = 0.1$ (10) and $\alpha_{max} = 10$ (11). Values of $\alpha > 1$ suppose that there are substantial additional energy sources, such as recombination energy and/or nuclear energy [230, 128] that contribute to the energy budget for CE ejection, in addition to the orbital energy. The extreme value of $\alpha_{max} = 10$ is more for illustration purposes rather than to mimic a particular physical interaction; in this case $\alpha_{max} = 10$ can only be explained if it comes from nuclear energy. The formation rates of DNSs and the log Bayes factors for variations in $\alpha$ are $\{\mathcal{R}_{10}, \mathcal{R}_{11}\} = \{7.59, 13.74\}$ per Galaxy per $\mathrm{Myr}^{-1}$ and log $\{\mathcal{K}_{10}, \mathcal{K}_{11}\} = \{1.76, -1.97\}$ respectively, neither clearly favouring nor disfavouring the $\alpha$ variations with respect to the `Fiducial` model. The choice of $\alpha$ varies not only the number of created DNSs, but also the amount of mergers. The fraction of all formed DNSs that will merge in a Hubble time is $\{f_{01}, f_{10}, f_{11}\} = \{0.73, 0.58, 0.36\}$.

Additionally, we also consider the "pessimistic" CE assumption (19). This assumption yields a DNS population which is a subset of the population under the `Fiducial` model, with binaries that enter the CE while the donor is classified as an HG star removed, as these are assumed to always lead to merger. The "pessimistic" CE assumption (19) is therefore expected to decrease DNS formation rates. The formation rates of DNSs and the log Bayes factors for these variations are $\{\mathcal{R}_{01}, \mathcal{R}_{19}\} = \{34.64, 20.60\}$ per Galaxy per $\mathrm{Myr}^{-1}$ and log $\{\mathcal{K}_{01}, \mathcal{K}_{19}\} = \{0, -0.16\}$ respectively. The likelihood of the "pessimistic" model (19) is similar to the one from the `Fiducial` model, which means the period–eccentricity distribution alone is insufficient to pick between these models. Additional constraints, such as merger rates, would be needed to determine the preferred model.

**On the effect of thermal eccentricity**

The only initial distribution we varied in this study was eccentricity. In order to simulate a population with non circular binaries at ZAMS we use the thermal eccentricity distribution (16), which has the form of $f_e(e) = 2e$ [116].

In this variation, the first episode of mass transfer commences once the primary expands to fill its Roche lobe at periastron. This changes the range of initial periods leading to interaction.

The formation rate and log Bayes factor of model 16 are $\mathcal{R} = 14.73$ per Galaxy per $\mathrm{Myr}^{-1}$ and log $\mathcal{K} = -0.07$ respectively. While formation rates drop by a factor of approximatively 3, the period–eccentricity distribution of forming DNS is not significantly affected. The drop in the formation rate is due to enhanced rates of interactions of main sequence stars that only need to fill their Roche lobe at periastron; if that mass transfer episode is unstable, the two main sequence stars merge.

### 2.4.3   On mass ratio distributions

Figure 2.5 shows the impact of the choice of the supernova remnant mass model on the DNS mass ratio distributions. The `Fiducial` model shows two distinct peaks in the mass ratio distribution around $q_{\mathrm{DCO}} = 0.87$ and $q_{\mathrm{DCO}} = 1$. The two peaks can be explained given the evolution of *Channel I* and *Channel II*, respectively. For the full discussion on the characteristics of the mass ratio for the `Fiducial` model, see section 2.4.1.

In the "delayed" prescription (03) most of the USSN mass change from 1.1 $\mathrm{M}_\odot$

to 1.28 $M_\odot$, with respect to the "rapid" mechanism; therefore, the mass ratio of systems in which the primary collapsed in an ECSN and the secondary in an USSN approaches 1, yielding an even more dominant peak at $q_{DCO} = 1$ in the overall mass ratio distribution. *Channel II* evolution leads to the second peak, with mass ratio $q_{DCO} = 1$, as in the `Fiducial` model. This results in a cumulative distribution function for the "delayed" mechanism (03) with a mass ratio between $0.52 \leq q_{DCO} \leq 1$, where 80% of the systems have $q_{DCO} > 0.80$, 55% have $q_{DCO} > 0.90$ and 40% have $q_{DCO} > 0.95$.

The remnant masses in the Müller prescription (04), as shown in figure 2.7 and A.2, have a wider spread and vary more at the low mass end. In this model, there is no significant pile-up. There is more scatter, with 70% of the systems having $q_{DCO} > 0.8$, 40% having $q_{DCO} > 0.9$ and 20% having $q_{DCO} > 0.95$.

### 2.4.4   On the chirp mass distribution

Figure 2.10 shows the predicted chirp mass distributions from some of our models. We compare the chirp mass distribution of DNSs which will merge within a Hubble time from our `Fiducial` model (01), which uses the "rapid" explosion mechanism, with different supernovae prescriptions: "delayed" (03) and "Müller" (04).

Additionally, we also show the COMPAS_$\alpha$ (00) chirp mass distribution, which uses the "delayed" mechanism. As expected, the chirp mass distributions show similarities with the mass ratio distributions, reproducing the same sharp features (peaks) explained in the previous section 2.4.3. In the same figure 2.10 we added all the confirmed DNSs with an estimated delay time smaller than the Hubble time, as well as GW170817.

We find that the "rapid" (01) mechanism predicts that most of the DNSs will have chirp mass lower than J1756-2251, which has the lowest chirp mass among confirmed DNS with good mass constraints. In fact, the "rapid" supernova mechanism (01) allows for light NSs which would be difficult to differentiate from NS–white dwarf binaries; there are several non-confirmed DNSs or poorly constrained DNS masses in the region favoured by the "rapid" mechanism (01) [209, 208]. On the other hand, the 7 existing well-constrained mass measurements are inconsistent with the predictions of the `Fiducial` model (01) at a $> 4\sigma$ level. None of these 7 measurements fall below a chirp mass of 1.1 $M_\odot$, while 83% of DNS in the `Fiducial` model have lower chirp masses. This suggests that the "rapid" mechanism under-predicts the amount of collapsed mass for the lowest-mass (electron-capture and ultra-stripped) neutron stars.

All other SN prescriptions considered here yield DNS chirp mass distributions starting above 1.1 $M_\odot$. Unsurprisingly, the "delayed" mechanism (03) has a very similar distribution to COMPAS_$\alpha$, which uses the same remnant mass prescription. They both predict systems matching all chirp masses included in the plot, with a peak close the lowest observed DNS chirp masses, J1756-2251 and J0737-3039. The "Müller" prescription (04) yields a similarly broad chirp mass distribution above 1.1 $M_\odot$. The "delayed" (03) and "Müller" (04) supernova fallback prescriptions cannot be distinguished based on existing mass measurements. However, the separation of $\approx 0.4$ between the predicted chirp mass cumulative distribution functions for these two models suggests that $\sim 10$ additional chirp mass measurements (whether from radio pulsars or merging DNSs) would be sufficient to tell these models apart.
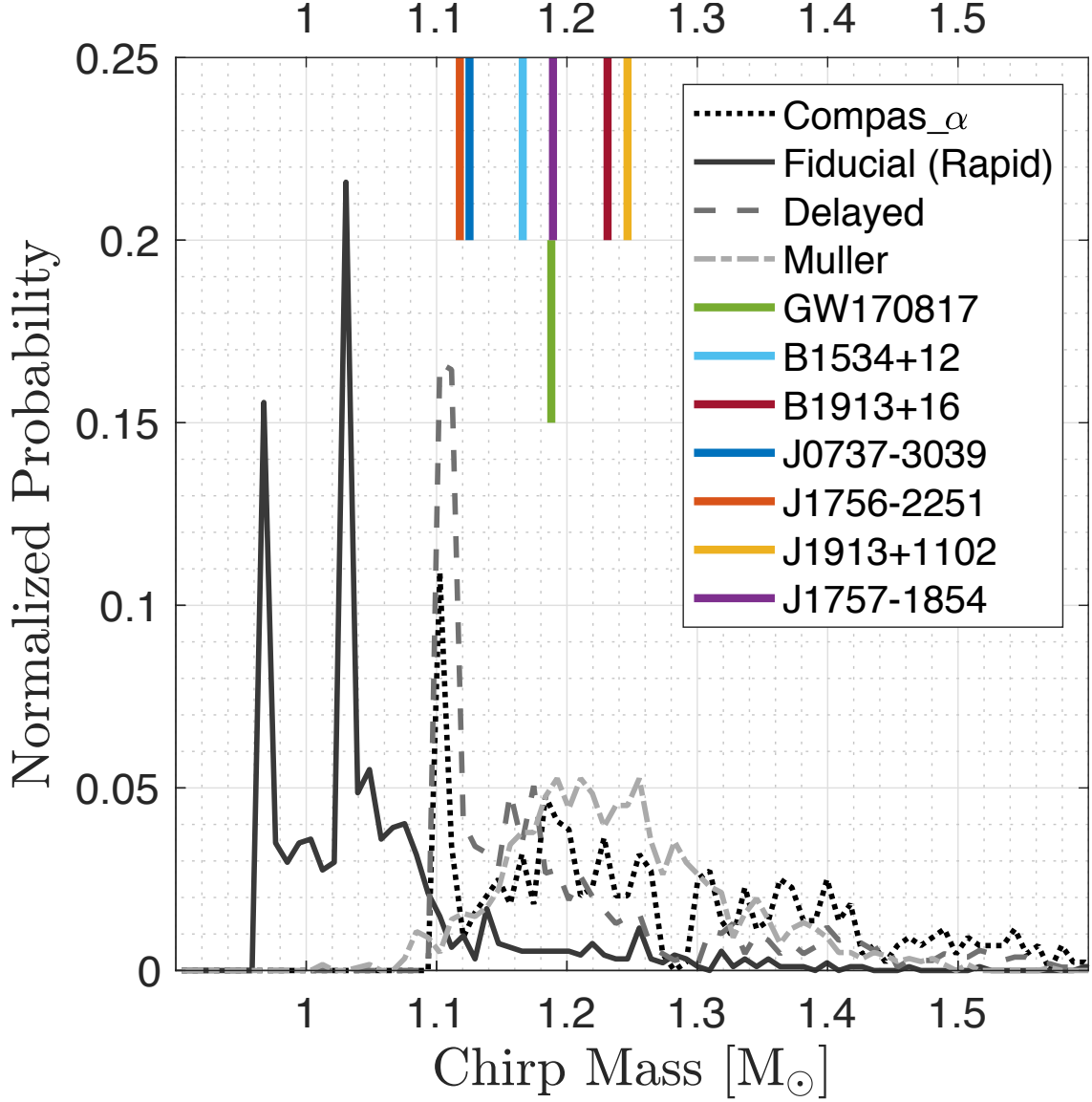
Figure 2.10: Chirp mass distribution of DNSs with a delay time smaller than a Hubble time: (00) COMPAS_α [black dotted], (01) `Fiducial` Fryer Rapid [dark gray solid], (03) Fryer Delayed [gray dashed] and (04) Müller [light gray dot-dashed]. Galactic DNSs with an estimated delay time smaller than a Hubble time are indicated at the top. GW170817, the only GW signal detected from DNSs to date, is shown as a vertically offset thick green line, with a similar chirp mass (1.188 $M_\odot$) as J1757-1854 in purple. All systems have precise mass measurements with error bars within the thickness of the line.

### 2.4.5   On kicks

When binaries undergo supernovae, they may get significant centre-of-mass kicks from both natal NS kicks and Blaauw recoil [34] from mass loss. The resulting DNS population should therefore be more broadly spatially distributed in the Galaxy than the regions of massive star formation. We have evolved a population of `Fiducial` model DNSs with the predicted kick distribution in a Galactic potential starting from birth in the thin disk. While we find that, as expected, kicks broaden the distribution of Galacto-centric distances (see figure A.3 in appendix A.3, where the details of this analysis are presented), the deep Galactic potential well means that this broadening is relatively small and challenging to test. In practice, the spreading of DNSs away from the thin disk may be even smaller than estimated here, because our simplified case BB mass loss models imply fairly high remaining core masses, between $1.6 \leq m_{\mathrm{O/C}}/\mathrm{M_\odot} \leq 4.6$, while detailed calculations of ultra-stripping suggest lower remnant core masses $1.45 \leq m/\mathrm{M_\odot} \leq 3.15$ [281]. Reducing COMPAS core masses in line with Tauris et al. [281] would both reduce Blaauw kicks and DNS eccentricities. On the other hand, three quarters of short GRBs are found outside the effective radius of the host galaxy [99], providing a strong constraint on the binary kick distribution; Fong and Berger [99] estimate total kicks of $\approx 20 - 140$ km s$^{-1}$.

### 2.4.6   On rates

**DNS merger rates**

DNS formation and merger rates are constrained by the observed sample of Galactic binary pulsars [e.g., 143, 204], by observations of short gamma ray bursts (sGRBs)

[99], and will ultimately be measured with gravitational-wave observations (see Mandel and O'Shaughnessy [177] for a review). Rates inferred from Galactic binary pulsars are dominated by a few systems and are sensitive to the imperfectly known pulsar radio luminosity distribution [138]. Short gamma ray bursts extend the observations beyond the Milky Way to cosmological distances, but inference from these is complicated by the difficulty of measuring jet opening angles and uncertain selection effects, and relies on the additional assumption of a one-to-one correspondence between SGRBs and DNS mergers [32]. Abadie et al. [1] combined the existing observational constraints to suggest that the DNS merger rate lies between 1 and 1000 $Myr^{-1}$ in a Milky Way equivalent galaxy (approximately 10 to 10000 $Gpc^{-3}$ $yr^{-1}$), with a likely value toward the middle of this range. All of the models presented in this paper fall within this range, although we focused on the Milky Way DNS population rather than the merger rate, and hence did not consider the convolution of the DNS formation rate and delay time distribution over cosmic history.

Other recent population synthesis studies give estimates that, like ours, fall in the two lower decades of this range. Chruslinska et al. [58] use `StarTrack` to predict a local merger rate density of 48 $Gpc^{-3}$ $yr^{-1}$ for their standard assumptions and $600^{+600}_{-300}$ $Gpc^{-3}$ $yr^{-1}$ for a very optimistic set of assumptions. Belczynski et al. [28] also use `StarTrack` to argue that even these rates are 2 orders of magnitude larger than the contribution from globular or nuclear clusters. Kruckow et al. [155] use $C_{OM}B_{IN}E$ to predict an upper limit to the local merger rate of 400 $Gpc^{-3}$ $yr^{-1}$.

Meanwhile, Abbott et al. [8] estimate a DNS merger rate of $1540^{+3200}_{-1220}$ $Gpc^{-3}$ $yr^{-1}$ based on GW170817 alone. However, given the significant Poisson uncertainty and sensitivity to rate priors from a single observation[2], the addition of this one (albeit, very special) event to the population of merging Galactic DNS and sGRBS

---

[2]For example, shifting from a flat-in-rate prior to a $p(R) \propto 1/\sqrt{R}$ Jeffreys prior [134] would reduce the peak of the posterior by a factor of 2 following one detection. Furthermore, the posterior peak is a factor of 1.67 lower than the posterior median quoted by [8].

does not significantly shift the observational constraints on the DNS merger rate. In fact, given the similarity of the predicted DNS formation rates among most models presented here, observational constraints on the rate alone will not be sufficient to distinguish between these models in the near future.

**Supernova rates**

We estimate the supernova rates for our `Fiducial` model (01). Given the ambiguity in supernova classification, we make simplifying assumptions to convert our models into observational predictions. We consider all progenitors with a hydrogen envelope to lead to hydrogen rich SNe (type II excluding type IIb) and the rest are considered stripped SNe (either hydrogen absent type Ib or Ic or hydrogen poor type IIb). Given the features of the SSE fitting formulae used throughout this study, pre-SN progenitors with any amount of hydrogen mass will be considered hydrogen rich. This leads to our hydrogen-rich/hydrogen-poor nomenclature to overlap with the hydrogen/no-hydrogen nomenclature from other studies. Our total rate of supernovae leading to NS formation is 0.0080 per $M_\odot$, which includes both ECSN and USSN. Among these, 75.6 per cent are hydrogen rich and the remaining 24.4 per cent are classified as stripped SNe, including all USSN. We predict that USSN that follow after case BB mass transfer onto a neutron star companion should make up 1.2 per cent of all stripped SNe and 0.3 per cent of all supernovae leading to NS formation.

Our total SN rate prediction is consistent with Zapartas et al. [318], a population synthesis study which reports CCSN rates in binaries between 0.0035–0.0253 per $M_\odot$, depending on the assumed IMF. Our estimates for the fraction of stripped supernovae compare well with observational results. Eldridge et al. [94] find that the fractions of hydrogen rich and stripped supernovae leading to NS formation are

61.9 and 38.1 per cent respectively; that study was made with supernovae discovered between 1998 and 2012 in galaxies with recessional velocities less than 2000 km s$^{-1}$. More recently, Shivvers et al. [260] report that 69.6 per cent of CCSN are hydrogen rich (according to the definition above), while the remaining 30.4 per cent come from stars with stripped envelopes.

## 2.5    Discussion & conclusions

We used the COMPAS rapid population synthesis code to evolve massive stellar binaries in order to generate a population of double compact objects. We quantitatively validated our models by comparing the predicted period–eccentricity distribution of double neutron stars against the observed Galactic DNS distribution, and qualitatively compared the predicted rate and mass distribution of Galactic DNS to observations. We considered variations relative to the `Fiducial` model in order to investigate the impact of uncertain evolutionary physics. We find that:

- *Case BB mass transfer during DNS formation must be predominantly stable.* We considered the possibility that post helium main sequence expansion of the secondary leads to dynamically unstable mass transfer and a second common envelope phase [77] in Variation (02). In fact, this was our initial default model, consistent with COMPAS_$\alpha$ (00) in this assumption. However, the lack of DNS with few-hour orbital periods (such as J0737-3039) in this variation (see figure 2.8), as well as our Bayesian analysis, indicates that most case BB mass transfer episodes must be stable. This finding is consistent with the detailed models of Tauris et al. [281]. However, some case BB dynamically unstable systems could exist without being detectable in the observed DNS population: the very short orbital periods of DNS that were hardened by two

common envelope phases would lead them to merge in less than a few hundred thousand years. While our study assumes constant star formation within the history of the Galaxy, the short orbital period DNSs would be disfavoured in Galactic star formation history models without recent periods of starbursts.

- *A bimodal supernova kick distribution is preferred over a single mode one.* We find that a bimodal kick distribution (with non-zero components) with lower kicks for electron-capture and ultra-stripped supernovae and higher kicks for standard core-collapse supernovae is preferred (see variations (05), (06), (07)). If ECSN and/or USSN are given the high kicks consistent with the observed velocities of isolated pulsars [111, 119], wider binaries are overwhelmingly disrupted by SNe, and observed wide DNS cannot be reproduced in the models. A bimodal supernova kick distribution is consistent with the findings of other population synthesis studies (see Pfahl et al. [223] and Belczynski et al. [23]) as well as with comparison to observations (see Beniamini and Piran [31] and Verbunt et al. [296]); although O'Shaughnessy et al. [206] didn't find evidence for multiple kick distributions.

The aforementioned findings in our paper, stability during case BB mass transfer and a bimodal kick distribution, are broadly in agreement with those in Andrews et al. [15], which used a smaller sample of 8 Galactic DNSs instead of the current 14 confirmed systems and carried out population synthesis by mainly varying common envelope parameters and kick magnitudes. Andrews et al. [15] find that it is likely that short-period low-eccentricity systems went through an evolutionary channel which includes stable case BB mass transfer. Their study also points out that the cores from ECSN progenitors should have relatively low mass, which can be related to lower natal kick magnitude.

- *Predicted DNS formation rates across variations are consistent with observations.* The formation rate of DNSs in the `Fiducial` model is 35 Myr$^{-1}$ in the Milky Way. The Milky Way DNS formation rate for all considered variations is 9 – 45 Myr$^{-1}$. All rates are consistent with observations [1], including the inferred rate from the GW170817 gravitational-wave detection [8], and cannot be used to differentiate between the models at this time.

- *Fryer "delayed" variation (03) is the preferred model with the highest log Bayes factor* $\log \mathcal{K}_{03} = 3.03$. The `Fiducial` model uses the Fryer "rapid" (01) explosion mechanism, which reproduces the first black-hole mass gap. Alternatively, the Fryer "delayed" (03) explosion mechanism has a continuous NS-BH remnant mass distribution. The statistical analysis in this chapter favours the Fryer "delayed" (03) over any other model variation. While this variation barely fits our criteria of being significantly favoured (see section 2.3.3), it suggests that an explosion mechanism which generates a continuous NS-BH remnant mass distribution is preferred. The chirp-mass distribution, as discussed in section 2.4.4, provides some additional support for the Fryer "delayed" (03) explosion mechanism, but still struggles to reproduce the observed chirp-mass distribution.

We also considered multiple SN models, including varying the fallback mass (Fryer "delayed" variation (03)) and a coupled mass–kick model calibrated to numerical calculations ("Müller" variation (04)). Low-mass iron-core CCSN may have reduced kicks, but are given standard CCSN kicks in the Fryer models, including the `Fiducial` model. The mass distribution of observed systems is not consistent with the very low masses predicted by the Fryer "rapid" fallback prescription used in the `Fiducial` model (01). Furthermore, observations do not show a peak in the mass distribution around 1.26 M$_\odot$ where ECSN should fall in our models. The

remnant mass of an ECSN depends on the NS equation-of-state and indicates that either ECSN are less common in binaries than we expected or the ECSN models should be revisited, as similarly noticed by Kruckow et al. [155]. With only $\sim 10$ additional DNS mass measurements it will be possible to further constrain the supernova fallback models, distinguishing between the "Müller" (04) and Fryer "delayed" (03) variants, both of which are consistent with existing observations.

Further input on kick velocity distributions should come from a better comparison with observed isolated pulsar kicks. At the moment, the observed isolated pulsar distribution is used to calibrate the CCSN kicks in binaries. However, the sample of observed isolated pulsars is contaminated by pulsars from disrupted binaries. Therefore, the approach we used here, which is also used by most population-synthesis codes, is not self-consistent: the observed single-pulsar velocity distribution should be checked for consistency against a model which includes contributions from both single and binary massive stars. In particular, observations should be tested for evidence of the predicted low kicks associated with ECSN, which may preferentially occur in binaries [229] that may subsequently be disrupted.

We assumed a solar metallicity $Z_\odot = 0.0142$ for massive stars in the Galaxy. In reality, the Galaxy has a distribution of metallicities at the present day, as well as a history of metallicity evolution over time, since present-day DNS systems and particularly DNS mergers may have formed in lower-metallicity regions (see Lamberts et al. [157] for a discussion of Galactic binary black hole formation). While figure 2.9 confirms that for a suitable choice of metallicity and initial conditions, the `Fiducial` model can produce compact binary mergers with masses matching all of the existing gravitational-wave observations; it also demonstrates that metallicity does impact the rate and properties of merging DNSs. Therefore, the metallicity-specific star formation history of the Milky Way will have an effect on the details of the modelled DNS population.

We do not account for selection effects in the observed Galactic DNS population in this study; see Tauris et al. [282] for a detailed discussion. Binaries with very short orbital periods may be selected against because of the orbital acceleration of the pulsar, which changes the apparent spin period; they will also have short merger times, and their location within the Galaxy will be sensitive to the details of recent star formation history. Meanwhile, binaries with extremely long orbital periods may also be challenging to detect, since they are less likely to be recycled during binary evolution, and detectable radio emission from non-recycled pulsars is expected to last for $\lesssim 50$ Myrs [168].

The DNS formation models presented here can also be tested against observable populations of massive stars during intermediate phases before DNS formation. Neutron star Be/X-ray binaries [e.g., 146] offer a particularly promising test case; for example, the observed correlation between the orbital period and the NS spin, with the latter appearing to be bimodal, could indicate distinct SN classes in their evolutionary history [146]. Spin distribution predictions could also be compared to observed pulsar spin periods in both isolated pulsars [e.g., 142] and in double neutron star systems [e.g., 79, 207, 282]. However, determining the NS spin-up or spin-down through binary interactions and pulsar evolution requires additional modelling assumptions, and hence spin models were not included in the present study. Meanwhile, more detailed studies of natal kicks in the Galactic potential could lead to additional constraints on kick distributions. Moreover, gravitational-wave detections will produce an ever larger catalogue of accurate mass measurements, at least for the chirp mass parameter. Together, these growing observational data sets will enable increasingly accurate tests of the massive stellar binary evolution models described here.

# Acknowledgments

# Chapter 3

# Common–Envelope Episodes en route to double neutron star formation

This chapter is a reformatted copy of a paper in preparation by Alejandro Vigna-Gómez, Morgan MacLeod, Ilya Mandel, et al. The current version of this work, as presented here, has been fully done by me. Morgan MacLeod and Ilya Mandel have helped with the interpretation of the results and made comments on the manuscript.

## 3.1   Abstract

DNSs have been observed as Galactic radio pulsars, gamma–ray bursts and gravitational–wave sources. They are believed to have experienced at least one CEE during their prior evolution to DNS formation. In the last decades, there have been numerous efforts to understand the details of the common–envelope phase, but there is still

no consensus. In this work we do rapid binary population synthesis of field-born double neutron stars in order to constrain the parameter space at the onset of the mass transfer episode leading to these CEEs. We provide a catalogue of CEEs that will eventually lead to DNS populations. In this catalogue we present and discuss the properties of the donor and the binary at the onset of the RLOF leading to that CEE. These properties can be used as initial conditions for detailed simulations of the common-envelope phase.

## 3.2   Introduction

An unstable mass transfer episode initiated by a post-MS donor is likely to lead to a CEE [211]. CEEs are proposed as a solution to the problem of how initially wide binaries, whose component stars may expand from a few tens to hundreds of solar radii during their lifetime, become close binaries at later stages of evolution [291]. Most evolutionary pathways leading to close binaries are expected to have experienced at least one CEE [128].

Astronomical transients, such as short gamma-ray bursts and gravitational-waves from DCO mergers, are also believed to have experienced and survived a CEE [23, 81, 28]. Models of Galactic DNSs predict than most of their progenitors experience a CEE [33, 279, 81, 15, 282, 299]. More recently, the CEE scenario has been used to explain luminous red novae transients [127, 173, 35] as a result from both successful ejections of the common envelope as well as mergers.

While CEEs are frequently evoked as a fundamental part of binary evolution,

the details of the physics remain poorly understood [211, 125, 127]. There have been efforts in modeling and understanding the phase from different approaches, such as hydrodynamics, from adaptive mesh refinement [253, 247, 248, 170, 172, 48], moving-mesh [200, 201] and smooth particle physics [242, 167, 213, 245] methods, detailed stellar modeling [78, 62] and binary population synthesis [277, 80, 15, 299]. There is currently no consensus on a thorough understanding of CEEs on all the relevant spatial and time scales.

Given the uncertainties in the initial conditions of the instability leading to the CEE, understanding the parameter space is important for more accurate modeling and predictions. In this chapter, we characterise the CEEs from binaries born in the field and on their way to forming DNS systems. We focus on the systems at the onset of the RLOF which experience dynamically unstable mass transfer phase leading to a CEE. We consider both Galactic-like DNSs as well as merging DNSs. While doing so, we constrain the plausible properties of DNS progenitors. We propose these constraints as initial conditions for studies of CEEs.

The chapter is structured as follows. Section 3.3 describe the rapid population synthesis as well as the initial distributions and relevant physical parameterisations. Section 3.4 presents the results of our study, particularly HR diagrams displaying different properties of the systems, as well as their distributions. Finally, section 3.5 presents the discussion and main conclusions of this work.

## 3.3 Population Synthesis Models

Characterisation of the CEEs is done by using the rapid population synthesis element of the COMPAS suite [270, 21, 299, 194]. Rapid population synthesis relies on simplified methods and parameterisations in order to simulate a single binary from ZAMS until stellar merger, binary disruption or DCO formation. This approach allows to do end-to-end simulations of binaries and to sample a multi-dimensional parameter space within hours, using a single processor. We follow the COMPAS `Fiducial` model (i.e. model variation 01) implementation and setup as defined in section 2.3, unless stated otherwise.

In COMPAS, a binary is defined as a gravitationally-bound system with a metallicity, component masses, a separation and an eccentricity, all of them specified at ZAMS. We assume that our binaries have a metallicity of $Z = 0.0142$, the same as solar metallicity bulk composition [18]. The mass of the primary ($m_1$), i.e. the most massive star in the binary at birth, is drawn from an initial mass function in the form $dN/dm_1 \propto m_1^{-2.3}$ [153] with masses between $5 \leq m_1/M_\odot \leq 100$. The mass of the secondary ($m_2$) is drawn from a flat distribution in mass ratio ($q = m_2/m_1$) in the form $dN/dq \propto 1$ with $0.1 < q_{\mathrm{ZAMS}} \leq 1$ [251]. The initial separation is drawn from a flat-in-the-log distribution in the form $dN/da \propto a^{-1}$ with separations between $0.01 < a_{\mathrm{ZAMS}}/\mathrm{AU} < 1000$ [202]. We assume our binaries follow a zero eccentricity distribution at birth. This assumption is made mainly for two reasons. The first one is that we expect tidal effects to play an important role in the formation of a short period binary. The second one is to be conservative when studying eccentricity at the onset of the CEE; all changes in eccentricity of an initially circular binary are only due to binary evolution (and not binary formation).

### 3.3.1 Adaptive Importance Sampling

In order to generate the initial distributions of masses and separation of the population, COMPAS originally relied fully on Monte Carlo methods. Monte Carlo performs adequately in fairly spanning the full parameter space of initial distributions, but becomes computationally more demanding for the study of unusual events. Given the shape of the initial mass function, progenitors of DNSs are more rare than progenitors of, for example, double White Dwarfs. In order to efficiently sample the parameter space leading to DNS formation, we adopt `STROOPWAFEL` as implemented in COMPAS [43].

`STROOPWAFEL` is an adaptive importance sampling (AIS) algorithm designed to improve the efficiency of sampling of unusual astrophysical events; it increases the abundance of DNSs more than an order of magnitude with respect to Monte Carlo. The algorithm is divided in three main steps:

1. **The exploratory phase:** it consists on performing regular Monte Carlo over the initial distributions and then follow the binary evolution until the end; if the binary becomes, e.g. in our case of interest, a DNS, then the initial conditions of this binary are recorded.

2. **The creation of a new sampling distribution:** once the parameter space leading to DNSs has been somewhat constrained, a multivariate Gaussian distribution is constructed around the initial parameters of each recorded event of interest. A mixture distribution is then constructed by combining the Gaussians.

3. **The sampling of the new distribution:** finally, the systems are sampled from the newly created distribution; each sample has an assigned weight that

reflects on the appropriate initial distribution, as they would be in a normal Monte Carlo sample.

Using AIS allow us to generate more DNSs per computer unit time as well as constraining our parameter space of interest in order to study it more thoroughly.

## 3.3.2   Underlying Physics

There are some physical parameterisations we want to highlight as they are particularly relevant for this work.

1. All mass transfer episodes from stripped post-helium-burning stars, i.e. case BB mass transfer [75], onto a NS, are assumed to be dynamically stable. The alternative, dynamically unstable case BB mass transfer, would lead to an additional CEE from a hot and luminous Wolf-Rayet-like donor. These late type of CEEs are not considered in the present work.

2. We deviate from Stevenson et al. [270] and Vigna-Gómez et al. [299] by allowing MS accretors in a CEE. Previously, any MS accretor was assumed to imminently lead to a stellar merger. Examination in the conditions for ablation of the accretor lead us to adapt our previous approach. We now apply energy formalism to systems with a MS accretor, just like with any other stellar type.

3. We follow de Kool [68] in the parameterization of the binding energy ($E_{\mathrm{bind}}$) of the donor star's envelope ($m_{\mathrm{donor,env}}$) given as:

$$E_{\mathrm{bind}} = \frac{-G m_{\mathrm{donor}} m_{\mathrm{donor,env}}}{\lambda R_{\mathrm{donor}}}, \tag{3.1}$$

where $m_{\mathrm{donor}}$ is the mass of the donor, $R_{\mathrm{donor}}$ is the radius of the donor, $G$ is

the gravitational constant and $\lambda$ is a numerical factor that parameterises the binding energy.

4. For the value of the $\lambda$ parameter, we follow the fitting formulae from detailed stellar models as calculated by Xu and Li [312]. This $\lambda$, originally referred to as $\lambda_{\mathrm{b}}$, includes internal energy and it is implemented in the same way as the $\lambda_{\mathrm{Nanjing}}$ is implemented in `StarTrack` [81].

5. We use the $\alpha\lambda$-formalism [305, 68] to model the evolution of the orbit in a CEE, with $\alpha = 1$ in all of our CEEs.

### 3.3.3 Tidal Timescales

Mass transfer episodes occur in close binaries which are assumed to experience tidal interactions. The tidal evolution of the orbit tends to make the binary synchronous and circular [64, 123, 317]. We estimate the synchronisation and circularisation timescales, $\tau_{\mathrm{sync}}$ and $\tau_{\mathrm{circ}}$ respectively, in order to parameterise the tidal evolution of the system. We follow the calculation as derived in Hurley et al. [122], which are based on the ones by Zahn [316] and Hut [123].

**The equilibrium tide for stars with convective envelopes**

For the equilibrium tide, the full synchronisation and circularisation evolution equations for the tidal effect a star of mass $m_{\mathrm{tide}}$ from a companion stars with mass $m_{\mathrm{comp}}$

are

$$\frac{d\Omega\text{spin}}{dt} = 3\left(\frac{k}{\tau_{\text{tide}}}\right)_c \frac{q^2}{r_g^2}\left(\frac{R_{\text{tide}}}{a}\right)^6 \frac{\Omega_{\text{orb}}}{(1-e^2)^6}$$
$$\times \left[f_2(e^2) - (1-e^2)^{3/2}f_5(e^2)\frac{\Omega_{\text{spin}}}{\Omega_{\text{orb}}}\right], \tag{3.2}$$

and

$$\frac{de}{dt} = -27\left(\frac{k}{\tau_{\text{tide}}}\right)_c q(1+q)\left(\frac{R_{\text{tide}}}{a}\right)^8 \frac{e}{(1-e^2)^{13/2}}$$
$$\times \left[f_3(e^2) - \frac{11}{18}(1-e^2)^{3/2}f_4(e^2)\frac{\Omega_{\text{spin}}}{\Omega_{\text{orb}}}\right], \tag{3.3}$$

where $f_n(e^2)$ are polynomial expressions given by Hut [123]. The structure of the tidally deformed star is parameterised in $k$, which is the apsidal motion constant [161] and the intrinsic tidal timescale ($\tau_{\text{tide}}$), usually associated with viscous dissipation [316]. We follow Hurley et al. [122] in the calculation of the $(k/\tau_{\text{tide}})_c$ factor, which depends on the evolutionary stage and structure of the star. The mass ratio is defined as $q = m_{\text{comp}}/m_{\text{tide}}$ and the gyration radius as $r_g = \sqrt{I_{\text{tide}}/(m_{\text{tide}}R_{\text{tide}}^2)}$, where $I_{\text{tide}}$ and $R_{\text{tide}}$ are the moment of inertia and the radius of the tidally deformed star, respectively.

Given that $a > R$, we expect synchronisation to be faster than circularisation. If we assume that the system is synchronous, we simplify Equation 3.3 and estimate

the circularisation timescale as

$$
\begin{aligned}
\tau_{\mathrm{circ}} &= \frac{e}{de/dt} \\
&= \left\{ 27\left(\frac{k}{\tau_{\mathrm{tide}}}\right)_c q(1+q)\left(\frac{R_{\mathrm{tide}}}{a}\right)^8 \frac{1}{(1-e^2)^{13/2}} \right. \\
&\qquad \left. \times \left[ f_3(e^2) - \frac{11}{18}(1-e^2)^{3/2} f_4(e^2) \right] \right\}^{-1}.
\end{aligned}
\tag{3.4}
$$

**The dynamical tide for stars with radiative envelopes**

For stars with radiative envelopes it is the dynamical tide [315], rather than the equilibrium tide, the mechanism in which drives synchronisation and circularisation. Following the derivation by Zahn [316] and expressing it in terms of Equations 3.2 and 3.3, as derived by Hut [123], we can write the synchronisation and circularisation timescale as

$$
\tau_{\mathrm{sync}} = 52^{-5/3}\left(\frac{R_{\mathrm{tide}}^3}{Gm_{\mathrm{tide}}}\right)^{1/2}\frac{r_{\mathrm{g}}^2}{q^2}(1+q)^{-5/6}E_2^{-1}\left(\frac{a}{R_{\mathrm{tide}}}\right)^{17/2},
\tag{3.5}
$$

and

$$
\tau_{\mathrm{circ}} = \frac{2}{21}\left(\frac{R_{\mathrm{tide}}^3}{Gm_{\mathrm{tide}}}\right)^{1/2}\frac{(1+q)^{-11/6}}{q}E_2^{-1}\left(\frac{a}{R_{\mathrm{tide}}}\right)^{21/2},
\tag{3.6}
$$

where $E_2 = 1.592 \times 10^{-9}(M/\mathrm{M}_\odot)^{2.84}$ is a second-order tidal coefficient as fitted by Hurley et al. [122] from the values given by Zahn [315]. In order to make a conservative estimate we approximate and $a \approx a_{\mathrm{p}} = a(1-e)$, which leads to shorter

tidal timescales. With this mechanism, we also expect synchronisation to be faster than circularisation.

**Radial Expansion Timescale**

An additional timescale, the radial expansion timescale ($\tau_{\mathrm{radial}}$), is computed as the rate of change of radius as a function of the current radius. This is done self-consistently within the fitting formulae provided by Hurley et al. [121] to the detailed stellar models from Pols et al. [234]. This radial expansion timescale depends on the pertinent stage of stellar evolution. It is used as a metric of efficiency against the tidal timescales, i.e. the synchronisation and circularisation timescales must be shorter than the radial expansion timescale in order for tides to be efficient in modifying the orbit.

**Uncertainties in timescales**

Some of the terms used in the aforementioned expressions can lead to uncertainties. For the radial expansion timescale, the stellar models our fitting formulae are based on are not accurate in representing the evolution of the star in a thermal timescale. For the tidal timescales, Kushnir et al. [156] noted the problem with $E_2$ being commonly used and widely extrapolated to massive stars. The intrinsic tidal timescale is uncertain for massive stars. It is important to compromise with the fact that all these timescales, as defined here, are being used as order of magnitude estimates in order to analyse the bulk properties of the systems, rather than accurate descriptions of stellar and binary evolution.

Table 3.1: Properties of the donor star at RLOF leading to a CEE. In this table, we present the symbols and units for each parameters, as well as a link the figure where they are presented.

| Property | Symbol | Units | Figure |
|---|---|---|---|
| Luminosity | $L_{\mathrm{d}}$ | $L_{\odot}$ | 3.1 |
| Effective temperature | $T_{\mathrm{eff,d}}$ | K | 3.1 |
| Stellar phase | - | - | 3.1 |
| Mass | $m_{\mathrm{donor}}$ | $M_{\odot}$ | 3.2 |
| Envelope mass | $m_{\mathrm{donor,env}}$ | $M_{\odot}$ | - |
| Core mass | $m_{\mathrm{donor,core}}$ | $M_{\odot}$ | 3.2 |
| Radius | $R$ | $R_{\odot}$ | 3.2 |
| Radial expansion timescale | $\tau_{\mathrm{radial}}$ | yr | 3.5 |

Table 3.2: Properties of the binary at RLOF leading to a CEE. In this table, we present the symbols and units for each parameters, as well as a link the figure where they are presented.

| Property | Symbol | Units | Figure |
|---|---|---|---|
| Eccentricity | $e$ | - | 3.3 |
| Semi-major axis | $a$ | $R_{\odot}$ | 3.3 |
| Total mass | $m_{\mathrm{tot}}$ | $M_{\odot}$ | 3.4 |
| Mass ratio | $q$ | - | 3.4 |
| Mass ratio at ZAMS | $q_{\mathrm{ZAMS}}$ | - | 3.4 |
| Circularisation timescale | $\tau_{\mathrm{circ}}$ | yr | 3.5 |
| Circularisation timescale factor | $f_{\mathrm{circ}}$ | - | 3.5 |

## 3.4 Results

We present the results of the population synthesis of binaries which become DNSs. We centre our attention on the properties of the systems at the onset of the CEE. If a star experiences RLOF, leading to an unstable mass transfer episode, the system is classified as experiencing a CEE. In that case, we record and report the properties of the system at the moment of the RLOF. Given that we are interested in DNS progenitors, all of these CEEs will experience a successful ejection of the envelope, i.e. no stellar mergers are reported in this study.

The data reported in this work contains information about 1,000,000 binaries evolved using COMPAS, which represent 2,774,952,000 $M_\odot$ of total mass across the full initial mass function. Out of the 1,000,000 binaries simulated, there are 32,710 CEEs leading to DNS formation. [1] For simplicity, we assume 100% binarity a priori. Nevertheless, given our assumptions for the separation distribution, up to 1000 AU, 46% of our systems never experience any mass transfer episode, resulting in two effectively single stars. We also consider a single metallicity, $Z = 0.0142$, for the whole population. While DNSs are believed to form in different environments, different studies have shown that metallicity does not play as much of a role in DNS properties, unlike binary black hole or neutron star/black hole formation [81, 299, 194].

The results section is structured as follows. Section 3.4.1 discusses the two most dominant formation channels leading to DNS formation in our model, i.e. the evolutionary history of the binary from ZAMS to DNS formation. In section 3.4.2 we characterise and present the basic properties at the onset of the CEE and report them according to the single stellar and binary parameters as used in COMPAS.

---

[1]This high DNS over binary ratio is a feature from AIS; Monte Carlo sampling of 1,000,000 binaries would give $\sim 2$ orders of magnitude less events of interest.

First we report the properties of the donor, most of them which are determined as specified in Pols et al. [234] and Hurley et al. [121]. Then we report the properties of the binary, particularly the orbital properties. For any given property, we present a color coded HR diagram, normalised distribution and cumulative distribution function (CDF).

## 3.4.1    Formation Channels of DNS systems

There is agreement within the literature regarding the most common evolutionary pathways leading to formation of DNS from isolated binary evolution [33, 279, 282]. There are two particular formation channels proposed as progenitors of DNS, with an unique CEE each. Following Vigna-Gómez et al. [299], we refer to these formation channels as *Channel I* and *Channel II* (see also section 2.4.1).

*Channel I* proceeds in the following way:

1. First, a hydrogen-shell-burning primary engages into stable mass transfer episode with a main sequence secondary.

2. The primary, now stripped, continues its evolution as a naked helium star until it explodes in a supernova, leaving a NS remnant in a bound orbit with a main sequence companion.

3. The secondary begins the post-main-sequence evolution, expanding and engaging in a CEE with the NS accretor.

4. After successfully ejecting the envelope, and hardening the orbit, the secondary becomes a naked helium star.

5. The stripped post-helium-burning secondary engages in a highly non-conservative

stable (case BB) mass transfer episode with the NS companion.

6. After being stripped again, the ultra-stripped secondary [280, 281, 110] continues its evolution until it explodes in a supernova, forming a DNS.

In *Channel I* the CEE occurs while the donor is crossing the HG, i.e. between the end of the MS and the start of the core helium burning (CHeB) phase. Rapid population synthesis modeling of CEEs sometimes parameterise these donors in two possible outcomes: "optimistic" and "pessimistic" [81]. The "optimistic" approach is where the donor has a clear core/envelope separation and it can engage and potentially survive a CEE. The "pessimistic" approach is where the dynamically unstable mass transfer leads imminently to a merger. This parameterisation is motivated by the structure of the star while it crosses the HG. The star has no clear core-envelope separation, as well as a large binding energy, likely leading the system to a merger. The pessimistic approach results in 19% of potential DNS candidates to merge before DCO formation. The pessimistic approach (imminent mergers) would lead to less energetic transients than the optimistic approach (potential ejections) [127]. Additionally, the optimistic approach could lead to additional CEEs at later evolutionary phases, where the ejected material would likely have a different compositions and generate different light curves.

*Channel II* proceeds in the following way:

1. There is an early unstable mass transfer episode leading to a CEE from both a post-main-sequence primary and secondary. During this early CEE, both stars have a clear core-envelope separation, and they engage in what is referred to in the literature as a double-core CEE [45, 80]. During this double-core CEE, both stars are stripped and become naked-helium-stars.

2. The stripped post-helium-burning primary engages in a stable (case BB) mass transfer episode with a stripped helium-burning primary.

3. The primary, now a naked metal star, explodes as an ultra-stripped SN and becomes a NS.

4. There is a final highly non-conservative stable (case BB) mass transfer episode from the stripped post-helium-burning secondary onto the NS.

5. The secondary then explodes as an ultra-stripped supernova, forming a DNS.

The two dominant channels, *Channel I* and *Channel II*, compose 61% and 34% of all DNSs respectively.

### 3.4.2   Common Envelope Episodes Leading to DNS formation

In figure 3.1, we present our synthesised population of DNS progenitors at the onset of RLOF leading to a CEE. They are coloured according to their particular stellar phase (following Hurley et al. [121]) at that point. The phase can also be inferred from their position in the HR diagram. Additionally, figure 3.1 shows the normalised distributions of luminosity, effective temperature and stellar type.

We use bootstrapping methods to estimate the uncertainty of our distributions given our sampling technique (AIS). Given any of our distributions, we randomly sample it with replacement in order to generate a bootstrapped distribution. We repeat this process $N = 100$ times to get a 10% accuracy of the bootstrapped standard deviation; i.e. the fluctuation of the bootstrapped bin scales as $1/\sqrt{N}$. We
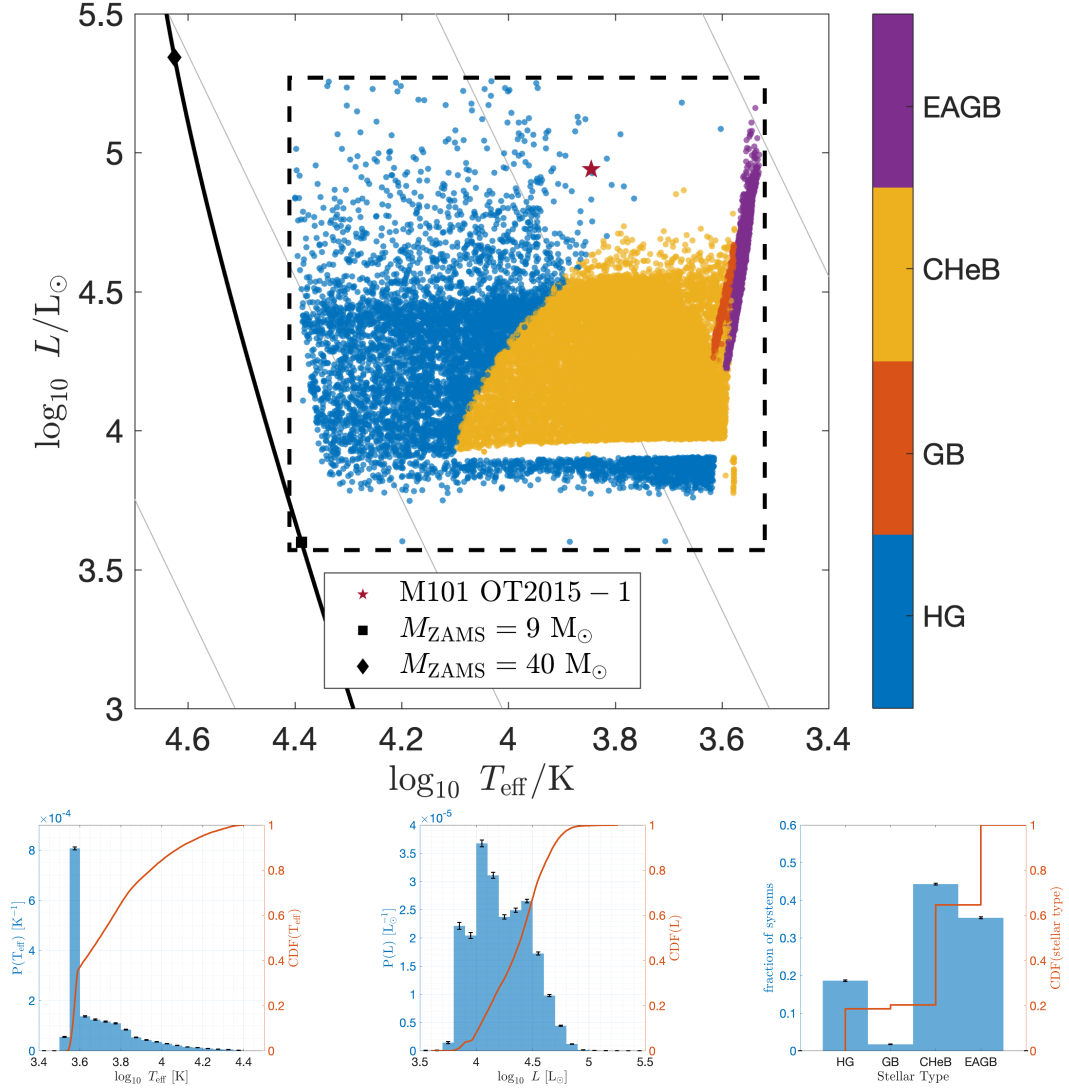
Figure 3.1: Main properties of the donor star at the onset of RLOF leading to the CEE. They are all systems en route to DNS formation. Top: HR diagram coloured by donor stellar phase: blue for HG, orange for GB, yellow for CHeB and purple for EAGB. We show the progenitor source for luminous red nova M101 OT2015-1 [35] in a wine color star around $\log_{10} T_{\mathrm{eff}} = 3.8$ K and $\log_{10} L = 4.9$ L$_\odot$. We show the position at ZAMS for a grid of SSE models [121] in a solid black line. We highlight the 9 and 40 M$_\odot$ models by marking them with a black filled square and black filled diamond respectively; we use this as a rough constrain on initial masses of interest. We draw a box with a thick dashed line around all systems in order to provide a visual constrain for the parameter space of interest. We also show iso-radial grey lines at $R = \{1, 10, 100, 1000\}$ R$_\odot$. Bottom: Normalised distributions and CDFs of the properties shown in the HR diagram. The properties shown are luminosity (left), effective temperature (middle) and stellar type (right). For each of them we show the binned normalised histogram in blue (left vertical axis) as well as the CDF in orange (right vertical axis). Sampling uncertainty error bars corresponding to $1\sigma$ are shown in black bars.

calculate and report the standard deviation of the bootstrapped distributions as $1\sigma$ error bars.

**Properties of the Donor**

We define the donor as the star which overflows its Roche lobe, initiating the mass transfer episode that leads to the CEE. We report the luminosity, effective temperature, stellar phase, mass, core mass and radius of the donor (see table 3.1).

The HR diagram in figure 3.1 contains arguably the most important properties of the donor. Each system is shown given the luminosity and effective temperature at the onset of the CEE. The luminosity and effective temperature limits are $\log_{10} [L_{\mathrm{d,min}}, L_{\mathrm{d,max}}] = [3.6, 5.3]$ $L_\odot$ and $\log_{10} [T_{\mathrm{eff,d,min}}, T_{\mathrm{eff,d,max}}] = [3.5, 4.4]$ K respectively. The property of interest in figure 3.1 is the stellar phase, which is color coded. While the evolution along the HR is an indicator itself of the evolutionary phase of the star, our stellar models models follow the stellar-type nomenclature as specified in Hurley et al. [121]. Donors which engage in a CEE leading to DNS formation can be in the HG (19%), GB (2%), CHeB (44%) or EAGB (35%) phase.

We estimate that, roughly, all DNSs can be enclosed in a sketch box with a bottom-left vertex around $\log_{10} \{T_{\mathrm{eff,left}}/\mathrm{K}, \mathrm{L_{bot}}/\mathrm{L_\odot}\} = \{4.41, 3.57\}$, a width and height of 0.89 dex and 1.7 dex respectively, and an upper-right vertex around $\log_{10} \{T_{\mathrm{eff,left}}/\mathrm{K}, \mathrm{L_{bot}}/\mathrm{L_\odot}\} = \{3.52, 5.27\}$. This region corresponds to the evolution of non-rotating single stellar models of ZAMS 9-40 $\mathrm{M_\odot}$ at $Z = 0.0142$.

In the case of *Channel I*, donors are HG or CHeB stars; they span most of the parameter space from terminal-age main-sequence until the end of core-helium burning, with a width of $\sim 1$ dex. In the case of *Channel II*, donors are GB or EAGB giant-like stars. The parameter space in the HR diagram for these giant-like donors is significantly smaller, having the spanned effective temperatures decrease to $\sim 0.1$ dex.

The mass properties of the donor are important to analyse in order to understand better the type of progenitors of these DNSs, as well as their observational properties. In figure 3.2, we show the mass of the donor. The limits are $[m_{\mathrm{donor,min}}, m_{\mathrm{donor,max}}] = [8.5, 34.4]$ M$_\odot$. The core mass, shown in figure 3.2, has limits of $[m_{\mathrm{donor,core,min}}, m_{\mathrm{donor,core,max}}] = [2.2, 11.5]$ M$_\odot$. The core mass plays an important role on the dynamics of the CEE. When a star is stripped, the core mass can also be used to estimate the final remnant mass.

We also show the radial properties of the donor. In figure 3.1, the iso-radial lines already give a sense of the radial evolution. We present the full radius distribution in figure 3.2. The limits in radius are $[R_{\mathrm{min}}, R_{\mathrm{max}}] = [13, 1183]$ R$_\odot$. The radial evolution will determine if a system begins Roche-lobe overflow, so the amount of CEEs varies with respect to the maximum radial expansion.

**Properties of the Binary**

We also report the properties that are intrinsic to the binary and, given the nature of the HR diagram, can only be understood by color coding the scatter plot. We report the eccentricity, semi-major axis, total mass, mass ratio, mass ratio at ZAMS and circularisation timescale factor (see table 3.2).
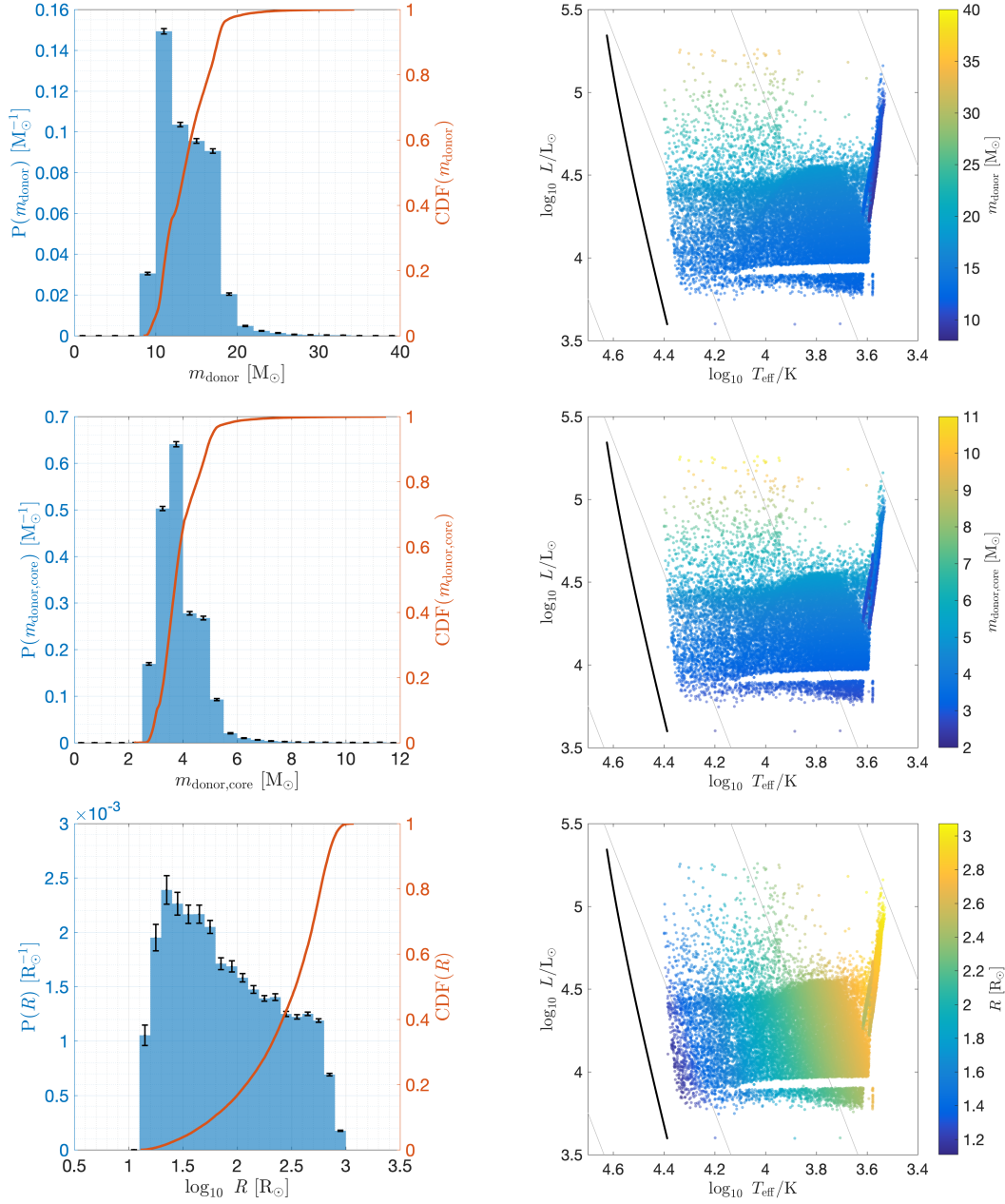
Figure 3.2: Pre-CEE donor properties of all DNS-forming systems. Left: Normalised distribution in blue (left vertical axis) and CDF in orange (right vertical axis). Sampling uncertainty error bars corresponding to $1\sigma$ are shown in black bars. Right: HR diagram color coded by the donor property of interest. The donor properties presented are mass (top), core mass (middle) and radius (bottom). For all HR diagrams we show the position at ZAMS for a grid of SSE models [121] spanning from 9 to 40 $M_\odot$. We also show iso-radial grey lines at $R = \{1, 10, 100, 1000\}$ $R_\odot$, derived using the Stefan-Boltzmann law.

We focus on the eccentricity, semi-major axis and masses of the system. These quantities are enough to estimate and characterise the orbital energy and angular momentum (at least in the two-point mass approximation). The eccentricity distribution, shown in figure 3.3, spans the whole parameter range $0 \leq e < 1$. The semi-major axis distribution, shown in figure 3.3, has limits of $[a_{\min}, a_{\max}] = [125, 152000]$ R$_\odot$. The very few very wide systems correspond to very eccentric binaries. The total mass distribution, shown in figure 3.4, has limits of $[m_{\text{tot,min}}, m_{\text{tot,max}}] = [9.8, 42]$ M$_\odot$. While these properties are enough to parameterise the binary evolution within the COMPAS framework, it is important to remember that other derived quantities are also relevant, such as periastron and Roche-lobe radius; both will determine if a system engages or not in unstable mass transfer.

We compute the mass ratio, both at the onset of the RLOF leading to the CEE and at ZAMS. The mass ratio, shown in figure 3.4, has limits of $[q_{\min}, q_{\max}] = [0.04, 1]$; while this range is quite broad, most of the systems lie in each of the ends of the mass ratio distribution, with a large gap between $0.15 \leq q \leq 0.9$. The sharp behaviour is shown in figure 3.4, where two significant peaks arise, one close to $q = 0$ and the other one close to $q = 1$. The extreme mass ratio systems correspond to CEEs from *Channel I*, where the companion is a NS. The $q \approx 1$ systems correspond to CEEs from *Channel II*, where there is a double-core CEE. The mass ratio at ZAMS is shown in figure 3.4. The mass ratio at ZAMS spread along $q > 0.3$, has limits of $[q_{\text{ZAMS,min}}, q_{\text{ZAMS,max}}] = [0.3, 1]$, and favours mass ratios closer to unity.

Mass ratio distributions are not the only way to distinguish DNS progenitors. Formation channels are also prominently distinguished when analysing the eccen-

tricity distribution. Figure 3.3 shows the eccentricity. The eccentricity distribution has a peak at $e = 0$, which can be associated to the initially circular orbits engaging in an early double-core CEE, as described in *Channel II*. This sharp features of the eccentricity distribution are directly related to our choice of initially circular orbits. The behaviour of the eccentricity distribution is expected to change for different choices of initial distribution. For a thermal distribution in the form $f_e(e) = 2e$ [116], the sharp feature at $q = 0$ is smoothed.

We calculate and parameterise the circularisation timescale of the binary. Given that the circularisation timescale is longer than the synchronisation timescale (see section 3.3.3), we focus on the former as an upper limit; if the binary is able to circularise, it will already be synchronous. We parametrise the circularisation timescale by dividing it over the radial expansion timescale, generating a dimensionless metric factor $f_{circ}$. If $f_{circ} > 1$, the circularisation timescale is longer than the rate of change in stellar structure, and we consider the binary will not be able to circularise by the time the CEE begins.

We pay particular attention to donors during the CHeB phase. These stars are expected to begin CHeB phase with a radiative envelope and develop a deep convective envelope by the end of it. The single stellar models from Hurley et al. [121] do not contain explicit information about when the deep convective envelope is formed. Hurley et al. [122] assumes CHeB stars have a radiative envelope. Belczynski et al. [24] assumes that stars with $\log T_{eff}/K > 3.73$ have a radiative envelope, while stars with $\log T_{eff}/K \leq 3.73$ have a convective envelope. In COMPAS, to check for mass transfer stability, we assume CHeB stars have a fully convective envelope. In order to see how the radiative/convective envelope affects the circularisation timescale, we calculate the timescale for the scenario where the tidal damping is driven by either purely convective or purely radiative envelope.

Figure 3.3:  Pre-CEE orbital properties of all DNS-forming systems.  Left:  Normalised distribution in blue (left vertical axis) and CDF in orange (right vertical axis).  Sampling uncertainty error bars corresponding to $1\sigma$ are shown in black bars. Right:  HR diagram color coded by the donor property of interest.  The binary properties presented are eccentricity (top) and semi-major axis (bottom).  For all HR diagrams we show the position at ZAMS for a grid of SSE models [121] spanning from 9 to 40 $M_\odot$.  We also show iso-radial grey lines at $R = \{1, 10, 100, 1000\}$ $R_\odot$, derived using the Stefan-Boltzmann law.

Figure 3.5 shows the circularisation timescales under the radiative/convective assumption for CHeB.  For our default assumption in which CHeB star have convective envelopes, 20% of the systems are not able to circularise.  If instead CHeB envelopes were assumed to be radiative, 58% of the systems are not able to circularise.  While radiative CHeB systems are the main systems which we expect to remain eccentric, most HG and some GB donors might not circularise.  The dynamics of an initially eccentric CEE has not been studied in detail and may have significant deviations from the canonical studies of CEEs.  This adds to the multiple uncertainties in theory and modeling of CEEs [127].
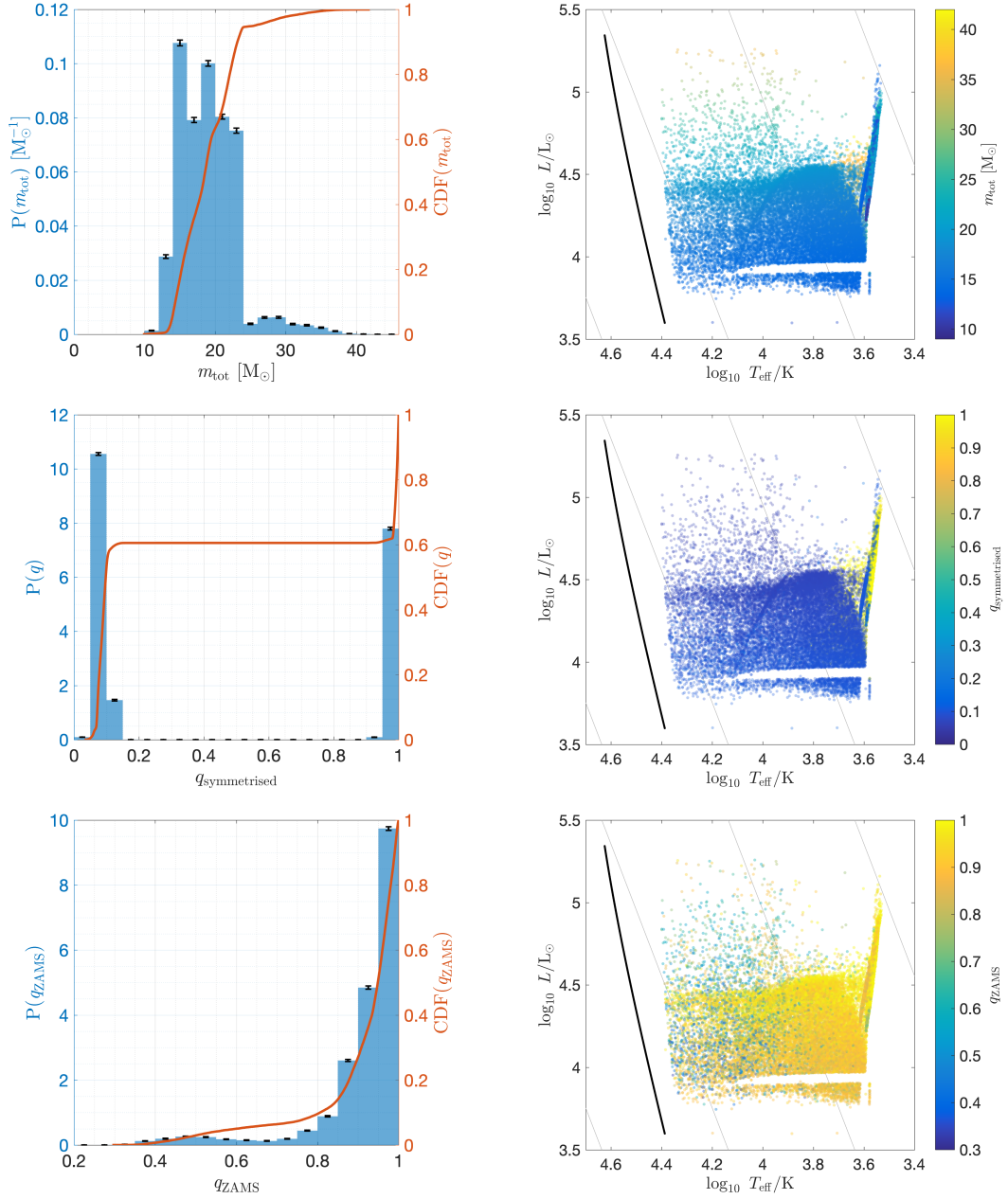
Figure 3.4: Pre-CEE mass of all DNS-forming systems. Left: Normalised distribution in blue (left vertical axis) and CDF in orange (right vertical axis). Sampling uncertainty error bars corresponding to $1\sigma$ are shown in black bars. Right: HR diagram color coded by the donor property of interest. The binary properties presented are total mass (top), mass ratio (middle) and mass ratio at ZAMS (bottom). For all HR diagrams we show the position at ZAMS for a grid of SSE models [121] spanning from 9 to 40 $M_\odot$. We also show iso-radial grey lines at $R = \{1, 10, 100, 1000\}$ $R_\odot$, derived using the Stefan-Boltzmann law.
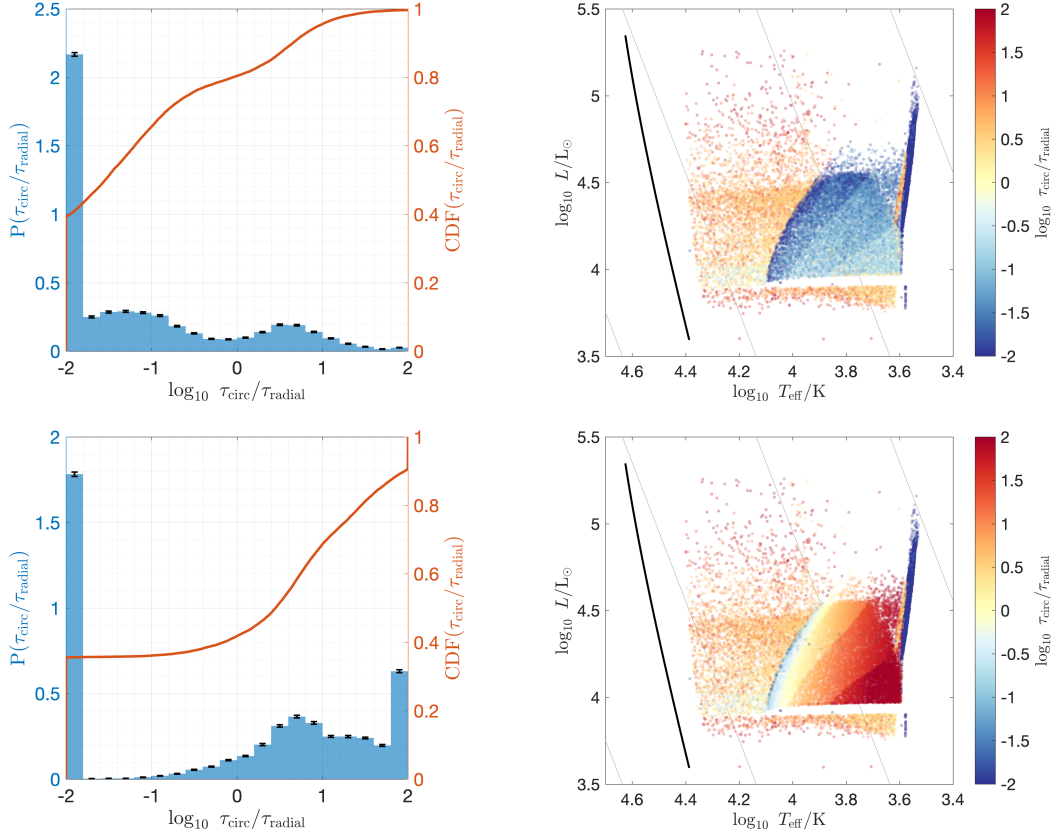
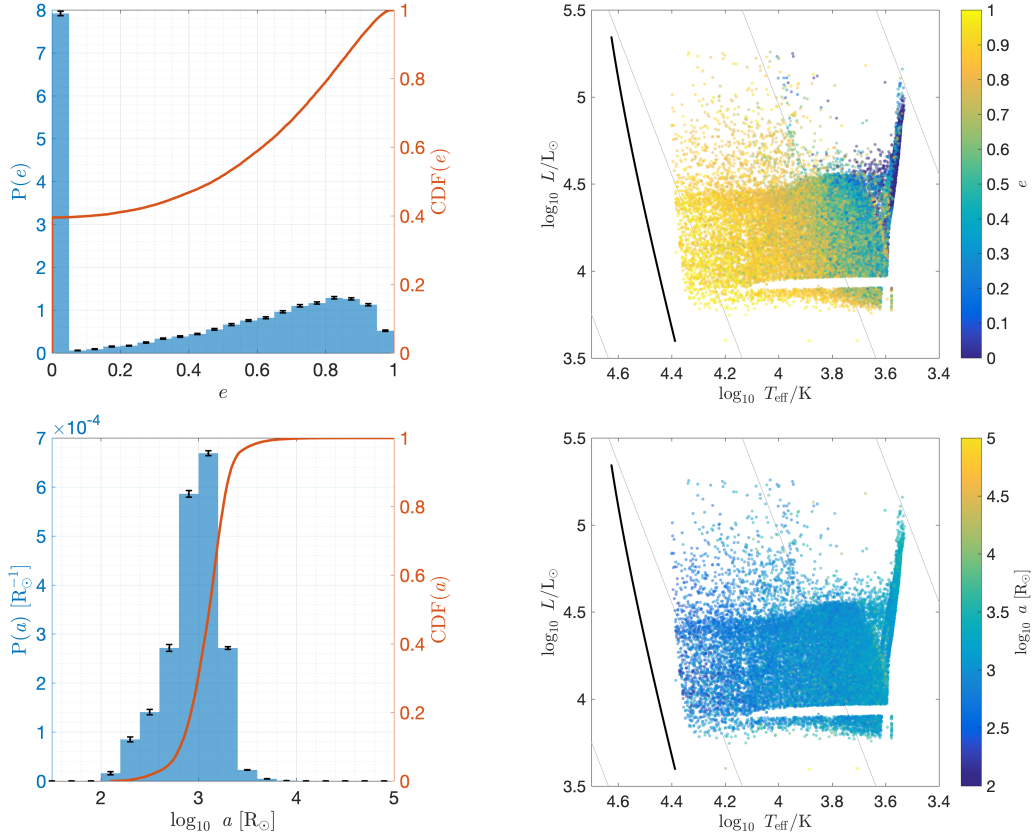Figure 3.5: Pre-CEE circularisation timescale factor for all DNS-forming systems. Left: Normalised distribution in blue (left vertical axis) and CDF in orange (right vertical axis). Sampling uncertainty error bars corresponding to $1\sigma$ are shown in black bars. Right: HR diagram color coded by the circularisation timescale factor. We compare the extreme scenarios where CHeB star are assumed to either have a deep convective (top) or fully radiative (bottom) envelope. If $\log_{10} \tau_{\mathrm{circ}}/\tau_{\mathrm{radial}} \leq 0$, we consider systems will circularise between RLOF and the beginning of the CEE; alternatively, they won't. For all HR diagrams we show the position at ZAMS for a grid of SSE models [121] spanning from 9 to 40 $M_\odot$. We also show iso-radial grey lines at $R = \{1, 10, 100, 1000\}$ $R_\odot$, derived using the Stefan-Boltzmann law.

## 3.5   Discussion and Conclusions

We used COMPAS to do rapid population synthesis of DNSs. We provide a catalogue of the properties of the binary at the onset of the RLOF leading to the CEE. Next, we discuss and elaborate the main conclusions of this work.

### 3.5.1   DNS populations have two distinctive CEEs phases

There are two main formation channels leading to DNS formation. Each of these formation channels has a single CEE each. They are both quite distinctive: the properties of the binary at the onset of the RLOF leading to the CEE will let you determine which formation history the binary experiences. *Channel I* has a NS primary with a post-MS secondary; this results in a high mass ratio single-core CEE. *Channel II* has similar post-MS primary and secondary; this results in an approximately equal mass ratio double-core CEE.

### 3.5.2   CEEs are strong candidates for luminous red novae transients

Recently, the luminous red novae transient M101 OT2015-1 was detected and reported by Blagorodnova et al. [35]. This event is similar to other luminous red novae associated with CEEs [127]. Following the discovery of M101 OT2015-1, additional photometric data from previous archival epochs was found. Blagorodnova et al. [35] use this to derive the characteristics of the progenitor. The inferred properties for M101 OT2015-1 are a luminosity of $L_{\mathrm{d}} \sim 8.7 \times 10^4$ $L_{\odot}$, an effective temperature of $T_{\mathrm{eff}} \approx 7000$ K and a mass of $M_{\mathrm{d}} = 18 \pm 1$ $M_{\odot}$ (see figure 3.1 for location in the HR

diagram). The progenitor is crossing the HG, and while doing so expands, which agrees with our proposed models for CEE progenitors. This progenitor is luminous, cool and massive. While these type of progenitors are not the most common in our synthesised population, it is important to notice that no selection effects are taken into account in presenting our catalogue. Selection effects should strongly favour more luminous sources, particularly for extra-Galactic transients.

### 3.5.3 DNSs progenitors can be constrained

The donor at the onset of the RLOF phase leading to the CEE has some distinctive properties. The minimum and maximum masses are 8.5 and 34.4 $M_\odot$ respectively. The minimum and maximum effective temperatures are $10^{3.5} \approx 3160$ and $10^{4.4} \approx 25200$ K respectively. The minimum and maximum luminosities are $10^{3.6} \approx 3980$ and $10^{5.3} \approx 199530$ $L_\odot$ respectively. With these limits we can constrain the initial conditions in which a CEE occurs as well as inferring the type of progenitors of luminous red novae. We also constrain the minimum and maximum ZAMS masses which are 7.3 and 25.9 $M_\odot$ respectively, and determine that the CEE is most likely to occur during the giant-phase and, depending on the structure of the envelope of the donor star, during the CHeB phase. This can also be of use to trace back the progenitor type of luminous red novae transients.

### 3.5.4 CEEs might not begin circular

Finally, we found that our estimation of the tidal timescales, similar to the ones used by most population synthesis codes, predict long circularisation timescales with respect to the intrinsic radial timescales of the tidally distorted stars. This suggests that some systems are not able to circularise between the onset of the RLOF and the

beginning of the CEE, i.e. some binaries would be eccentric at the beginning of the CEE. There have been some efforts in the literature to describe and parameterise mass transfer in eccentric binaries (e.g. [258, 82, 83]), but a complete understanding of the evolution from the onset of the RLOF to the dynamical instability is yet to be achieved. If confirmed, eccentric CEEs would change our understanding of the initial conditions leading to a CEE, which is usually assumed to begin synchronous and circular. This would further complicate the modeling and understanding of the common-envelope phase.

# Chapter 4

# Massive stellar mergers as precursors of hydrogen-rich Pulsational Pair Instability Supernovae

Alejandro Vigna-Gómez[1,2,3], Stephen Justham[4,5,6,7,3], Ilya Mandel[1,2,3] Selma E. de Mink[3,6,7], Philipp Podsiadlowski[3,8],

[1] Birmingham Institute for Gravitational Wave Astronomy, University of Birmingham, Birmingham, B15 2TT, UK

[2] Monash Centre for Astrophysics, School of Physics and Astronomy, Monash University, Clayton, Victoria 3800, Australia

[3] DARK, Niels Bohr Institute, University of Copenhagen, Blegdamsvej 17, 2100, Copenhagen, Denmark

[4] School of Astronomy & Space Science, University of the Chinese Academy of

Sciences, Beijing, China

[5] National Astronomical Observatories, Chinese Academy of Sciences, Beijing 100012, China

[6] Anton Pannekoek Institute for Astronomy, University of Amsterdam, 1090 GE Amsterdam, The Netherlands

[7] GRAPPA, University of Amsterdam, Science Park 904, 1098 XH Amsterdam, The Netherlands

[8] Department of Astronomy, Oxford University, Oxford OX1 3RH, United Kingdom

This chapter is a reformatted copy of Vigna-Gómez et al. [300], published in ApJ Letters and with arXiv number 1903.02135. My contribution to this work was to (i) write the routine to simulate mergers, (ii) simulate the single and merger models, (iii) interpret the results, (iv) make figures 4.3 and 4.4 (figures 4.1 and 4.2 were jointly made by Stephen Justham and Selma E. de Mink), and (v) write and edit the text.

## 4.1   Abstract

Interactions between massive stars in binaries are thought to be responsible for much of the observed diversity of supernovae. As surveys probe rarer populations of events, we should expect to see supernovae arising from increasingly uncommon progenitor channels. Here we examine a scenario in which massive stars merge after they have both formed a hydrogen-exhausted core. We suggest this could produce stars which explode as PISNe with significantly more hydrogen, at a given metallicity, than in single-star models with the same pre-explosion oxygen-rich core mass. We investigate the subset of those stellar mergers which later produce pulsational PISNe,

and estimate that the rate of such post-merger, hydrogen-rich pulsational PISNe could approach a few in a thousand of all core-collapse supernovae. The nature and predicted rate of such hydrogen-rich pulsational PISNe are reminiscent of the very unusual supernova iPTF14hls [16]. For plausible assumptions, PISNe from similar mergers might dominate the rate of PISNe in the local Universe.

## 4.2   Introduction

The diversity of ways in which massive stars die is heavily affected by the interactions which they undergo during their lifetimes [228]. It is natural to consider binary-star pathways towards all outcomes of massive star evolution, as these stars are typically born in interacting binaries [251]. Moreover, since the binary-interaction parameter space is large and multi-dimensional, ongoing SN discoveries may reveal new diversity arising from novel binary evolution routes. One relatively unexplored question is the influence of binarity on the diversity of pair-instability supernovae (PISNe).

PISNe are predicted to occur in stars with sufficiently massive O/C cores. In those cores, the temperatures become high enough for photons to produce electron-positron pairs, which results in a decrease of the radiation pressure support, and can lead to a dynamical instability. The core then contracts until the temperature is high enough to initiate explosive oxygen fusion [20, 241]. If nuclear burning reverses the contraction, this process may result in a single explosion as a PISN, completely disrupting the star.

Models of less massive stellar cores, with O/C core masses between approximately

28 and 52 $M_\odot$[1] find that they can avoid disruption by the first pulse of explosive burning [20, 308]. Those stars may experience multiple pair-instability eruptions, collectively called pulsational PISNe, after which there is insufficient nuclear fuel remaining to reverse the next collapse. Pulsational PISNe have been proposed as being responsible for a possible limit to the masses of black holes so far detected by gravitational wave detections [285], and as explanations for some very luminous SNe [310], but there has been no unambiguous identification of such a pair-instability driven stellar death.

Most newly-observed SNe fit within existing classes, but iPTF14hls is an extraordinary exception. The inferred bolometric luminosity stayed above $10^{42}$ erg s$^{-1}$ for over 600 rest-frame days, a duration more than 6 times longer than that of a canonical SN, and the light curve during this time displayed at least 5 peaks. This is different from the single plateaus seen in other hydrogen-rich Type II-P SNe to which iPTF14hls is spectroscopically similar [16]. The total energy radiated during those 600 days was a couple of times $10^{50}$ erg, well above the energy inferred for any previously known Type II-P SN. After 600 days, iPTF14hls remained more luminous than a typical Type II-P SN at peak luminosity. The multiple-peaked light curve is somewhat reminiscent of a pulsational PISN [20, 308]. However, one challenge with interpreting iPTF14hls as a pulsational PISN is that single stars sufficiently massive to produce luminous pulsational PISNe at metallicities similar to that of the apparent host galaxy of iPTF14hls are typically expected to retain too little hydrogen by the time of the explosion to produce the observed hydrogen-rich iPTF14hls [16, 309].

Here we investigate whether a class of stellar mergers could produce stars that later explode in a hydrogen-rich pulsational PISN. In this model, two stars in

---

[1]This range is found for pure helium cores in Woosley [308]. Different assumptions lead to different ranges, e.g., Chatzopoulos and Wheeler [52].
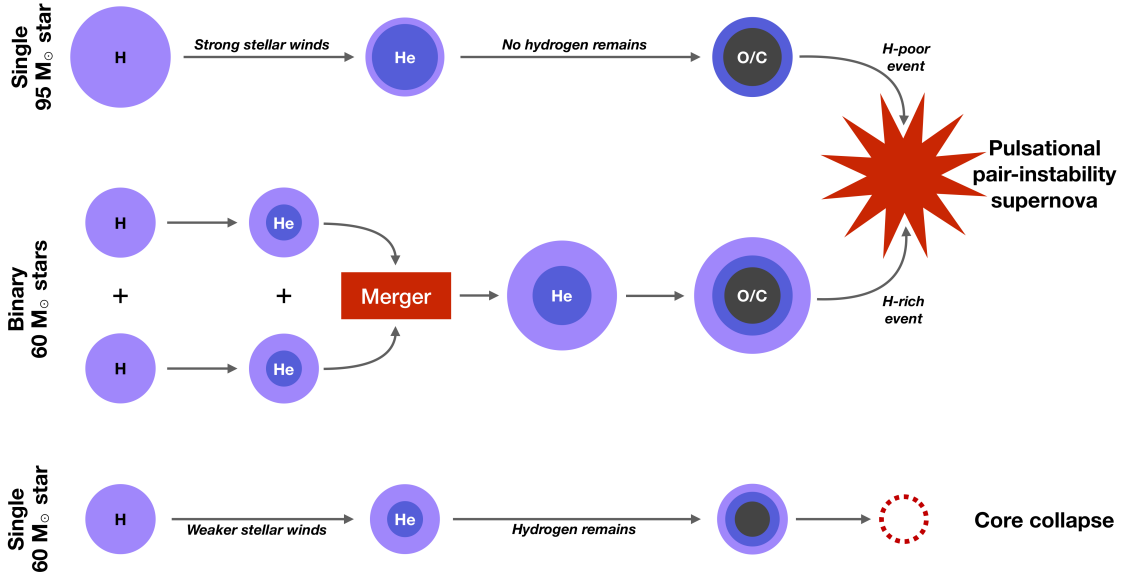
Figure 4.1: Schematic representation of three possible outcomes of stellar evolution. Top: single stellar evolution of a 95 $M_\odot$ star leading to a canonical pulsational PISN. Middle: merger scenario of two stars of initially 60 $M_\odot$ each, as investigated in this Letter; this scenario leads to a hydrogen-rich pulsational PISN. Bottom: single stellar evolution of non-rotating 60 $M_\odot$ star, which doesn't produce a O/C core massive enough to be a pulsational PISN.

a binary system merge to form the SN progenitor after the end of the relatively long phase of hydrogen fusion in each of their cores [137]. A merger during this evolutionary stage is natural, due to the expansion of the stars after the end of their core hydrogen fusion, and the pre-merger stars will have experienced significantly less fractional mass loss by winds than a single star of the same total mass and evolutionary state. The merger creates a combined helium core sufficiently massive to lead to a pair-unstable O/C core. Figure 4.1 displays a schematic representation of a single star leading to a pulsational PISN, as well as this merger formation channel. We find that this progenitor scenario could lead to a more substantial hydrogen-rich envelope at the onset of the explosion than in single-star pulsational PISN models with otherwise identical assumptions. We estimate that this evolutionary route could well be significant in producing pulsational PISNe in the local Universe.

## 4.3   Massive stellar mergers

### 4.3.1   Astrophysical case

Two similarly massive stars transferring mass at an appropriate orbital separation can merge. When both stars are expanding after their MS, mass transfer can cause the accreting star to also over-fill its Roche lobe. Subsequent loss of mass and angular momentum from one or both of the outer Lagrangian points can cause runaway shrinking of the binary orbit. For such stars, it appears likely that this situation would at least sometimes, and perhaps typically, lead to a merger (see, e.g., Pasquali et al. [212]; Podsiadlowski [227]; Justham et al. [137]).

Cases in which unstable mass transfer occurs when two similar-mass stars have completed their MS, but in which successful common-envelope ejection prevents a merger, have been proposed as a pathway to explain the formation of some double-neutron-star binaries [45, 80] and low-mass binary systems [136]. Those cases typically require binary components with initial masses similar to within, at most, a few per cent. However, at higher masses the probability for two stars to interact during the post MS evolution of both stars becomes larger. This is because the duration of the MS becomes a very shallow function of initial mass [see, e.g., 44]. Hence stars from a wider relative range in mass can simultaneously be between the end of core hydrogen fusion and the start of core oxygen fusion, ideal for mergers in our scenario. (Such systems with similar masses and appropriate orbital periods have been observed, e.g. R139/VFTS 527, for which see §4.4.)

Figure 4.2 illustrates two dimensions of the parameter space for (pulsational) PISNe arising from non-interacting single stars and merger products.
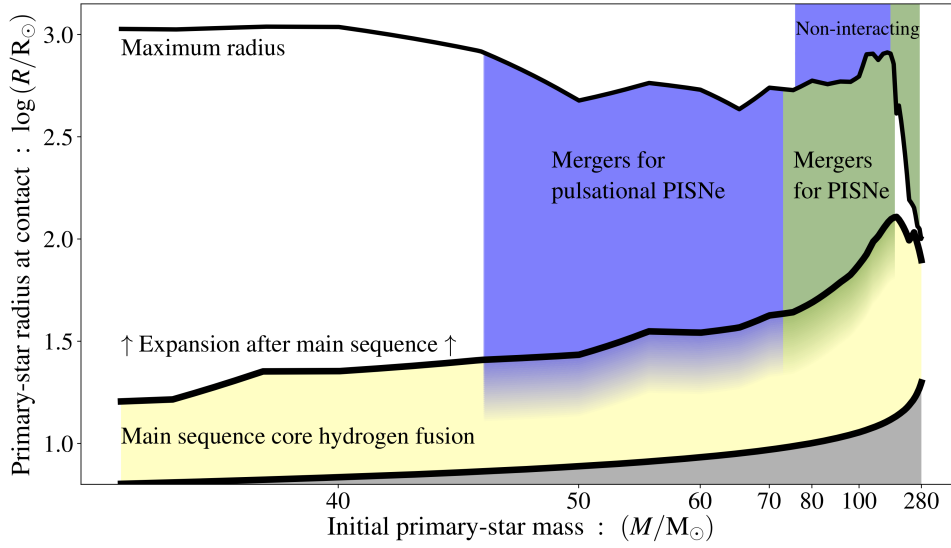
Figure 4.2: Depiction of the parameter space that is expected to lead to PISNe, including pulsational PISNe. The figure shows stellar radii as a function of initial mass. Primary stars evolve vertically upwards in this plot as they expand, and will interact with a companion if they overflow their Roche lobe. The shaded regions indicate where pulsational (blue) and normal (green) PISNe may be produced. For non-interacting binaries or single stars, this is based on the helium core mass range [308]. For post-main sequence binary mergers the extremes of the shaded regions assume equal-mass mergers. The shading extends to lower radii to indicate a possible contribution from binaries which start mass transfer on the main sequence. The scalings along both axes are chosen such that equal areas represent equal number density. Stellar radii and helium core masses for this figure are taken from the MIST library of MESA models [56] for non-rotating models with an initial metallicity of $[\mathrm{Fe/H}] = -0.75$, similar to the SMC metallicity of our MESA models.

To investigate the subsequent evolution of such a merger product, we model a case with two identical merging stars, each 60 $\mathrm{M}_\odot$ at ZAMS. For a given primary-star mass, an equal-mass case should be the least favourable for retaining hydrogen, since the total fractional core mass at the time of merger will be higher than in cases with non-equal masses, i.e., the fraction of mass in hydrogen at the time of the merger is the lowest. Less massive secondary stars would also retain a larger fraction of their H envelope before the merger because of their reduced stellar winds.

## 4.3.2   Numerical modeling

The merger of two stars is complex. Realistic simulations of such events and their outcome are still beyond our reach. However, making reasonable simplifying assumptions, it is possible to study the properties of the products that are the likely outcome of such mergers. We model a single star and a merger product using Modules for Experiments in Stellar Astrophysics (MESA) [216, 217, 218, 219] (version 10108). We adopt the same assumptions for the single and merger models, unless stated otherwise. The MESA inlists used in this chapter can be found in `http://doi.org/10.5281/zenodo.2644593` [298]. We use the `mesa_67.net` nuclear network, and assume a metallicity of 0.0035, representative of star-forming regions in the Small Magellanic Cloud, corresponding to [Fe/H] $\approx -0.76$ ([Z/H] = [Fe/H] adopting solar-scaled abundances as specified in Choi et al. [56]). For wind mass loss, we use the "Dutch" wind scheme in MESA [108], reduced by multiplication with a factor of 0.3 [240, 264]. Cool and hot wind schemes are used for effective temperatures below 10,000 K and above 11,000 K, respectively, interpolating when at intermediate temperatures. For hot winds, the mass loss rate scales with metallicity as $\dot{M} \propto Z^{0.85}$ [301]. Convective overshooting extends 0.25 pressure scale heights above convective regions during the MS – specifically until hydrogen is exhausted in the core for the single stars – and until the moment of merger, which happens shortly after the end of the MS in our models.

The ZAMS mass of our single-star model is 95 M$_\odot$, and is 60 M$_\odot$ for each star that we assume to merge. There is significantly more main-sequence mass loss for the 95 M$_\odot$ single star than for the 60 M$_\odot$ pre-merger star (see Figure 4.3), as expected.

We assume that the structure of the merger product depends on the entropy profile of the merging progenitors, consistent with earlier hydrodynamic situations of mergers between less massive stars [166] and non-rotating massive-star collisions

(Glebbeek et al. [109]; although see Gaburov et al. [105]). For equal-mass components, this assumption means that the relative internal composition structure of the merger product is initially the same as that of the progenitor star. Hence we keep the relative internal structure of the pre-merger model fixed whilst doubling the total mass through relaxation, with no abundance change due to nuclear burning during the merger, and with no additional mixing. However the thermal structure then readjusts in response to the new hydrostatic balance, which can lead to mixing. Our models are non-rotating and spherically symmetric, but the strong molecular-weight gradients likely suppress rotational mixing [see, e.g., 137, and references therein]. We do not remove mass on a dynamical timescale during the merger, as might be expected, but $\approx 7$ per cent of the post-merger mass is removed by intense winds during the first $\approx 20$ kyr after the merger (just visible in Figure 4.3), during the time when the model merger product is relaxing towards gravo-thermal equilibrium. Simulations of head-on mergers between two 40 M$_\odot$ stars at and just after the end of the main sequence found mass loss of $\approx 8$ per cent [109]. The amount of mass loss is probably the main uncertainty in our predictions for hydrogen-rich pulsational PISNe. This uncertainty affects hydrogen retention, and so whether our merger scenario would produce hydrogen-rich explosions.

We model the post-merger evolution with the same assumptions as for the single-star model. Figure 4.3 shows the stellar structures during these evolutionary phases for both models. These models were chosen so that the O/C core masses are very similar at the onset of pair instability, but the post-merger model retains a massive hydrogen-rich envelope. The dominant composition structures of these models, just before the onset of the first pulsation, are shown in figure 4.4. The single-star model has a 6.0 M$_\odot$ helium envelope and less than $10^{-2}$ M$_\odot$ of hydrogen, while the post-merger model retains a hydrogen-rich envelope with 19.0 M$_\odot$ of helium and 9.8 M$_\odot$ of hydrogen.
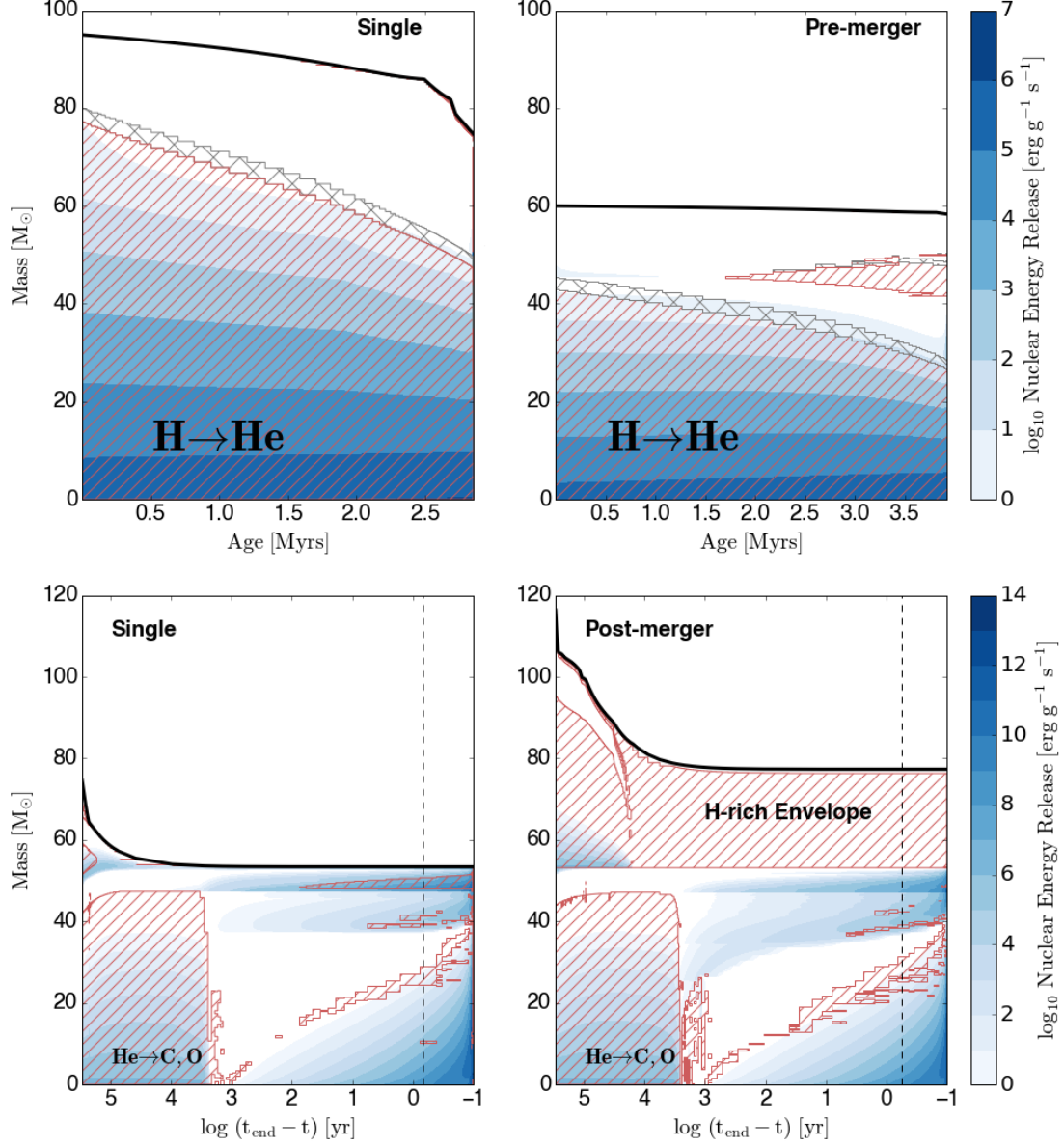
Figure 4.3: Structures of the single (left) and merger (right) models described in the text. Both main sequence (top) and post-main-sequence or post-merger (bottom) evolution are shown. The total mass of each star is shown with a thick solid black curve, nuclear burning regions in shaded blue and convective regions in hatched red. For the post-main-sequence models, the vertical dashed lines (black) show when the central temperature reaches $T_c \approx 10^9$ K.
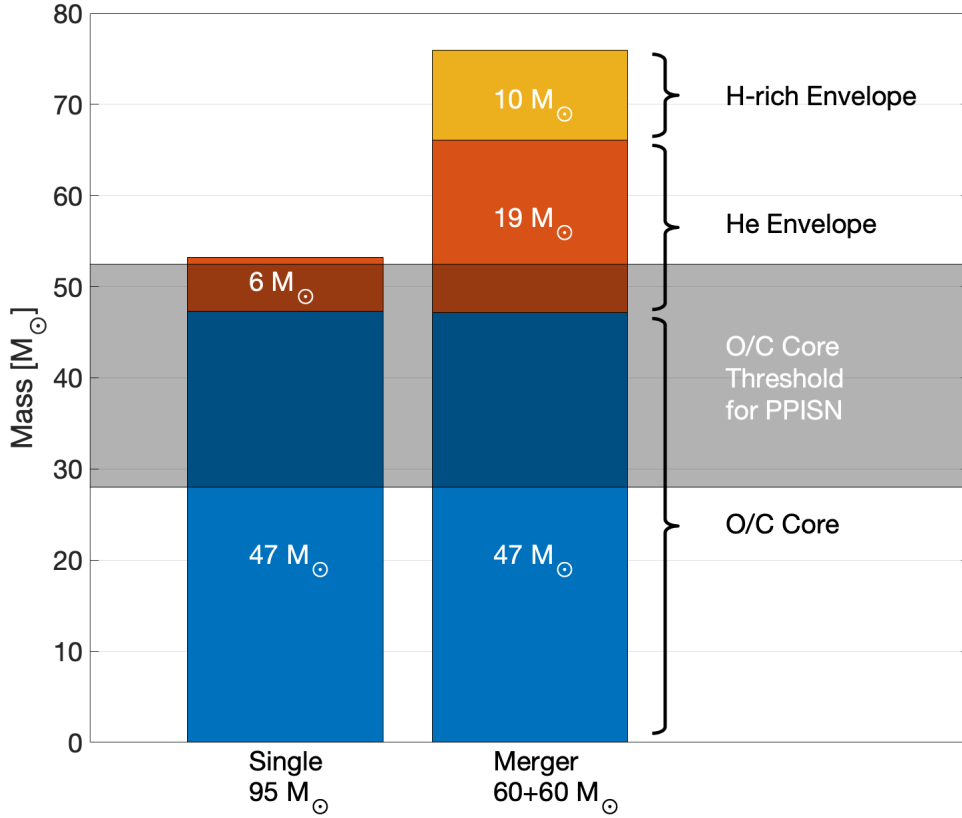
Figure 4.4: Schematic diagram of the dominant compositions of our single (left) and post-merger (right) models at the moment when the central temperature $T_c \approx 10^9$ K, less than a year before the first pair-instability driven outburst. The bottom (blue) represents the O/C core, whilst the middle (red) and top (yellow) show the masses of helium and hydrogen outside the O/C core. The grey shaded region represents the range of masses of O/C cores leading to pulsational PISNe according to Woosley [308]: $28 \leq M/M_\odot \leq 52$. Both cases are expected to lead to a pulsational PISN, but the single-star model has less than 0.01 $M_\odot$ of hydrogen at explosion, while the merger model has approximately 10 $M_\odot$.

### 4.3.3   Rate estimates

We estimate the hydrogen-rich pulsational PISN rate, $\mathcal{R}$, as a ratio between the number of pulsational PISNe from mergers in our scenario, $N_{\mathrm{PPISN,mergers}}$, and the total number of CCSNe, $N_{\mathrm{CCSN}}$, for a fixed amount of star formation:

$$
\begin{aligned}
\mathcal{R} &= \frac{N_{\mathrm{PPISN,mergers}}}{N_{\mathrm{CCSN}}} \\
&= f_{\mathrm{binarity}} \times f_{\mathrm{primary}} \times f_{\mathrm{secondary}} \times f_{\mathrm{separation}}.
\end{aligned}
\tag{4.1}
$$

The factor $f_{\mathrm{binarity}}$ describes the fraction of massive stellar systems which contain close binaries; we assume it to be $f_{\mathrm{binarity}} = 0.7$ [251].

The factor $f_{\mathrm{primary}}$ represents the ratio between the number of binaries in which the initially more massive star is in the correct mass range to produce a pulsational PISN if a suitable post-main sequence merger occurs, and the number of stars with the right mass to undergo a CCSN.

We assume that stars with ZAMS masses in the range $[8, 40]$ M$_\odot$ undergo CCSNe, and use the Salpeter [250] initial mass function $p(m) \propto m^{-2.3}$.

We estimate $f_{\mathrm{primary}}$ using terminal-age main sequence helium core masses calculated with MESA (for more details, see appendix B.2). We double those core masses to give notional post-merger core masses, and compare those to the range from Woosley [308]. This gives a primary mass range $[40, 64]$ M$_\odot$. As a pessimistic alternative, we only allow the primary to be within $[56, 64]$ M$_\odot$, with mass ranges symmetric about our calculated example merger model. These assumptions lead to $f_{\mathrm{primary}} \in [0.01, 0.06]$.

The factor $f_{\mathrm{secondary}}$ is the fraction of binaries with a suitable primary in which

the lighter companion is sufficiently massive for our merger scenario.

As a pessimistic assumption we include only mergers between components with nearly equal masses, $q = m_{\mathrm{secondary}}/m_{\mathrm{primary}} \geq 0.99$ at ZAMS. For the more optimistic assumption, we consider that mergers between two stars that have both evolved beyond the main sequence can yield pulsational PISN progenitors. For massive stars, the luminosity-mass relation flattens out and evolutionary timescales vary slowly with mass [44, 147]. This leads to a threshold $q \geq 1 + f_{\mathrm{postMS}} \left(\tau/M\right) \left(dM/d\tau\right) \approx 0.85$, where $\tau$ is the main sequence lifetime [96] and $f_{\mathrm{postMS}} \approx 0.1$ is the fraction of time the star spends beyond the main sequence. These assumptions lead to $f_{\mathrm{secondary}} \in [0.01, 0.15]$.

Finally, $f_{\mathrm{separation}}$ accounts for the fraction of otherwise suitable binary stars with the appropriate separation to merge in the correct evolutionary phase.

We assume the flat-in-the-log distribution of initial separations $p(a) \propto a^{-1}$ (consistent with, e.g., Sana et al. [251]). Depending on whether we require the merger to happen whilst the primary star is close to the end of the MS – within a factor of two in radius – or optimistically allow for mergers at any point until the star's maximum radial expansion ($\approx 800$ R$_\odot$), we find that $f_{\mathrm{separation}}$ falls in the range $[0.13, 0.46]$.

These assumptions predict a range of rates of suitable mergers leading to pulsational PISNe that goes from $\mathcal{R}_{\mathrm{min}} = 1.3 \times 10^{-5}$ CCSN$^{-1}$ for conservative assumptions to $\mathcal{R}_{\mathrm{max}} = 3.2 \times 10^{-3}$ CCSN$^{-1}$ for more optimistic ones. Empirical estimates indicate that events such as iPTF14hls could constitute about $10^{-3} - 10^{-2}$ of the Type II SN rate [16], where Type II SNe make up $\approx 70\%$ of all CCSNe [260].

Our rate estimate does not include a potentially significant contribution of stellar mergers from binaries with initially closer separations. These massive overcontact

binaries [179] may experience several mass transfer episodes during the MS, which could lead the stars to approach terminal-age main sequence at the same time. Our rate estimates are also sensitive to mass loss rate prescriptions, which are in turn a function of metallicity. Metallicity-dependent stellar winds reduce both the size of the core and the amount of hydrogen retained in the envelope at the onset of a pulsational PISN. Furthermore, radial expansion, which determines the range of binary separations for which suitable mergers can occur, is also a function of mass and metallicity. We generally expect lower metallicity environments to yield a higher rate of hydrogen-rich pulsational PISNe. Their total rate in the local Universe is an integral over all metallicities at which star formation occurs.

## 4.4 Discussion and conclusions

The R139 binary in the Tarantula nebula in the LMC, also known as VFTS 527, consists of two very similar supergiant Of stars of about 60 $M_\odot$ and an orbital period of about 150 days [see 284, 12]. This is a near-perfect example for our scenario. Apart from the metallicity, this system is a real-world illustration that systems exist which may follow the merger scenario we have described. Another well-studied close analogue is WR20a, containing two stars each of 82 $M_\odot$ [243, 38, 244], which would be an excellent candidate for a future binary-merger progenitor of a PISN if the orbit were slightly wider.

This merger route is not the only way to potentially increase the rate of pulsational and non-pulsational PISNe. Rotational mixing increases the core mass of stars with a given initial mass, which may allow initially less-massive stars to reach the pair-unstable regime, although with less hydrogen in their envelope than for stars of the same mass when evolving without rotational mixing [159, 72, 52, 53, 180].

Runaway mergers of massive stars in stellar clusters have also been discussed as potential progenitors of PISNe [236, 108]; however, this is not obviously more likely to lead to hydrogen-rich progenitors at the time of the PISN than for single stars.

An intriguing question remains whether iPTF14hls represents a case for a hydrogen-rich PISN resulting from the scenario explored here. While the metallicity of our models is below the estimated range of $\approx 0.4 - 0.9\,Z_\odot$ for the host galaxy of iPTF14hls [16], uncertainties in the metallicity estimate for the progenitor star are significant. We do not claim that this evolutionary scenario has explained all the specific features observed or inferred for the iPTF14hls transient [see, e.g., 16, 308], but we consider the possibility worth further modelling and investigation. Other models, including circumstellar material interaction in a regular CCSN and events powered by the spin-down of a magnetar, have not fully explained iPTF14hls [309, 76].

There is tentative observational evidence for an eruption at the location of iPTF14hls 50 years previously [187]. If this was an earlier pulse related to iPTF14hls, it may be challenging for the simpler pulsational PISN to explain it, as much of the hydrogen would likely be expelled during that early pulsation. One very speculative alternative is that this earlier optical transient was related to an extremely late merger, in which case iPTF14hls would be following a very fine-tuned scenario.

Another unusual event that has been discussed as a possible pulsational PISN is SN 2009ip [102, 214], with progenitor metallicity similar to that of the SMC [67]. It may be interesting to re-consider whether this event, originating from a luminous blue variable star, may also have been a hydrogen-rich pulsational PISN from a merger product.

Our scenario does not only produce a pathway for some hydrogen-rich pulsational PISNe, it also increases the range of initial stellar masses and metallicities

from which PISNe can originate, whether hydrogen-rich or not. PISNe from mergers may even dominate the PISN rate in the local Universe if stellar winds are sufficiently high to suppress PISN production at even moderate metallicities in single stars. This formation channel may therefore have significant consequences for the chemical yields from PISNe. A strong nucleosynthetic signature of enrichment by PISNe had been expected in low-metallicity stars, but searches for that abundance pattern have had limited success [see, e.g., 197]. However, increasing the rate of PISNe at high metallicity would not exacerbate this problem, because the distinctive PISN elemental abundance pattern would be damped when a PISN enriches gas that has already been enriched by previous generations of regular supernovae. The new age of wide-field transient surveys is already producing unexpected discoveries, as shown by iPTF14hls. The ongoing development of such surveys should provide further examples of similar events with which to test our proposal.

# Acknowledgments

## Software

MESA [216, 217, 218, 219], Kippenhahn plotter for MESA [178], MESA inlists used in this chapter [298].

# Chapter 5

# Conclusions

In this work we have studied different phases of massive binary stellar evolution using a mixture of methods. We do this in order to extend our understanding of the effect of binaries, particularly radio pulsars from Galactic DNSs, gravitational-waves, short gamma-ray bursts and (pulsational) PISNe. We also emphasise on the effect of binarity on astrophysical populations.

We performed rapid population synthesis studies in chapters 2 and 3. Chapter 2 discusses the formation of DNSs. We focussed on the effect that different physical parameters have on the resultant DNS population. We concluded that there are two features that are important to reproduce the observed Galactic DNS population: (i) mass transfer from a stripped post-helium-burning secondary on to a NS is more likely to be stable, and (ii) a bimodal natal kick distribution with a low ($\sigma \sim 30$ km s$^{-1}$) and high ($\sigma \sim 265$ km s$^{-1}$) component is preferred over a single high mode natal kick distribution. These two assumptions could be correlated; this correlation has been suggested in the literature in ultra-stripped SNe. Incorporating ultra-stripped SNe to our model allowed us to jointly reproduce the

period-eccentricity Galactic DNS and gravitational-wave mass distributions of the observed populations. The statistical framework used in chapter 2 favours the Fryer "delayed" supernova explosion mechanism, which has a continuous NS-BH remnant mass distribution, i.e. does not reproduce the first black-hole mass gap. The model variation using the Fryer "delayed" remnant mass prescription is the most likely to reproduce the Galactic DNS period-eccentricity distribution. On the other hand, we also showed that current supernova models used in chapter 2 struggle to reproduce the DNS mass distribution. A successful population synthesis model should be able to reproduce the full orbital parameters of the observed Galactic DNS population.

We studied previous evolutionary phases of DNSs in chapter 3, using the preferred model defined in the previous chapter 2. We catalogued the mass transfer phases leading to CEEs. We constrained orbital and donor properties at the onset of mass transfer. We find that there are, dominantly, two distinctive types of CEEs leading to DNSs. We proposed to use these findings and constrains as initial conditions for detailed simulation of CEEs. We also found that a significant amount of systems will not have time to circularise between the first moment of RLOF and the beginning of the CEE. This suggests that our current understanding of tidal interactions and orbital evolution during a mass transfer phase should be revisited.

It is important to note that there are several uncertainties in the underlying models used in chapters 2 and 3. The uncertainties in binary evolution are frequently discussed in the literature, including this thesis. However, there are other uncertainties which are worth mentioning. Single stellar models are a major uncertainty in population synthesis. These models are numerically expensive to simulate and usually contain very particular parameterisations of single stellar physics. Deviations from those parameterisations and more extensive collection of models require a particular framework and an extensive amount of work. In the case of massive single stars, the lack of observational constrains also makes these models difficult to

calibrate.

Other uncertainties are the properties of binaries at birth, usually referred to as initial distributions. The uncertainty on initial distributions comes from observations rather than theory. However, a better constraint on them will lead to more accurate initial conditions for both detailed model simulations and population studies.

Besides the rapid population synthesis approach, we performed a detailed stellar structure and composition study in chapter 4. We modeled Pulsational PISNe from a single and a merger model. While the properties of the core are very similar, the merger product has a significantly larger envelope, which is also very rich in hydrogen. We proposed a stellar merger leading to a Pulsational PISN as a progenitor for iPTF14hls. This proof-of-concept work also highlights the role of binaries and mergers in astrophysical transients, which is sometimes neglected or overly simplified. The natural evolution of this study is to investigate how changes in physical parameterisations of the models, such as metallicity and mass loss rates, affect the SN progenitor. This study would allow us to incorporate our findings to our population synthesis models and use them to predict rates. These rate predictions could be then be directly compared with the observed rates and help us undertand the main uncertainties in the physics.

Throughout this thesis we focussed on two particular scenarios: (i) massive binaries which form DCOs, particularly DNSs, and (ii) massive binaries which merge and become (pulsational) PISNe. The former was done in a rapid population synthesis approach and the latter using detailed stellar structure methods. Results from detailed simulations can be implemented in population synthesis models and vice versa. For example, details in the physics of DNS progenitors can be incorporated in the parameterised models to see how they affect synthesised populations. Some of the main uncertainties come from the lack of understanding of supernovae and

mass transfer phases, both from observations and theory. Detailed modeling of supernovae include computationally expensive hydrodynamic simulations which can be used to parameterise natal kicks and remnant mass distributions. Results from mass transfer simulations, including CEE evolution, can be used to parameterise the orbital evolution and post-mass-transfer properties of the component stars. These parameterisations can be included and tested with population synthesis studies.

The opposite approach is also possible: use results from population synthesis to decide what to simulate in more detail. Population studies give an understanding of the broad features of a population, which is useful to diagnose the parameter space of interest to model in detail. This not only constrains the parameter space of interest, but also highlights the more plausible physical configurations and initial conditions.

Population synthesis and detailed modeling must be used in complement to predict and corroborate astrophysical events. The combined strengths of both approaches can provide more rapid progress than the use of a single method. The combined method must be thought and developed holistically in order to make the best use of both. The efforts made in this thesis, alongside others in the literature, hint that the proposal of a combined method approach is plausible.

One of the main goals in the field for the coming years is to further understand and constrain the main uncertainties in the theory and observations of massive binaries. The growing number of observations of different astrophysical phenomena will be the main asset to do so. Gravitational-wave detections from DCO mergers have increased to a few tens since the detection of the first binary-black hole merger GW150914 [2]. The inferred mass distribution will allow us to test our binary evolution models, particularly natal kicks and remnant mass distribution from supernovae. Current and future radio observatories may provide additional infor-

mation of Galactic DNSs, which would increase our current sample and make our model comparison to observations more robust. Future gravitational-wave observatories with different frequency sensitivity bands, from mili-Hertz to micro-Hertz frequencies, could potentially detect some local DNSs. Optical observatories will increase number of transients associated to massive binary evolution. While future optical detections are expected, archival data is likely to contain a large number of interesting transients that have already been observed but not yet reported. The next few years will provide us with important observational constraints in massive binary evolution. The next decades will give us enough evidence to refine our current models or revisit the basics of massive binary evolution.

# Appendix A

# "On the formation history of Galactic double neutron stars"

This appendix is a reformatted copy of Vigna-Gómez et al. [299], published in MN-RAS and with arXiv number 1805.07974. My contribution to this work was to make the figures A.1 and A.2. Appendix A.1 was written by Simon Stevenson. Appendix A.2 was written by Bernhard Müller. All contents from appendix A.3 were written and created by Ilya Mandel. All appendices were edited by me.

## A.1  Likelihood calculation

Our methodology follows Andrews et al. [15]. We can write the base $e$ log-likelihood $\log \mathcal{L}$ as

$$\log \mathcal{L} = \sum_{b=1}^{N_{\mathrm{obs}}} \log\, p(\log P_b, e_b | M), \tag{A.1}$$

where $e_b$ and $\log P_b$ are the eccentricity and log of the orbital period in days for the $b$-th observed DNS, respectively; $N_{\mathrm{obs}} = 14$ observations were used here (see table I and associated discussion). The term $p(\log P_b, e_b|M)$ describes the likelihood of observing the $b$-th DNS given a model $M$, where our models are described in table 2.2 and shown in figure A.1. We therefore need a way of calculating the 2D probability density given the discrete simulated DNS binaries we have for each model.

We evolve the eccentricity and period of each simulated DNS as it emits gravitational radiation according to Peters [220]. We stop the inspiral evolution when the system either merges or reaches 10 Gyr (a proxy for the age of the Galactic thin disk, see [74]). We place systems into linearly spaced bins in eccentricity, with the lowest bin spanning $e \in [0, 10^{-4}]$, and determine the log period $\log P_k$ when the system enters each bin with eccentricity $e_k$ and the time the system spends in that bin $\Delta t_k$, which is subject to

$$\sum_k \Delta t_k = t_{\mathrm{delay}}. \tag{A.2}$$

We weigh the contribution of each binary at each point in its evolutionary history to the probability density map by $\Delta t_k$, since a system is more likely to be observed in the part of the orbit where it spends more of its time. Since tight, highly eccentric binaries evolve the fastest due to gravitational radiation, this has the effect of down weighting those binaries in our analysis (see figure 2.2).

We construct the probability density map from a discrete sample of simulated binaries by means of a weighted kernel density estimator. We found that density maps estimated via a 2D binned histogram, as used by Andrews et al. [15], were extremely sensitive to the chosen number of bins. We model the 2D probability

density as a sum of weighted Gaussians

$$p(\log P, e|M) = \sum_{j=1}^{n_{\text{binaries}}} \sum_{k=1}^{n_{\text{timesteps,j}}} \frac{\Delta t_k}{T} N(\boldsymbol{\mu}_k, \boldsymbol{\Sigma}_k), \tag{A.3}$$

where

$$T = \sum_{j=1}^{n_{\text{binaries}}} \sum_{k=1}^{n_{\text{timesteps,j}}} \Delta t_k = \sum_{j=1}^{n_{\text{binaries}}} t_{\text{delay,j}}; \tag{A.4}$$

$N(\boldsymbol{\mu}, \boldsymbol{\Sigma})$ is the 2D normal distribution with mean

$$\boldsymbol{\mu}_k = (\log P_k, e_k), \tag{A.5}$$

and the covariance $\boldsymbol{\Sigma}_k$ is chosen to be the same for all samples

$$\boldsymbol{\Sigma}_k = \begin{bmatrix} b_{\log P}^2 & 0 \\ 0 & b_e^2 \end{bmatrix}, \tag{A.6}$$

where $b_{\log P}$ and $b_e$ are the "rule-of-thumb" [261] bandwidth parameters which determine how much we 'smooth' the distribution. We choose $e_{\max} = 1$, $e_{\min} = 0$, $\log(P_{\min}/\text{days}) = -6$ and $\log(P_{\max}/\text{days}) = 4$ for our analysis.

The log-likelihoods fluctuate by $\mathcal{O}(1)$ depending on the choice of bandwidth. This systematic uncertainty in the estimated likelihoods arises because our theoretical distributions are built from a finite number of samples, and could be improved with larger simulation campaigns.
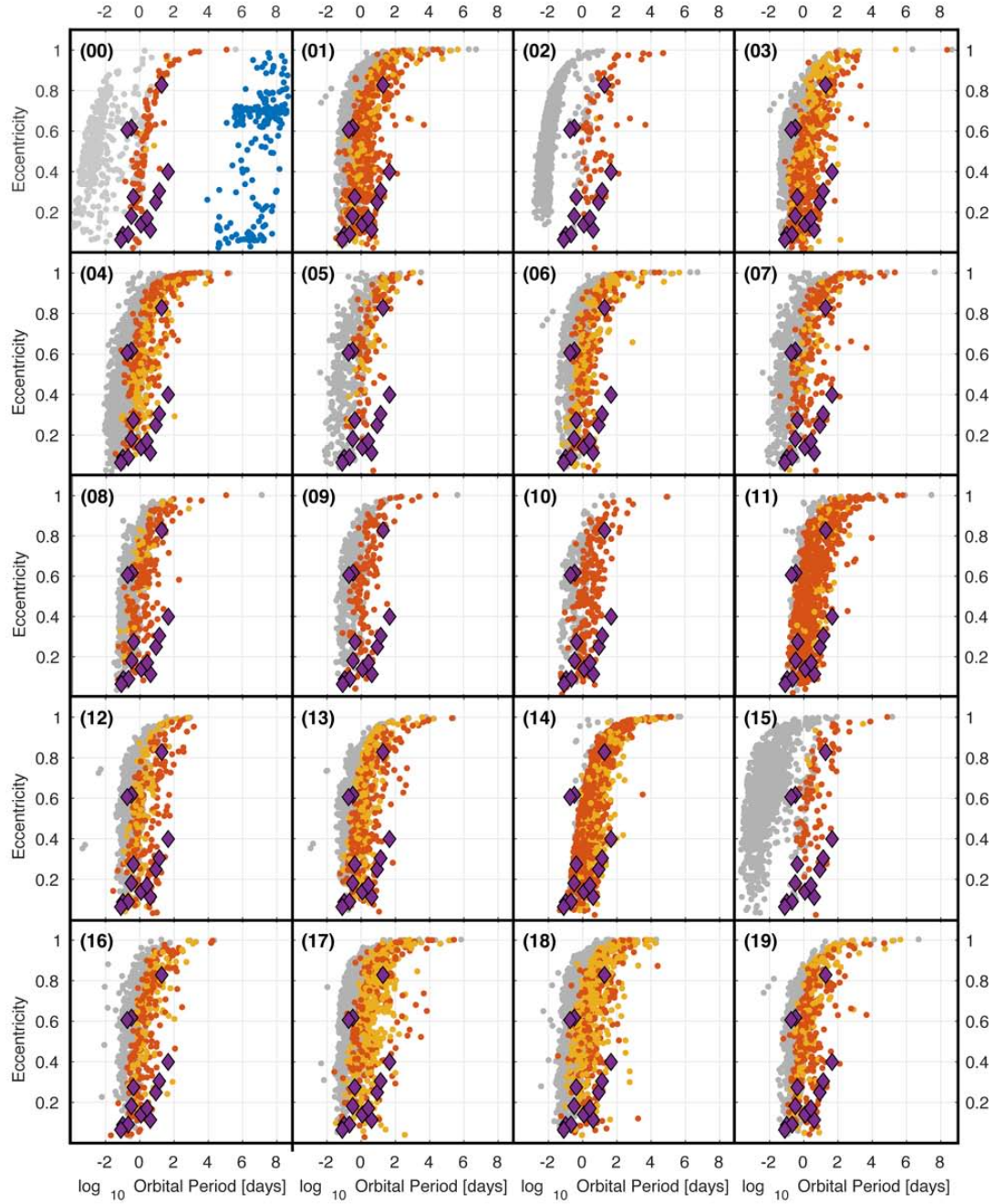
Figure A.1: Predicted period-eccentricity distribution of Galactic DNSs under the `Fiducial` model. Gray dots in the back are all DNSs at DCO formation. DCO period and eccentricity are evolved forward from birth until present age given gravitational-wave radiation emission, likely removing short-lived short-period binaries from the observable population. Coloured dots represent the DNS distribution at present age. Colour denotes the type of common envelope phase: blue for no CE phase, red for a single-core and yellow for a double-core common envelope phase. The single-core and double-core can be, in most cases, associated with *Channel I* and Channel II respectively (see section 2.4.1). Purple diamonds represent the observed Galactic DNS; all observed systems have precise period–eccentricity measurements with error bars within the thickness of the symbol.

# A.2 Model for the dependence of the kick velocity on explosion parameters

The most viable mechanism for producing sizeable kicks in core-collapse supernova explosions is the gravitational tug-boat mechanism, which relies on the acceleration of the neutron star due to the net gravitational pull exerted by anisotropic ejecta during the first few seconds after shock revival [254, 255, 198, 307]. Bray and Eldridge [42] suggested that this kick could be correlated with other explosion properties. An attempt to clarify these correlations based on the phenomenology of multi-dimensional simulations was then made by Janka [132], whose kick estimate we briefly review here, since it largely agrees with the one we developed for COM-PAS. Invoking total momentum conservation, Janka [132] considered the momentum $|\mathbf{p}_{\mathrm{ej}}|$ of the ejecta at a time when the kick asymptotes to its final value. Introducing an anisotropy parameter $\alpha_{\mathrm{kick}}$ to relate $|\mathbf{p}_{\mathrm{ej}}|$ to the spherical quasi-momentum of the ejecta as

$$\alpha_{\mathrm{kick}} = \frac{|\mathbf{p}_{\mathrm{ej}}|}{\int_{\mathrm{ejecta}} \rho |\mathbf{v}| \, dV}, \tag{A.7}$$

Janka [132] then invoked dimensional analysis to relate the ejecta (and neutron star) momentum to the kinetic energy $E_{\mathrm{kin}}$ and mass $m_{\mathrm{ej}}$ of the anisotropic ejecta behind the shock as

$$|\mathbf{p}_{\mathrm{ej}}| = \alpha_{\mathrm{kick}} \sqrt{2 E_{\mathrm{kin}} m_{\mathrm{ej}}}. \tag{A.8}$$

In the early phase when the kick is determined, $E_{\mathrm{kin}}$ is of the order of the diagnostic explosion energy $E_{\mathrm{expl}}$ (i.e. the net energy of unbound material), within a factor of 2–3 in recent 3D neutrino hydrodynamics simulations. Unlike Janka [132], we

simply identify $E_{kin}$ and $E_{expl}$ so that we obtain the kick velocity $v_{kick}$ as

$$v_{kick} = \frac{\alpha_{kick}\sqrt{2E_{expl}m_{ej}}}{m_{NS}}, \tag{A.9}$$

where $m_{NS}$ is the gravitational neutron star mass. To obtain $m_{ej}$, Janka [132] related $E_{expl}$ to the mass $m_\nu$ of the *neutrino–heated* ejecta via the nucleon recombination energy and then expressed $m_{ej}$ as a multiple thereof. The semi-analytical models of Müller et al. [190] directly predict $m_{ej}$, $E_{expl}$ and $m_{NS}$ (see below), up to parameters based on 3D simulations and observational constraints. These parameters are calibrated slightly differently than in Müller et al. [190] (see section 2.4.2). We can therefore work directly with equation (A.9).

Equation (A.9) needs to be evaluated at the time when the kick asymptotes to its final value. One possibility, suggested by Janka [132], is to relate the freeze-out of the kick to the termination of accretion onto the neutron star, which happens roughly when the post-shock velocity equals the escape velocity [181, 190]; this is the criterion we adopt here.

Our key assumption is that the expectation value of the anisotropy parameter $\alpha_{kick}$ is independent of the progenitor. This is based on the observation that three-dimensional explosion models [185, 162, 191] with multi-group neutrino transport typically develop unipolar or bipolar explosions, i.e. there is limited variation in explosion geometry. Moreover, there is a convergence to similar turbulent Mach number around [274] and after shock revival, which implies a similar density contrast between the under–dense neutrino-heated bubbles and the surrounding down flows. This is somewhat dissimilar from parameterised models [307], which show larger variations in $\alpha_{kick}$ because they can vary the explosion energy independently of the progenitor structure.

While the assumption of uniform $\alpha_{\mathrm{kick}}$ is well motivated, some caveats about its limitations are in order. Even though the distribution of $\alpha_{\mathrm{kick}}$ may be relatively uniform across different progenitors (which remains to be confirmed by more 3D explosion models), $\alpha_{\mathrm{kick}}$ will show stochastic variations. Moreover, supernova models for progenitors with small O/C cores are characterised by medium-scale asymmetries [303, 186] instead of unipolar/bipolar modes during the explosion phase.

Since theoretical arguments can only constrain the assumed uniform value of $\alpha_{\mathrm{kick}}$ within an order of magnitude, calibration is still required to roughly match the observed distribution of neutron star kicks. The fit formulae presented below are based on a normalisation $\alpha_{\mathrm{kick}} = 0.08$ that yields a match to the observed kick distribution of Hobbs et al. [119].

For the neutron star mass $m_{\mathrm{NS}}$, we use

$$\frac{m_{\mathrm{NS}}}{\mathrm{M}_\odot} = \begin{cases} 1.21 - 0.40(m_{\mathrm{O/C}} - 1.372), & 1.37 \le m_{\mathrm{O/C}} < 1.49 \\ 1.16, & 1.49 \le m_{\mathrm{O/C}} < 1.65 \\ 1.32 + 0.30(m_{\mathrm{O/C}} - 1.65), & 1.65 \le m_{\mathrm{O/C}} < 2.40 \\ 1.42 + 0.70(m_{\mathrm{O/C}} - 2.4), & 2.40 \le m_{\mathrm{O/C}} < 3.20 \\ 1.32 + 0.25(m_{\mathrm{O/C}} - 3.2), & 3.20 \le m_{\mathrm{O/C}} < 3.60 \\ 1.50, & 4.05 \le m_{\mathrm{O/C}} < 4.60 \\ 1.64 - 0.20(m_{\mathrm{O/C}} - 5.7), & 5.70 \le m_{\mathrm{O/C}} < 6.00 \end{cases} \quad , \tag{A.10}$$

where $m_{\mathrm{O/C}}$ is the O/C core mass in units of $\mathrm{M}_\odot$. BH formation is assumed to happen for $3.6 \le m_{\mathrm{O/C}} < 4.05$, $4.6 \le m_{\mathrm{O/C}} < 5.7$, and $m_{\mathrm{O/C}} > 6.0$.
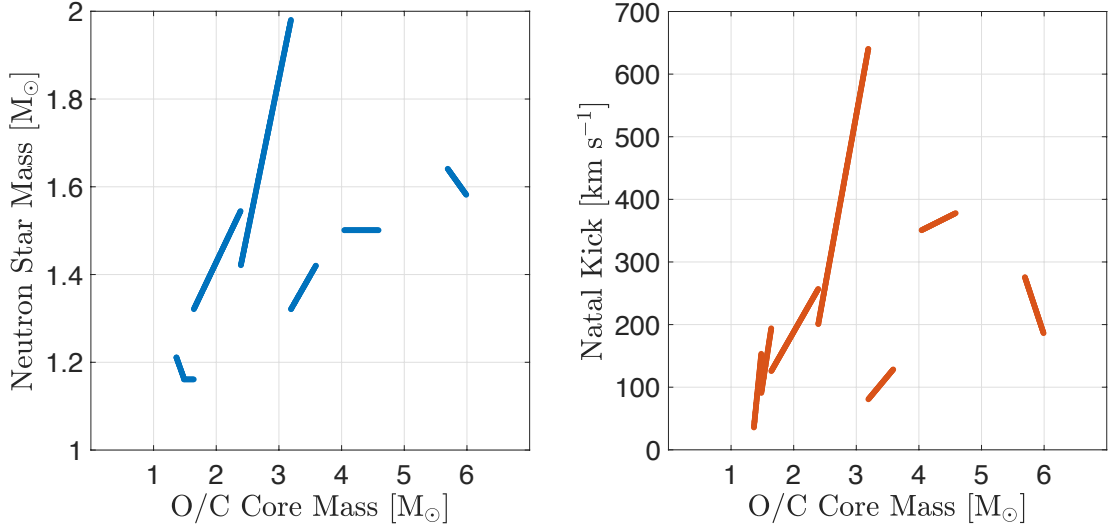
Figure A.2: Müller supernova prescription of the best-fitting relation to the models described by Müller et al. [190] with parameters adjusted for better agreement with inferred supernova progenitor masses [263]. Gravitational mass (left) and natal kick (right) of the neutron star as a function of the carbon–oxygen core mass. BH formation is assumed to happen for $3.6 \leq m_{O/C} < 4.05$, $4.6 \leq m_{O/C} < 5.7$, and $m_{O/C} > 6.0$, where $m_{O/C}$ is the oxygen–carbon core mass in $M_\odot$ units.

The natal kicks are computed as

$$\frac{v_{\text{kick}}}{\text{km s}^{-1}} = \begin{cases} 35 + 1000(m_{O/C} - 1.372), & 1.37 \leq m_{O/C} < 1.49 \\ 90 + 650(m_{O/C} - 1.49), & 1.49 \leq m_{O/C} < 1.65 \\ 100 + 175(m_{O/C} - 1.65), & 1.65 \leq m_{O/C} < 2.40 \\ 200 + 550(m_{O/C} - 2.4), & 2.40 \leq m_{O/C} < 3.20 \\ 80 + 120(m_{O/C} - 3.2), & 3.20 \leq m_{O/C} < 3.60 \\ 350 + 50(m_{O/C} - 4.05), & 4.05 \leq m_{O/C} < 4.60 \\ 275 - 300(m_{O/C} - 5.7), & 5.70 \leq m_{O/C} < 6.00 \end{cases} . \tag{A.11}$$

## A.3   Movement in the Galactic potential

Double neutron star centre-of-mass velocities in our `Fiducial` model, in which the second supernova is typically a USSN with a low natal kick, are dominated by the Blaauw kick received as a result of the mass loss accompanying the collapse of the secondary. This kick is proportional to the orbital velocity of the secondary before the collapse, which is greatest for the most compact binaries. Therefore, the binary's velocity is anti-correlated with the coalescence time, as shown on the left panel of figure A.3. If the USSN progenitors are stripped even deeper than in COMPAS models during case BB mass transfer [281], as discussed in section 2.5, the mass lost during the supernova and the associated Blaauw kick would be further reduced.

These kicks have the effect of broadening the distribution of observed DNS systems in the Galaxy. We assume that each DNS is formed in the thin disk, at $z = 0$ in cylindrical coordinates, with a radial distribution proportional to the disk mass projected onto the Galactic equatorial plane. We use model 2 of Irrgang et al. [126] for the Galactic matter distribution and total gravitational potential. We do not account for scattering in this simplified analysis; while dynamical heating would increase the scale height of older populations, it does not appreciably impact the distribution of distances from the Galactic centre, which we estimate here. After choosing a random initial location for the binary as above, we apply an additional initial velocity relative to the local rotational velocity with a magnitude equal to the binary's simulated kick velocity and a random direction. The trajectory of the binary in the Galactic potential is solved with a Runge-Kutta integrator. We sample the binary's subsequent motion at fixed time intervals between birth and merger (or a maximum age of 10 Gyr). The right panel of figure A.3 shows the cumulative distribution function of the birth location, and the broader cumulative distribution function at which DNS systems are expected to reside for a snapshot of all DNS
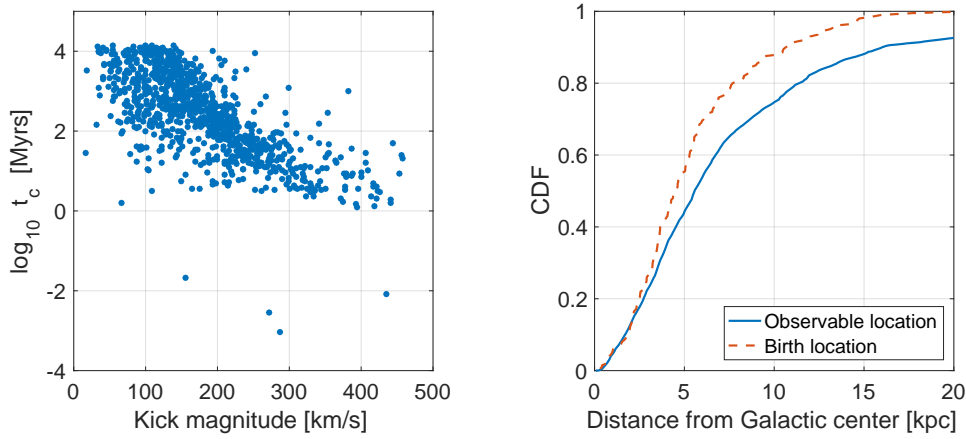
Figure A.3: Scatter plot of the binary coalescence time against the DNS kicks magnitude in the `Fiducial` model (left panel). DNS kicks are dominated by the Blaauw kick during the collapse of the secondary, which is proportional to the orbital velocity of the progenitor and therefore inversely correlated with the coalescence time of the binary. These kicks spread the binaries in the Milky Way gravitational potential relative to birth sites, which are presumed to be in the disk plane (cumulative distribution function of the Galacto-centric distance for binaries born in the disk is shown in the right panel).

existing at the present moment. The broadening of the distribution would be more significant in shallower gravitational potentials of less massive galaxies, which are probed with short GRBs.

# Appendix B

# "Massive stellar mergers as precursors of hydrogen-rich Pulsational Pair Instability Supernovae"

I wrote this appendix and created all the figures on it. All the contents of this appendix were created for this thesis.

## B.1 Detail on stellar models

In chapter 4 we compared a single and a merger model; figure 4.3 shows the structure in a Kippenhahn diagram, while figure 4.4 shows a summary of the composition. We use this appendix to show additional details on the structure of our models.
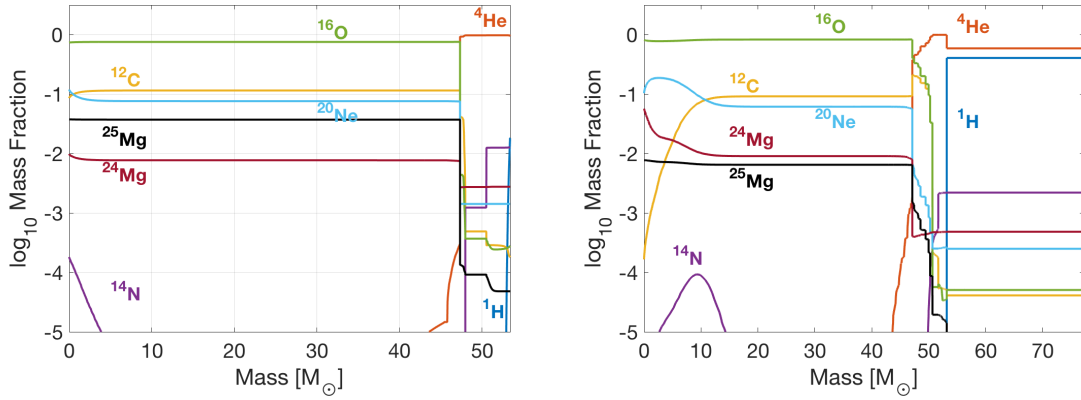
Figure B.1: Chemical composition when the star reaches a central temperature $T_c \approx 10^9$ K for the 95 $M_\odot$ single (left) and 60+60 $M_\odot$ merger (right) models, both with $\approx 1$ yr left before the first pulse. The merger model has a more massive and hydrogen-rich envelope than the single one.

To simulate the models we used the `mesa_67.net` nuclear network, which includes 67 isotopes. Figure 4.4 of chapter 4 shows only hydrogen, helium and O/C. Figure B.1 shows more detailed chemical composition profiles including $^1$H, $^4$He, $^{12}$C, $^{14}$N, $^{16}$O, $^{20}$Ne, $^{24}$Mg and $^{25}$Mg; heavier isotopes are not shown within the scale of this figure. The quantitative and qualitative composition analysis of chapter 4 was made using the profiles displayed in figure B.1.

Chapter 4 reports results at the moment when $T_c \approx 10^9$ K. In reality, we kept evolving each model until the beginning of oxygen deflagration, which is the beginning of the sub-sonic oxygen burning front. Both models crashed shortly after this stage, when the spatial and time resolutions become finer and need to be solved using detailed hydrodynamics methods. Figure B.2 shows the rapid increase in temperature and power emission during this later stages. This rapid increase is expected for pulsational PISN progenitors, which are believed to leave a black hole remnant. A more rapid and overal energetic curve is expected for the canonical PISN, which is believed to leave no remnant.
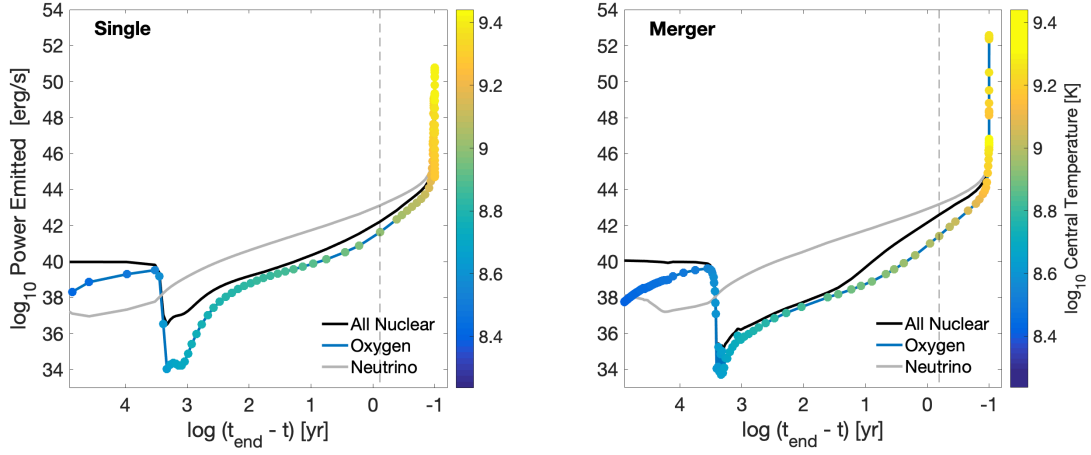
Figure B.2: Power emitted as a function of time before the first pulse, for the 95 $M_\odot$ single model post-main-sequence evolution (left) and the 60+60 $M_\odot$ merger model post-merger evolution (right). Power from all nuclear reactions is shown in black. Power from reactions involving oxygen fusion is in blue, with coloured circles representing the central temperature at that moment (the colour scale goes from lower temperatures in blue to higher temperatures in yellow). Power transported out by thermal and nuclear neutrinos is in grey. The dashed vertical line on each plot shows the moment when the central temperature reaches $T_{\rm c} \approx 10^9$ K: the rate of reactions involving oxygen fusion increases significantly beyond that point, as expected from pulsational PISN progenitors at late stages.

# B.2   Visualisation of rate estimates

In figure B.3 we make a visual comparison between the observational iPTF14hls-like event rates, pulsational PISNe rates according to other studies and pulsational PISNe from our proposed merger channel.

We estimate rates from our channel using a Drake-like equation 4.1: $\mathcal{R} = f_{\rm binarity} \times f_{\rm primary} \times f_{\rm secondary} \times f_{\rm separation}$. To determine the optimistic $f_{\rm primary}$ factor, we evolve a small grid of single stars at $Z = Z_{\rm SMC}$ from ZAMS to terminal-age main sequence. The one-dimensional grid spans the ZAMS mass space with $30 \leq M_{\rm ZAMS}/{\rm M}_\odot \leq 70$. Once the stars reach terminal-age main sequence, we stop the evolution and estimate the helium core mass. Given that this is the optimistic approach, we simulate a $q = 1$ merger without mass loss. We then compare the

post-merger helium core masses to the ones leading to pulsational PISN according to Woosley [308]. This gives us mass limits of $[M_{\text{primary,min}}, M_{\text{primary,max}}] = [40, 64]$ $M_\odot$. We illustrate this rationale in figure B.4.

We also estimate an empirical rate based on the observation of R139, which we predict will explode as a hydrogen-rich pulsation PISN (for more details see section 4.4). To do so, we assume a local continuous star formation rate and that the merger occurs roughly within the volume of a Milky-Way Equivalent Galaxy (MWEG). Given this single system we would expect a local rate of hydrogen-rich pulsation PISN to be $\mathcal{R}_{\text{HPPSIN,local}} = 1 \times \tau_{\text{merge}}^{-1}$ MWEG$^{-1}$, where $\tau_{\text{explosion}}$ is the time it takes the system between formation and explosion. According to the stellar models from chapter 4, $\tau_{\text{explosion}} \approx 4$ Myrs. If we compare this to the observed local CCSNe rate, $\mathcal{R}_{\text{CCSN,local}} = \frac{1}{100}$ yr$^{-1}$ MWEG$^{-1}$, we get the empirical rate $\mathcal{R}_{\text{empirical}} = \mathcal{R}_{\text{HPPISN,local}}/\mathcal{R}_{\text{CCSN,local}} \approx 2.5 \times 10^{-5}$. This suggests that $\approx 1$ of every $\approx 10^5$ SNe would be a hydrogen-rich pulsational PISN. This empirical rate lies between the estimates from section 4.3.3, which predicts a range of rate of pulsational PISNe between $1.3 \times 10^{-5} \leq \mathcal{R} \leq 3.2 \times 10^{-3}$ CCSN$^{-1}$.

$$f_{\text{binary}} \quad \times \quad f_{\text{primary}} \quad \times \quad f_{\text{secondary}} \quad \times \quad f_{\text{separation}} = \mathcal{R}$$
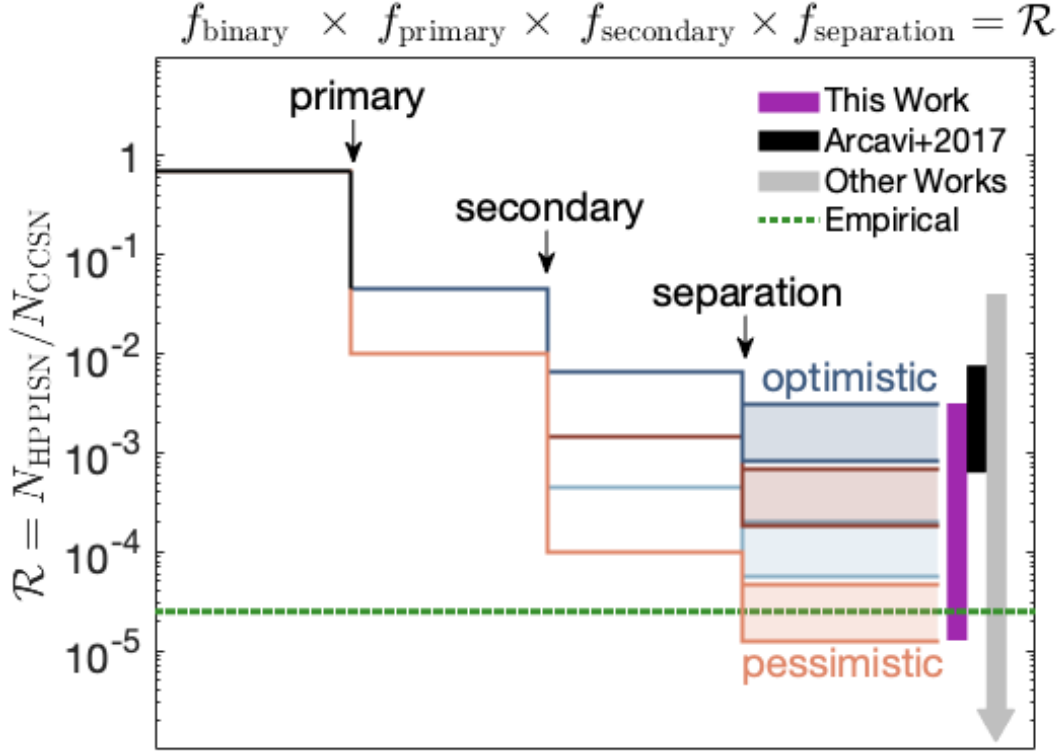
Figure B.3: Diagram illustrating our rate estimate for post-merger pulsational PISN events, presented as a fraction $\mathcal{R}$ of the total rate of CCSNe. Reading left-to-right, each downward step shows the result of an additional requirement for the systems which produce pulsational PISNe via mergers. At each step we show outcomes for optimistic and pessimistic assumptions. The first step represents the restricted mass range of primary stars in binaries which can lead to pulsational PISNe, the second the suitable mass range of secondary stars in each binary, and the third step our assumptions for the range of binary separations at which a suitable merger can occur. The shaded regions indicate the range of uncertainty in $\mathcal{R}$, with the most optimistic and pessimistic combinations of assumptions presented spanning more than two orders of magnitude (vertical purple bar). This estimate is consistent with the empirical estimate for iPTF14hls-like events at all metallicities [16, 260] (vertical black bar). Theoretical rate estimates for single pulsational PISNe at this metallicity start from above our rate estimate but extend down to zero [308, 266, 26] (vertical grey arrow). We also include in a green-dashed line the empirical rate based on the observed candidate R139 as estimated in appendix B.2.
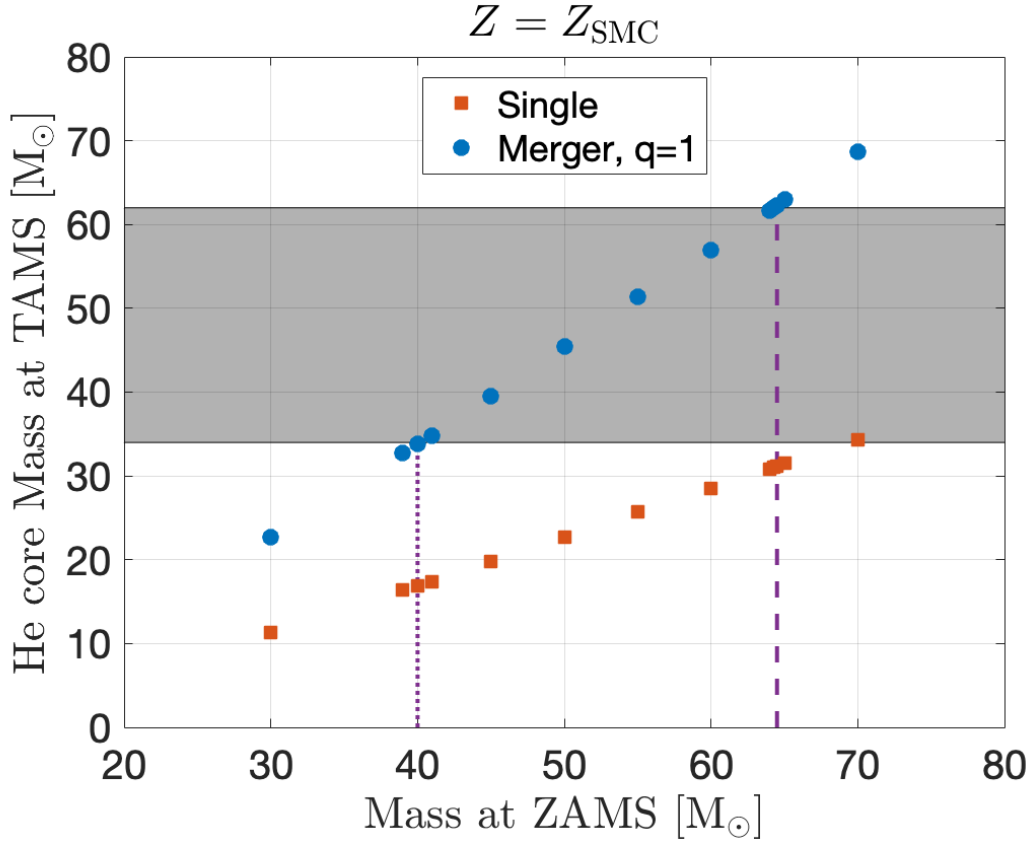
Figure B.4: Comparison between ZAMS mass (horizontal axis) against helium core mass at terminal-age main sequence (vertical axis). Red squares correspond to single stars. Blue circles correspond to a terminal-age main sequence merger product of a binary with mass ratio unity, i.e. twice the mass of the single stellar models. Grey shaded region corresponds to the helium core mass ranges leading to pulsational PISN according to Woosley [308]. Purple vertical lines correspond to the primary mass limits. The lower limit corresponds to the dotted line at $M_{\mathrm{ZAMS}}/\mathrm{M}_\odot = 40$. The upper limit corresponds to the dashed line at $M_{\mathrm{ZAMS}}/\mathrm{M}_\odot = 64$. Data courtesy of Ellen Butler.

# Bibliography

[1] J. Abadie et al. Predictions for the Rates of Compact Binary Coalescences Observable by Ground-based Gravitational-wave Detectors. *Classical and Quantum Gravity*, 27(17):173001–+, Sept. 2010. doi: 10.1088/0264-9381/27/17/173001.

[2] B. P. Abbott, R. Abbott, T. D. Abbott, M. R. Abernathy, F. Acernese, K. Ackley, C. Adams, T. Adams, P. Addesso, R. X. Adhikari, and et al. Observation of Gravitational Waves from a Binary Black Hole Merger. *Physical Review Letters*, 116(6):061102, Feb. 2016. doi: 10.1103/PhysRevLett.116.061102.

[3] B. P. Abbott, R. Abbott, T. D. Abbott, M. R. Abernathy, F. Acernese, K. Ackley, C. Adams, T. Adams, P. Addesso, R. X. Adhikari, and et al. GW151226: Observation of Gravitational Waves from a 22-Solar-Mass Binary Black Hole Coalescence. *Physical Review Letters*, 116(24):241103, June 2016. doi: 10.1103/PhysRevLett.116.241103.

[4] B. P. Abbott, R. Abbott, T. D. Abbott, M. R. Abernathy, F. Acernese, K. Ackley, C. Adams, T. Adams, P. Addesso, R. X. Adhikari, and et al. Binary Black Hole Mergers in the First Advanced LIGO Observing Run. *Physical Review X*, 6(4):041015, Oct. 2016. doi: 10.1103/PhysRevX.6.041015.

[5] B. P. Abbott, R. Abbott, T. D. Abbott, F. Acernese, K. Ackley, C. Adams, T. Adams, P. Addesso, R. X. Adhikari, V. B. Adya, and et al. GW170104:

Observation of a 50-Solar-Mass Binary Black Hole Coalescence at Redshift
0.2. *Physical Review Letters*, 118(22):221101, June 2017. doi: 10.1103/
PhysRevLett.118.221101.

[6] B. P. Abbott, R. Abbott, T. D. Abbott, F. Acernese, K. Ackley, C. Adams,
T. Adams, P. Addesso, R. X. Adhikari, V. B. Adya, and et al. GW170608:
Observation of a 19 Solar-mass Binary Black Hole Coalescence. *ApJ*, 851(2):
L35, Dec 2017. doi: 10.3847/2041-8213/aa9f0c.

[7] B. P. Abbott, R. Abbott, T. D. Abbott, F. Acernese, K. Ackley, C. Adams,
T. Adams, P. Addesso, R. X. Adhikari, V. B. Adya, and et al. GW170814:
A Three-Detector Observation of Gravitational Waves from a Binary Black
Hole Coalescence. *Physical Review Letters*, 119(14):141101, Oct. 2017. doi:
10.1103/PhysRevLett.119.141101.

[8] B. P. Abbott, R. Abbott, T. D. Abbott, F. Acernese, K. Ackley, C. Adams,
T. Adams, P. Addesso, R. X. Adhikari, V. B. Adya, and et al. GW170817: Ob-
servation of Gravitational Waves from a Binary Neutron Star Inspiral. *Physi-
cal Review Letters*, 119(16):161101, Oct. 2017. doi: 10.1103/PhysRevLett.119.
161101.

[9] B. P. Abbott, R. Abbott, T. D. Abbott, F. Acernese, K. Ackley, C. Adams,
T. Adams, P. Addesso, R. X. Adhikari, V. B. Adya, and et al. Gravitational
waves and gamma-rays from a binary neutron star merger: Gw170817 and grb
170817a. *The Astrophysical Journal Letters*, 848(2):L13, 2017.

[10] B. P. Abbott, R. Abbott, T. D. Abbott, F. Acernese, K. Ackley, C. Adams,
T. Adams, P. Addesso, R. X. Adhikari, V. B. Adya, and et al. Multi-messenger
observations of a binary neutron star merger. *Astrophys. J. Lett*, 848(2):L12,
2017.

[11] H. A. Abt. Normal and abnormal binary frequencies. *ARA&A*, 21:343–372, Jan 1983. doi: 10.1146/annurev.aa.21.090183.002015.

[12] L. A. Almeida, H. Sana, W. Taylor, R. Barbá, A. Z. Bonanos, P. Crowther, A. Damineli, A. de Koter, S. E. de Mink, C. J. Evans, M. Gieles, N. J. Grin, V. Hénault-Brunet, N. Langer, D. Lennon, S. Lockwood, J. Maíz Apellániz, A. F. J. Moffat, C. Neijssel, C. Norman, O. H. Ramírez-Agudelo, N. D. Richardson, A. Schootemeijer, T. Shenar, I. Soszyński, F. Tramper, and J. S. Vink. The Tarantula Massive Binary Monitoring. I. Observational campaign and OB-type spectroscopic binaries. *A&A*, 598:A84, Feb. 2017. doi: 10.1051/0004-6361/201629844.

[13] L. G. Althaus, A. H. Córsico, J. Isern, and E. García-Berro. Evolutionary and pulsational properties of white dwarf stars. *A&A Rev.*, 18(4):471–566, Oct 2010. doi: 10.1007/s00159-010-0033-1.

[14] S. B. Anderson, P. W. Gorham, S. R. Kulkarni, T. A. Prince, and A. Wolszczan. Discovery of two radio pulsars in the globular cluster M15. *Nature*, 346:42–44, July 1990. doi: 10.1038/346042a0.

[15] J. J. Andrews, W. M. Farr, V. Kalogera, and B. Willems. Evolutionary Channels for the Formation of Double Neutron Stars. *ApJ*, 801:32, Mar. 2015. doi: 10.1088/0004-637X/801/1/32.

[16] I. Arcavi, D. A. Howell, D. Kasen, L. Bildsten, G. Hosseinzadeh, C. McCully, Z. C. Wong, S. R. Katz, A. Gal-Yam, J. Sollerman, F. Taddia, G. Leloudas, C. Fremling, P. E. Nugent, A. Horesh, K. Mooley, C. Rumsey, S. B. Cenko, M. L. Graham, D. A. Perley, E. Nakar, N. J. Shaviv, O. Bromberg, K. J. Shen, E. O. Ofek, Y. Cao, X. Wang, F. Huang, L. Rui, T. Zhang, W. Li, Z. Li, J. Zhang, S. Valenti, D. Guevel, B. Shappee, C. S. Kochanek, T. W.-S. Holoien, A. V. Filippenko, R. Fender, A. Nyholm, O. Yaron, M. M. Kasli-

wal, M. Sullivan, N. Blagorodnova, R. S. Walters, R. Lunnan, D. Khazov, I. Andreoni, R. R. Laher, N. Konidaris, P. Wozniak, and B. Bue. Energetic eruptions leading to a peculiar hydrogen-rich explosion of a massive star. *Nature*, 551:210–213, Nov. 2017. doi: 10.1038/nature24030.

[17] P. Artymowicz and S. H. Lubow. Dynamics of binary-disk interaction. 1: Resonances and disk gap sizes. *ApJ*, 421:651–667, Feb. 1994. doi: 10.1086/173679.

[18] M. Asplund, N. Grevesse, A. J. Sauval, and P. Scott. The Chemical Composition of the Sun. *ARA&A*, 47:481–522, Sept. 2009. doi: 10.1146/annurev.astro.46.060407.145222.

[19] C. D. Bailyn, R. K. Jain, P. Coppi, and J. A. Orosz. The Mass Distribution of Stellar Black Holes. *ApJ*, 499(1):367–374, May 1998. doi: 10.1086/305614.

[20] Z. Barkat, G. Rakavy, and N. Sack. Dynamics of supernova explosion resulting from pair formation. *Physical Review Letters*, 18(10):379, 1967.

[21] J. W. Barrett, S. M. Gaebel, C. J. Neijssel, A. Vigna-Gómez, S. Stevenson, C. P. L. Berry, W. M. Farr, and I. Mandel. Accuracy of inference on the physics of binary evolution from gravitational-wave observations. *MNRAS*, 477(4):4685–4695, Jul 2018. doi: 10.1093/mnras/sty908.

[22] K. Belczyński and T. Bulik. The effect of supernova natal kicks on compact object merger rate. *A&A*, 346:91–100, June 1999.

[23] K. Belczynski, V. Kalogera, and T. Bulik. A Comprehensive Study of Binary Compact Objects as Gravitational Wave Sources: Evolutionary Channels, Rates, and Physical Properties. *ApJ*, 572:407–431, June 2002. doi: 10.1086/340304.

[24] K. Belczynski, V. Kalogera, F. A. Rasio, R. E. Taam, A. Zezas, T. Bulik, T. J. Maccarone, and N. Ivanova. Compact Object Modeling with the StarTrack Population Synthesis Code. *ApJS*, 174:223-260, Jan. 2008. doi: 10.1086/521026.

[25] K. Belczynski, M. Dominik, T. Bulik, R. O'Shaughnessy, C. Fryer, and D. E. Holz. The Effect of Metallicity on the Detection Prospects for Gravitational Waves. *ApJ*, 715(2):L138–L141, Jun 2010. doi: 10.1088/2041-8205/715/2/L138.

[26] K. Belczynski, A. Heger, W. Gladysz, A. J. Ruiter, S. Woosley, G. Wiktorowicz, H.-Y. Chen, T. Bulik, R. O'Shaughnessy, D. E. Holz, C. L. Fryer, and E. Berti. The effect of pair-instability mass loss on black-hole mergers. *A&A*, 594:A97, Oct. 2016. doi: 10.1051/0004-6361/201628980.

[27] K. Belczynski, D. E. Holz, T. Bulik, and R. O'Shaughnessy. The first gravitational-wave source from the isolated evolution of two stars in the 40-100 solar mass range. *Nature*, 534:512–515, June 2016. doi: 10.1038/nature18322.

[28] K. Belczynski, A. Askar, M. Arca-Sedda, M. Chruslinska, M. Donnari, M. Giersz, M. Benacquista, R. Spurzem, D. Jin, G. Wiktorowicz, and D. Belloni. The origin of the first neutron star - neutron star merger. *A&A*, 615: A91, July 2018. doi: 10.1051/0004-6361/201732428.

[29] K. Belczyński and V. Kalogera. A new formation channel for double neutron stars without recycling: Implications for gravitational wave detection. *The Astrophysical Journal Letters*, 550(2):L183, 2001. URL `http://stacks.iop.org/1538-4357/550/i=2/a=L183`.

[30] M. Benacquista. *An Introduction to the Evolution of Single and Binary Stars.* 2013. doi: 10.1007/978-1-4419-9991-7.

[31] P. Beniamini and T. Piran. Formation of double neutron star systems as implied by observations. *MNRAS*, 456:4089–4099, Mar. 2016. doi: 10.1093/ mnras/stv2903.

[32] E. Berger. Short-Duration Gamma-Ray Bursts. *ARA&A*, 52:43–105, Aug. 2014. doi: 10.1146/annurev-astro-081913-035926.

[33] D. Bhattacharya and E. P. J. van den Heuvel. Formation and evolution of binary and millisecond radio pulsars. *Phys. Rep.*, 203:1–124, 1991. doi: 10. 1016/0370-1573(91)90064-S.

[34] A. Blaauw. On the origin of the O- and B-type stars with high velocities (the "run-away" stars), and some related problems. *Bull. Astron. Inst. Netherlands*, 15:265, May 1961.

[35] N. Blagorodnova, R. Kotak, J. Polshaw, M. M. Kasliwal, Y. Cao, A. M. Cody, G. B. Doran, N. Elias-Rosa, M. Fraser, C. Fremling, C. Gonzalez-Fernandez, J. Harmanen, J. Jencson, E. Kankare, R.-P. Kudritzki, S. R. Kulkarni, E. Magnier, I. Manulis, F. J. Masci, S. Mattila, P. Nugent, P. Ochner, A. Pastorello, T. Reynolds, K. Smith, J. Sollerman, F. Taddia, G. Terreran, L. Tomasella, M. Turatto, P. M. Vreeswijk, P. Wozniak, and S. Zaggia. Common Envelope Ejection for a Luminous Red Nova in M101. *ApJ*, 834:107, Jan. 2017. doi: 10.3847/1538-4357/834/2/107.

[36] S. I. Blinnikov, I. D. Novikov, T. V. Perevodchikova, and A. G. Polnarev. Exploding Neutron Stars in Close Binaries. *Soviet Astronomy Letters*, 10: 177–179, Apr 1984.

[37] E. Böhm-Vitense. Über die wasserstoffkonvektionszone in sternen verschiedener effektivtemperaturen und leuchtkräfte. mit 5 textabbildungen. *Zeitschrift fur Astrophysik*, 46:108, 1958.

[38] A. Z. Bonanos, K. Z. Stanek, A. Udalski, L. Wyrzykowski, K. Żebruń, M. Kubiak, M. K. Szymański, O. Szewczyk, G. Pietrzyński, and I. Soszyński. WR 20a Is an Eclipsing Binary: Accurate Determination of Parameters for an Extremely Massive Wolf-Rayet System. *ApJ*, 611:L33–L36, Aug. 2004. doi: 10.1086/423671.

[39] H. E. Bond. Pre-Cataclysmic Binaries. In D. Q. Lamb and J. Patterson, editors, *Cataclysmic Variables and Low-Mass X-ray Binaries*, page 15, Jan 1985. doi: 10.1007/978-94-009-5319-2_2.

[40] S. Bowyer, E. Byram, T. Chubb, and H. Friedman. Cosmic x-ray sources. *Science*, 147(3656):394–398, 1965.

[41] N. Brandt and P. Podsiadlowski. The effects of high-velocity supernova kicks on the orbital properties and sky distributions of neutron-star binaries. *MNRAS*, 274:461–484, May 1995. doi: 10.1093/mnras/274.2.461.

[42] J. C. Bray and J. J. Eldridge. Neutron star kicks and their relationship to supernovae ejecta mass. *MNRAS*, 461:3747–3759, Oct. 2016. doi: 10.1093/mnras/stw1275.

[43] F. S. Broekgaarden, S. Justham, S. E. de Mink, J. Gair, I. Mandel, S. Stevenson, J. W. Barrett, A. Vigna-Gómez, and C. J. Neijssel. Stroopwafel: Simulating rare outcomes from astrophysical populations, with application to gravitational-wave sources. *arXiv preprint arXiv:1905.00910*, 2019.

[44] I. Brott, S. E. de Mink, M. Cantiello, N. Langer, A. de Koter, C. J. Evans, I. Hunter, C. Trundle, and J. S. Vink. Rotating massive main-sequence stars. I. Grids of evolutionary models and isochrones. *A&A*, 530:A115, June 2011. doi: 10.1051/0004-6361/201016113.

[45] G. E. Brown. Neutron star accretion and binary pulsar formation. *ApJ*, 440: 270–279, Feb. 1995. doi: 10.1086/175268.

[46] A. D. Cameron, D. J. Champion, M. Kramer, M. Bailes, E. D. Barr, C. G. Bassa, S. Bhandari, N. D. R. Bhat, M. Burgay, S. Burke-Spolaor, R. P. Eatough, C. M. L. Flynn, P. C. C. Freire, A. Jameson, S. Johnston, R. Karuppusamy, M. J. Keith, L. Levin, D. R. Lorimer, A. G. Lyne, M. A. McLaughlin, C. Ng, E. Petroff, A. Possenti, A. Ridolfi, B. W. Stappers, W. van Straten, T. M. Tauris, C. Tiburzi, and N. Wex. The High Time Resolution Universe Pulsar Survey - XIII. PSR J1757-1854, the most accelerated binary pulsar. *MNRAS*, 475:L57–L61, Mar. 2018. doi: 10.1093/mnrasl/sly003.

[47] M. Cantiello, S. C. Yoon, N. Langer, and M. Livio. Binary star progenitors of long gamma-ray bursts. *A&A*, 465(2):L29–L33, Apr 2007. doi: 10.1051/0004-6361:20077115.

[48] L. Chamandy, A. Frank, E. G. Blackman, J. Carroll-Nellenback, B. Liu, Y. Tu, J. Nordhaus, Z. Chen, and B. Peng. Accretion in common envelope evolution. *MNRAS*, 480:1898–1911, Oct. 2018. doi: 10.1093/mnras/sty1950.

[49] D. J. Champion, D. R. Lorimer, M. A. McLaughlin, J. M. Cordes, Z. Arzoumanian, J. M. Weisberg, and J. H. Taylor. PSR J1829+2456: a relativistic binary pulsar. *MNRAS*, 350:L61–L65, June 2004. doi: 10.1111/j.1365-2966.2004.07862.x.

[50] S. Chandrasekhar. The highly collapsed configurations of a stellar mass (Second paper). *MNRAS*, 95:207–225, Jan 1935. doi: 10.1093/mnras/95.3.207.

[51] S. Chandrasekhar. *An introduction to the study of stellar structure*. 1967.

[52] E. Chatzopoulos and J. C. Wheeler. Effects of rotation on the minimum mass of primordial progenitors of pair-instability supernovae. *The Astrophysical Journal*, 748(1):42, 2012.

[53] E. Chatzopoulos and J. C. Wheeler. Hydrogen-poor circumstellar shells from

pulsational pair-instability supernovae with rapidly rotating progenitors. *The Astrophysical Journal*, 760(2):154, 2012.

[54] R. A. Chevalier. Cassiopeia A, faint supernovae, and heavy-element ejection by supernovae. *ApJ*, 208:826–828, Sep 1976. doi: 10.1086/154669.

[55] C. Chiosi and A. Maeder. The evolution of massive stars with mass loss. *ARA&A*, 24:329–375, Jan 1986. doi: 10.1146/annurev.aa.24.090186.001553.

[56] J. Choi, A. Dotter, C. Conroy, M. Cantiello, B. Paxton, and B. D. Johnson. Mesa Isochrones and Stellar Tracks (MIST). I. Solar-scaled Models. *ApJ*, 823:102, June 2016. doi: 10.3847/0004-637X/823/2/102.

[57] L. Chomiuk and M. S. Povich. Toward a Unification of Star Formation Rate Determinations in the Milky Way and Other Galaxies. *AJ*, 142:197, Dec. 2011. doi: 10.1088/0004-6256/142/6/197.

[58] M. Chruslinska, K. Belczynski, J. Klencki, and M. Benacquista. Double neutron stars: merger rates revisited. *MNRAS*, 474:2937–2958, Mar. 2018. doi: 10.1093/mnras/stx2923.

[59] R. P. Church, A. J. Levan, M. B. Davies, and N. Tanvir. Implications for the origin of short gamma-ray bursts from their observed positions around their host galaxies. *MNRAS*, 413:2004–2014, May 2011. doi: 10.1111/j.1365-2966.2011.18277.x.

[60] J. S. W. Claeys, O. R. Pols, R. G. Izzard, J. Vink, and F. W. M. Verbunt. Theoretical uncertainties of the Type Ia supernova rate. *A&A*, 563:A83, Mar. 2014. doi: 10.1051/0004-6361/201322714.

[61] D. D. Clayton. *Principles of stellar evolution and nucleosynthesis.* 1968.

[62] M. Clayton, P. Podsiadlowski, N. Ivanova, and S. Justham. Episodic mass

ejections from common-envelope objects. *MNRAS*, 470:1788–1808, Sept. 2017. doi: 10.1093/mnras/stx1290.

[63] A. Corongiu, M. Kramer, B. W. Stappers, A. G. Lyne, A. Jessner, A. Possenti, N. D'Amico, and O. Löhmer. The binary pulsar PSR J1811-1736: evidence of a low amplitude supernova kick. *A&A*, 462:703–709, Feb. 2007. doi: 10.1051/0004-6361:20054385.

[64] I. Counselman, Charles C. Outcomes of Tidal Evolution. *ApJ*, 180:307–316, Feb 1973. doi: 10.1086/151964.

[65] J. P. Cox and R. T. Giuli. *Principles of stellar structure* . 1968.

[66] G. H. Darwin. The Determination of the Secular Effects of Tidal Friction by a Graphical Method. *Proceedings of the Royal Society of London Series I*, 29: 168–181, Jan 1879.

[67] B. Davies, R.-P. Kudritzki, Z. Gazak, B. Plez, M. Bergemann, C. Evans, and L. Patrick. Red Supergiants as Cosmic Abundance Probes: The Magellanic Clouds. *ApJ*, 806:21, June 2015. doi: 10.1088/0004-637X/806/1/21.

[68] M. de Kool. Common envelope evolution and double cores of planetary nebulae. *ApJ*, 358:189–195, July 1990. doi: 10.1086/168974.

[69] O. De Marco and R. G. Izzard. Dawes Review 6: The Impact of Companions on Stellar Evolution. *PASA*, 34:e001, Jan 2017. doi: 10.1017/pasa.2016.52.

[70] S. E. de Mink and I. Mandel. The chemically homogeneous evolutionary channel for binary black hole mergers: rates and properties of gravitational-wave events detectable by advanced LIGO. *MNRAS*, 460(4):3545–3553, Aug 2016. doi: 10.1093/mnras/stw1219.

[71] S. E. de Mink, O. R. Pols, and R. W. Hilditch. Efficiency of mass transfer in

massive close binaries. Tests from double-lined eclipsing binaries in the SMC. *A&A*, 467:1181–1196, June 2007. doi: 10.1051/0004-6361:20067007.

[72] S. E. de Mink, M. Cantiello, N. Langer, O. R. Pols, I. Brott, and S.-C. Yoon. Rotational mixing in massive binaries. Detached short-period systems. *A&A*, 497:243–253, Apr. 2009. doi: 10.1051/0004-6361/200811439.

[73] S. E. de Mink, N. Langer, R. G. Izzard, H. Sana, and A. de Koter. The Rotation Rates of Massive Stars: The Role of Binary Interaction through Tides, Mass Transfer, and Mergers. *ApJ*, 764(2):166, Feb 2013. doi: 10.1088/0004-637X/764/2/166.

[74] E. F. del Peloso, L. da Silva, G. F. Porto de Mello, and L. I. Arany-Prado. The age of the Galactic thin disk from Th/Eu nucleocosmochronology. III. Extended sample. *A&A*, 440:1153–1159, Sept. 2005. doi: 10.1051/0004-6361:20053307.

[75] A. J. Delgado and H.-C. Thomas. Mass transfer in a binary system - The evolution of the mass-giving helium star. *A&A*, 96:142–145, Mar. 1981.

[76] L. Dessart. A magnetar model for the hydrogen-rich super-luminous supernova iPTF14hls. *A&A*, 610:L10, Feb. 2018. doi: 10.1051/0004-6361/201732402.

[77] J. D. M. Dewi and O. R. Pols. The late stages of evolution of helium star-neutron star binaries and the formation of double neutron star systems. *MNRAS*, 344:629–643, Sept. 2003. doi: 10.1046/j.1365-8711.2003.06844.x.

[78] J. D. M. Dewi and T. M. Tauris. On the energy equation and efficiency parameter of the common envelope evolution. *A&A*, 360:1043–1051, Aug. 2000.

[79] J. D. M. Dewi, P. Podsiadlowski, and O. R. Pols. The spin period-eccentricity

relation of double neutron stars: evidence for weak supernova kicks? *MNRAS*, 363:L71–L75, Oct. 2005. doi: 10.1111/j.1745-3933.2005.00085.x.

[80] J. D. M. Dewi, P. Podsiadlowski, and A. Sena. Double-core evolution and the formation of neutron star binaries with compact companions. *MNRAS*, 368: 1742–1748, June 2006. doi: 10.1111/j.1365-2966.2006.10233.x.

[81] M. Dominik, K. Belczynski, C. Fryer, D. E. Holz, E. Berti, T. Bulik, I. Mandel, and R. O'Shaughnessy. Double Compact Objects. I. The Significance of the Common Envelope on Merger Rates. *ApJ*, 759:52, Nov. 2012. doi: 10.1088/0004-637X/759/1/52.

[82] F. Dosopoulou and V. Kalogera. Orbital Evolution of Mass-transferring Eccentric Binary Systems. I. Phase-dependent Evolution. *ApJ*, 825(1):70, Jul 2016. doi: 10.3847/0004-637X/825/1/70.

[83] F. Dosopoulou and V. Kalogera. Orbital Evolution of Mass-transferring Eccentric Binary Systems. II. Secular Evolution. *ApJ*, 825(1):71, Jul 2016. doi: 10.3847/0004-637X/825/1/71.

[84] G. Duchêne and A. Kraus. Stellar Multiplicity. *ARA&A*, 51(1):269–310, Aug 2013. doi: 10.1146/annurev-astro-081710-102602.

[85] P. Eggenberger, G. Meynet, A. Maeder, R. Hirschi, C. Charbonnel, S. Talon, and S. Ekström. The Geneva stellar evolution code. *Ap&SS*, 316(1-4):43–54, Aug 2008. doi: 10.1007/s10509-007-9511-y.

[86] P. Eggleton. Composition Changes in Stellar Evolution. In A. G. D. Philip, editor, *The Evolution of Population II Stars*, pages 203–206, Apr 1972.

[87] P. Eggleton. *Evolutionary Processes in Binary and Multiple Stars*. 2006.

[88] P. P. Eggleton. The evolution of low mass stars. *MNRAS*, 151:351, Jan 1971. doi: 10.1093/mnras/151.3.351.

[89] P. P. Eggleton. A numerical treatment of double shell source stars. *MNRAS*, 163:279, Jan 1973. doi: 10.1093/mnras/163.3.279.

[90] P. P. Eggleton. Approximations to the radii of Roche lobes. *ApJ*, 268:368, May 1983. doi: 10.1086/160960.

[91] D. Eichler and V. Usov. Particle Acceleration and Nonthermal Radio Emission in Binaries of Early-Type Stars. *ApJ*, 402:271, Jan 1993. doi: 10.1086/172130.

[92] S. Ekström, C. Georgy, P. Eggenberger, G. Meynet, N. Mowlavi, A. Wytten-bach, A. Granada, T. Decressin, R. Hirschi, U. Frischknecht, C. Charbonnel, and A. Maeder. Grids of stellar models with rotation. I. Models from 0.8 to 120 M at solar metallicity (Z = 0.014). *A&A*, 537:A146, Jan 2012. doi: 10.1051/0004-6361/201117751.

[93] J. J. Eldridge and E. R. Stanway. BPASS predictions for binary black hole mergers. *MNRAS*, 462(3):3302–3313, Nov 2016. doi: 10.1093/mnras/stw1772.

[94] J. J. Eldridge, M. Fraser, S. J. Smartt, J. R. Maund, and R. M. Crockett. The death of massive stars - II. Observational constraints on the progenitors of Type Ibc supernovae. *MNRAS*, 436:774–795, Nov. 2013. doi: 10.1093/mnras/stt1612.

[95] R. Emden. *Gaskugeln: Anwendungen der mechanischen Wärmetheorie auf kosmologische und meteorologische Probleme*. B. Teubner., 1907.

[96] W. M. Farr and I. Mandel. Comment on "An excess of massive stars in the local 30 Doradus starburst". *Science*, 361:aat6506, July 2018. doi: 10.1126/science.aat6506.

[97] W. M. Farr, N. Sravan, A. Cantrell, L. Kreidberg, C. D. Bailyn, I. Mandel, and V. Kalogera. The Mass Distribution of Stellar-mass Black Holes. *ApJ*, 741:103, Nov. 2011. doi: 10.1088/0004-637X/741/2/103.

[98] A. J. Faulkner, M. Kramer, A. G. Lyne, R. N. Manchester, M. A. McLaughlin, I. H. Stairs, G. Hobbs, A. Possenti, D. R. Lorimer, N. D'Amico, F. Camilo, and M. Burgay. PSR J1756-2251: A New Relativistic Double Neutron Star System. *ApJ*, 618:L119–L122, Jan. 2005. doi: 10.1086/427776.

[99] W. Fong and E. Berger. The Locations of Short Gamma-Ray Bursts as Evidence for Compact Object Binary Progenitors. *ApJ*, 776:18, Oct. 2013. doi: 10.1088/0004-637X/776/1/18.

[100] E. Fonseca, I. H. Stairs, and S. E. Thorsett. A Comprehensive Study of Relativistic Gravity Using PSR B1534+12. *ApJ*, 787:82, May 2014. doi: 10.1088/0004-637X/787/1/82.

[101] W. A. Fowler and F. Hoyle. Neutrino Processes and Pair Formation in Massive Stars and Supernovae. *ApJS*, 9:201, Dec. 1964. doi: 10.1086/190103.

[102] M. Fraser, C. Inserra, A. Jerkstrand, R. Kotak, G. Pignata, S. Benetti, M.-T. Botticella, F. Bufano, M. Childress, S. Mattila, A. Pastorello, S. J. Smartt, M. Turatto, F. Yuan, J. P. Anderson, D. D. R. Bayliss, F. E. Bauer, T.-W. Chen, F. Förster Burón, A. Gal-Yam, J. B. Haislip, C. Knapic, L. Le Guillou, S. Marchi, P. Mazzali, M. Molinaro, J. P. Moore, D. Reichart, R. Smareglia, K. W. Smith, A. Sternberg, M. Sullivan, K. Takáts, B. E. Tucker, S. Valenti, O. Yaron, D. R. Young, and G. Zhou. SN 2009ip à la PESSTO: no evidence for core collapse yet. *MNRAS*, 433:1312–1337, Aug. 2013. doi: 10.1093/mnras/stt813.

[103] C. L. Fryer and V. Kalogera. Theoretical Black Hole Mass Distributions. *ApJ*, 554(1):548–560, Jun 2001. doi: 10.1086/321359.

[104] C. L. Fryer, K. Belczynski, G. Wiktorowicz, M. Dominik, V. Kalogera, and D. E. Holz. Compact Remnant Mass Function: Dependence on the Explosion

Mechanism and Metallicity. *ApJ*, 749:91, Apr. 2012. doi: 10.1088/0004-637X/749/1/91.

[105] E. Gaburov, J. C. Lombardi, and S. Portegies Zwart. Mixing in massive stellar mergers. *MNRAS*, 383:L5–L9, Jan 2008. doi: 10.1111/j.1745-3933.2007.00399.x.

[106] H. Ge, R. F. Webbink, X. Chen, and Z. Han. Adiabatic Mass Loss in Binary Stars. II. From Zero-age Main Sequence to the Base of the Giant Branch. *ApJ*, 812:40, Oct. 2015. doi: 10.1088/0004-637X/812/1/40.

[107] N. Giacobbo, M. Mapelli, and M. Spera. Merging black hole binaries: the effects of progenitor's metallicity, mass-loss rate and Eddington factor. *MNRAS*, 474(3):2959–2974, Mar 2018. doi: 10.1093/mnras/stx2933.

[108] E. Glebbeek, E. Gaburov, S. E. de Mink, O. R. Pols, and S. F. Portegies Zwart. The evolution of runaway stellar collision products. *A&A*, 497:255–264, Apr. 2009. doi: 10.1051/0004-6361/200810425.

[109] E. Glebbeek, E. Gaburov, S. Portegies Zwart, and O. R. Pols. Structure and evolution of high-mass stellar mergers. *MNRAS*, 434:3497–3510, Oct. 2013. doi: 10.1093/mnras/stt1268.

[110] Y. Götberg, S. E. de Mink, and J. H. Groh. Ionizing spectra of stars that lose their envelope through interaction with a binary companion: role of metallicity. *A&A*, 608:A11, Nov. 2017. doi: 10.1051/0004-6361/201730472.

[111] B. M. S. Hansen and E. S. Phinney. The pulsar kick velocity distribution. *MNRAS*, 291:569, Nov. 1997. doi: 10.1093/mnras/291.3.569.

[112] A. Heger and N. Langer. Presupernova Evolution of Rotating Massive Stars. II. Evolution of the Surface Properties. *ApJ*, 544(2):1016–1035, Dec 2000. doi: 10.1086/317239.

[113] A. Heger and S. E. Woosley. The nucleosynthetic signature of population iii. *The Astrophysical Journal*, 567(1):532, 2002.

[114] A. Heger, N. Langer, and S. E. Woosley. Presupernova Evolution of Rotating Massive Stars. I. Numerical Method and Evolution of the Internal Stellar Structure. *ApJ*, 528(1):368–396, Jan 2000. doi: 10.1086/308158.

[115] A. Heger, C. L. Fryer, S. E. Woosley, N. Langer, and D. H. Hartmann. How massive single stars end their life. *The Astrophysical Journal*, 591(1):288, 2003.

[116] D. C. Heggie. Binary evolution in stellar dynamics. *Monthly Notices of the Royal Astronomical Society*, 173(3):729–787, 1975.

[117] W. Herschel. Xviii. catalogue of 500 new neb nebulous stars, planetary nebula:, and clusters of stars; with remarks on the construction of the heavens. *Philosophical transactions of the Royal Society of London*, (92):477–528, 1802.

[118] A. Hewish, S. J. Bell, J. D. H. Pilkington, P. F. Scott, and R. A. Collins. Observation of a Rapidly Pulsating Radio Source. *Nature*, 217:709–713, Feb. 1968. doi: 10.1038/217709a0.

[119] G. Hobbs, D. R. Lorimer, A. G. Lyne, and M. Kramer. A statistical study of 233 pulsar proper motions. *MNRAS*, 360:974–992, July 2005. doi: 10.1111/j.1365-2966.2005.09087.x.

[120] R. A. Hulse and J. H. Taylor. Discovery of a pulsar in a binary system. *ApJ*, 195:L51–L53, Jan. 1975. doi: 10.1086/181708.

[121] J. R. Hurley, O. R. Pols, and C. A. Tout. Comprehensive analytic formulae for stellar evolution as a function of mass and metallicity. *MNRAS*, 315:543–569, July 2000. doi: 10.1046/j.1365-8711.2000.03426.x.

[122] J. R. Hurley, C. A. Tout, and O. R. Pols. Evolution of binary stars and the

effect of tides on binary populations. *MNRAS*, 329:897–928, Feb. 2002. doi: 10.1046/j.1365-8711.2002.05038.x.

[123] P. Hut. Tidal evolution in close binary systems. *A&A*, 99:126–140, June 1981.

[124] J. Hwang, J. C. Lombardi, Jr., F. A. Rasio, and V. Kalogera. Stability and Coalescence of Massive Twin Binaries. *ApJ*, 806:135, June 2015. doi: 10.1088/0004-637X/806/1/135.

[125] I. Iben, Jr. and M. Livio. Common envelopes in binary star evolution. *PASP*, 105:1373–1406, Dec. 1993. doi: 10.1086/133321.

[126] A. Irrgang, B. Wilcox, E. Tucker, and L. Schiefelbein. Milky Way mass models for orbit calculations. *A&A*, 549:A137, Jan. 2013. doi: 10.1051/0004-6361/201220540.

[127] N. Ivanova, S. Justham, J. L. Avendano Nandez, and J. C. Lombardi. Identification of the Long-Sought Common-Envelope Events. *Science*, 339(6118): 433, Jan 2013. doi: 10.1126/science.1225540.

[128] N. Ivanova, S. Justham, X. Chen, O. De Marco, C. L. Fryer, E. Gaburov, H. Ge, E. Glebbeek, Z. Han, X.-D. Li, G. Lu, T. Marsh, P. Podsiadlowski, A. Potter, N. Soker, R. Taam, T. M. Tauris, E. P. J. van den Heuvel, and R. F. Webbink. Common envelope evolution: where we stand and how we can move forward. *A&A Rev.*, 21:59, Feb. 2013. doi: 10.1007/s00159-013-0059-2.

[129] R. G. Izzard, C. A. Tout, A. I. Karakas, and O. R. Pols. A new synthetic model for asymptotic giant branch stars. *MNRAS*, 350:407–426, May 2004. doi: 10.1111/j.1365-2966.2004.07446.x.

[130] R. G. Izzard, L. M. Dray, A. I. Karakas, M. Lugaro, and C. A. Tout. Population nucleosynthesis in single and binary stars. I. Model. *A&A*, 460:565–572, Dec. 2006. doi: 10.1051/0004-6361:20066129.

[131] R. G. Izzard, E. Glebbeek, R. J. Stancliffe, and O. R. Pols. Population synthesis of binary carbon-enhanced metal-poor stars. *A&A*, 508:1359–1374, Dec. 2009. doi: 10.1051/0004-6361/200912827.

[132] H.-T. Janka. Neutron Star Kicks by the Gravitational Tug-boat Mechanism in Asymmetric Supernova Explosions: Progenitor and Explosion Dependence. *ApJ*, 837:84, Mar. 2017. doi: 10.3847/1538-4357/aa618e.

[133] G. H. Janssen, B. W. Stappers, M. Kramer, D. J. Nice, A. Jessner, I. Cognard, and M. B. Purver. Multi-telescope timing of PSR J1518+4904. *A&A*, 490: 753–761, Nov. 2008. doi: 10.1051/0004-6361:200810076.

[134] H. Jeffreys. An Invariant Form for the Prior Probability in Estimation Problems. *Proceedings of the Royal Society of London Series A*, 186:453–461, Sept. 1946. doi: 10.1098/rspa.1946.0056.

[135] Y.-F. Jiang, M. Cantiello, L. Bildsten, E. Quataert, O. Blaes, and J. Stone. Outbursts of luminous blue variable stars from variations in the helium opacity. *Nature*, 561(7724):498, 2018.

[136] S. Justham, P. Podsiadlowski, and Z. Han. On the formation of single and binary helium-rich subdwarf O stars. *MNRAS*, 410:984–993, Jan. 2011. doi: 10.1111/j.1365-2966.2010.17497.x.

[137] S. Justham, P. Podsiadlowski, and J. S. Vink. Luminous blue variables and superluminous supernovae from binary mergers. *The Astrophysical Journal*, 796(2):121, 2014.

[138] V. Kalogera, C. Kim, D. R. Lorimer, M. Burgay, N. D'Amico, A. Possenti, R. N. Manchester, A. G. Lyne, B. C. Joshi, M. A. McLaughlin, M. Kramer, J. M. Sarkissian, and F. Camilo. The Cosmic Coalescence Rates for Double Neutron Star Binaries. *ApJ*, 601:L179–L182, Feb. 2004. doi: 10.1086/382155.

[139] J. I. Katz. Two kinds of stellar collapse. *Nature*, 253:698, Feb. 1975. doi: 10.1038/253698a0.

[140] M. J. Keith, M. Kramer, A. G. Lyne, R. P. Eatough, I. H. Stairs, A. Possenti, F. Camilo, and R. N. Manchester. PSR J1753-2240: a mildly recycled pulsar in an eccentric binary system. *MNRAS*, 393:623–627, Feb. 2009. doi: 10.1111/j.1365-2966.2008.14234.x.

[141] C. Keller. X-rays from the sun. *Experientia*, 51(7):710–720, 1995.

[142] P. Kiel, J. Hurley, M. Bailes, and J. Murray. Populating the Galaxy with pulsars I: stellar & binary evolution. *Mon. Not. Roy. Astron. Soc.*, 388:393–415, 2008. doi: 10.1111/j.1365-2966.2008.13402.x.

[143] C. Kim, V. Kalogera, and D. R. Lorimer. The Probability Distribution of Binary Pulsar Coalescence Rates. I. Double Neutron Star Systems in the Galactic Field. *ApJ*, 584:985–995, Feb. 2003. doi: 10.1086/345740.

[144] R. Kippenhahn and A. Weigert. Entwicklung in engen Doppelsternsystemen I. Massenaustausch vor und nach Beendigung des zentralen Wasserstoff-Brennens. *ZAp*, 65:251, 1967.

[145] R. Kippenhahn and A. Weigert. *Stellar Structure and Evolution*. 1990.

[146] C. Knigge, M. J. Coe, and P. Podsiadlowski. Two populations of X-ray pulsars produced by two types of supernova. *Nature*, 479:372–375, Nov. 2011. doi: 10.1038/nature10529.

[147] K. Köhler, N. Langer, A. de Koter, S. E. de Mink, P. A. Crowther, C. J. Evans, G. Gräfener, H. Sana, D. Sanyal, F. R. N. Schneider, and J. S. Vink. The evolution of rotating very massive stars with LMC composition. *A&A*, 573:A71, Jan. 2015. doi: 10.1051/0004-6361/201424356.

[148] Z. Kopal. *Close binary systems*. 1959.

[149] Y. Kozai. Secular perturbations of asteroids with high inclination and eccentricity. *The Astronomical Journal*, 67:591, 1962.

[150] M. Kramer, I. H. Stairs, R. N. Manchester, M. A. McLaughlin, A. G. Lyne, R. D. Ferdman, M. Burgay, D. R. Lorimer, A. Possenti, N. D'Amico, J. M. Sarkissian, G. B. Hobbs, J. E. Reynolds, P. C. C. Freire, and F. Camilo. Tests of General Relativity from Timing the Double Pulsar. *Science*, 314:97–102, Oct. 2006. doi: 10.1126/science.1132305.

[151] W. Kraushaar, G. W. Clark, G. Garmire, H. Helmken, P. Higbie, and M. Agogino. Explorer XI Experiment on Cosmic Gamma Rays. *ApJ*, 141: 845, Apr. 1965. doi: 10.1086/148179.

[152] L. Kreidberg, C. D. Bailyn, W. M. Farr, and V. Kalogera. Mass Measurements of Black Holes in X-Ray Transients: Is There a Mass Gap? *ApJ*, 757:36, Sept. 2012. doi: 10.1088/0004-637X/757/1/36.

[153] P. Kroupa. On the variation of the initial mass function. *MNRAS*, 322:231–246, Apr. 2001. doi: 10.1046/j.1365-8711.2001.04022.x.

[154] M. U. Kruckow, T. M. Tauris, N. Langer, D. Szécsi, P. Marchant, and P. Podsiadlowski. Common-envelope ejection in massive binary stars. Implications for the progenitors of GW150914 and GW151226. *A&A*, 596:A58, Nov. 2016. doi: 10.1051/0004-6361/201629420.

[155] M. U. Kruckow, T. M. Tauris, N. Langer, M. Kramer, and R. G. Izzard. Progenitors of gravitational wave mergers: binary evolution with the stellar grid-based code COMBINE. *MNRAS*, 481(2):1908–1949, Dec 2018. doi: 10.1093/mnras/sty2190.

[156] D. Kushnir, M. Zaldarriaga, J. A. Kollmeier, and R. Waldman. Dynamical tides reexpressed. *MNRAS*, 467:2146–2149, May 2017. doi: 10.1093/mnras/stx255.

[157] A. Lamberts, S. Garrison-Kimmel, P. F. Hopkins, E. Quataert, J. S. Bullock, C. A. Faucher-Giguère, A. Wetzel, D. Kereš, K. Drango, and R. E. Sand erson. Predicting the binary black hole population of the Milky Way with cosmological simulations. *MNRAS*, 480(2):2704–2718, Oct 2018. doi: 10. 1093/mnras/sty2035.

[158] N. Langer, K. J. Fricke, and D. Sugimoto. Semiconvective diffusion and energy transport. *A&A*, 126(1):207, Sep 1983.

[159] N. Langer, C. A. Norman, A. de Koter, J. S. Vink, M. Cantiello, and S.-C. Yoon. Pair creation supernovae at low and high redshift. *A&A*, 475:L19–L23, Nov. 2007. doi: 10.1051/0004-6361:20078482.

[160] P. Lazarus, P. C. C. Freire, B. Allen, C. Aulbert, O. Bock, S. Bogdanov, A. Brazier, F. Camilo, F. Cardoso, S. Chatterjee, J. M. Cordes, F. Crawford, J. S. Deneva, H.-B. Eggenstein, H. Fehrmann, R. Ferdman, J. W. T. Hessels, F. A. Jenet, C. Karako-Argaman, V. M. Kaspi, B. Knispel, R. Lynch, J. van Leeuwen, B. Machenschalk, E. Madsen, M. A. McLaughlin, C. Patel, S. M. Ransom, P. Scholz, A. Seymour, X. Siemens, L. G. Spitler, I. H. Stairs, K. Stovall, J. Swiggum, A. Venkataraman, and W. W. Zhu. Einstein@Home Discovery of a Double Neutron Star Binary in the PALFA Survey. *ApJ*, 831: 150, Nov. 2016. doi: 10.3847/0004-637X/831/2/150.

[161] M. Lecar, J. C. Wheeler, and C. F. McKee. Tidal circularization of the binary X-ray sources Hercules X-1 and Centaurus X-3. *ApJ*, 205:556–562, Apr. 1976. doi: 10.1086/154311.

[162] E. J. Lentz, S. W. Bruenn, W. R. Hix, A. Mezzacappa, O. E. B. Messer, E. Endeve, J. M. Blondin, J. A. Harris, P. Marronetti, and K. N. Yakunin. Three-dimensional Core-collapse Supernova Simulated Using a 15 M Progenitor. *ApJ*, 807:L31, July 2015. doi: 10.1088/2041-8205/807/2/L31.

[163] M. Lidov. The evolution of orbits of artificial satellites of planets under the action of gravitational perturbations of external bodies. *Planetary and Space Science*, 9(10):719–759, 1962.

[164] V. M. Lipunov, K. A. Postnov, and M. E. Prokhorov. The Scenario Machine: restrictions on key parameters of binary evolution. *A&A*, 310:489–507, Jun 1996.

[165] V. M. Lipunov, K. A. Postnov, M. E. Prokhorov, and A. I. Bogomazov. Description of the "Scenario Machine". *Astronomy Reports*, 53(10):915–940, Oct 2009. doi: 10.1134/S1063772909100047.

[166] J. C. Lombardi, Jr., J. S. Warren, F. A. Rasio, A. Sills, and A. R. Warren. Stellar Collisions and the Interior Structure of Blue Stragglers. *ApJ*, 568: 939–953, Apr. 2002. doi: 10.1086/339060.

[167] J. C. Lombardi, Jr., Z. F. Proulx, K. L. Dooley, E. M. Theriault, N. Ivanova, and F. A. Rasio. Stellar Collisions and Ultracompact X-Ray Binary Formation. *ApJ*, 640:441–458, Mar. 2006. doi: 10.1086/499938.

[168] D. R. Lorimer and M. Kramer. *Handbook of Pulsar Astronomy*. Cambridge University Press, Dec. 2004.

[169] R. S. Lynch, P. C. C. Freire, S. M. Ransom, and B. A. Jacoby. The Timing of Nine Globular Cluster Pulsars. *ApJ*, 745:109, Feb. 2012. doi: 10.1088/ 0004-637X/745/2/109.

[170] M. MacLeod and E. Ramirez-Ruiz. Asymmetric Accretion Flows within a Common Envelope. *ApJ*, 803:41, Apr. 2015. doi: 10.1088/0004-637X/803/1/ 41.

[171] M. MacLeod and E. Ramirez-Ruiz. On the Accretion-fed Growth of Neutron

Stars during Common Envelope. *ApJ*, 798:L19, Jan. 2015. doi: 10.1088/ 2041-8205/798/1/L19.

[172] M. MacLeod, A. Antoni, A. Murguia-Berthier, P. Macias, and E. Ramirez-Ruiz. Common Envelope Wind Tunnel: Coefficients of Drag and Accretion in a Simplified Context for Studying Flows around Objects Embedded within Stellar Envelopes. *ApJ*, 838:56, Mar. 2017. doi: 10.3847/1538-4357/aa6117.

[173] M. MacLeod, P. Macias, E. Ramirez-Ruiz, J. Grindlay, A. Batta, and G. Montes. Lessons from the Onset of a Common Envelope Episode: the Remarkable M31 2015 Luminous Red Nova Outburst. *ApJ*, 835:282, Feb. 2017. doi: 10.3847/1538-4357/835/2/282.

[174] A. Maeder and G. Meynet. Rotating massive stars: From first stars to gamma ray bursts. *Reviews of Modern Physics*, 84(1):25–63, Jan 2012. doi: 10.1103/ RevModPhys.84.25.

[175] R. N. Manchester, G. B. Hobbs, A. Teoh, and M. Hobbs. The Australia Telescope National Facility Pulsar Catalogue. *AJ*, 129(4):1993–2006, Apr 2005. doi: 10.1086/428488.

[176] I. Mandel and S. E. de Mink. Merging binary black holes formed through chemically homogeneous evolution in short-period stellar binaries. *MNRAS*, 458(3):2634–2647, May 2016. doi: 10.1093/mnras/stw379.

[177] I. Mandel and R. O'Shaughnessy. Compact binary coalescences in the band of ground-based gravitational-wave detectors. *Classical and Quantum Gravity*, 27(11):114007–+, June 2010. doi: 10.1088/0264-9381/27/11/114007.

[178] P. Marchant. Kippenhahn plotter for mesa (version 1.0.0). `http://doi.org/ 10.5281/zenodo.2602098`, 2019.

[179] P. Marchant, N. Langer, P. Podsiadlowski, T. M. Tauris, and T. J. Moriya. A new route towards merging massive black holes. *A&A*, 588:A50, Apr. 2016. doi: 10.1051/0004-6361/201628133.

[180] P. Marchant, N. Langer, P. Podsiadlowski, T. M. Tauris, S. de Mink, I. Mandel, and T. J. Moriya. Ultra-luminous X-ray sources and neutron-star-black-hole mergers from very massive close binaries at low metallicity. *A&A*, 604:A55, Aug. 2017. doi: 10.1051/0004-6361/201630188.

[181] A. Marek and H. Janka. Delayed Neutrino-Driven Supernova Explosions Aided by the Standing Accretion-Shock Instability. *ApJ*, 694:664–696, Mar. 2009. doi: 10.1088/0004-637X/694/1/664.

[182] J. G. Martinez, K. Stovall, P. C. C. Freire, J. S. Deneva, F. A. Jenet, M. A. McLaughlin, M. Bagchi, S. D. Bates, and A. Ridolfi. Pulsar J0453+1559: A Double Neutron Star System with a Large Mass Asymmetry. *ApJ*, 812:143, Oct. 2015. doi: 10.1088/0004-637X/812/2/143.

[183] J. G. Martinez, K. Stovall, P. C. C. Freire, J. S. Deneva, T. M. Tauris, A. Ridolfi, N. Wex, F. A. Jenet, M. A. McLaughlin, and M. Bagchi. Pulsar J1411+2551: A Low-mass Double Neutron Star System. *ApJ*, 851:L29, Dec. 2017. doi: 10.3847/2041-8213/aa9d87.

[184] C. A. Meakin and D. Arnett. Anelastic and Compressible Simulations of Stellar Oxygen Burning. *ApJ*, 665(1):690–697, Aug 2007. doi: 10.1086/519372.

[185] T. Melson, H.-T. Janka, R. Bollig, F. Hanke, A. Marek, and B. Müller. Neutrino-driven Explosion of a 20 Solar-mass Star in Three Dimensions Enabled by Strange-quark Co ntributions to NeutrinoNucleon Scattering. *ApJ*, 808:L42, Aug. 2015. doi: 10.1088/2041-8205/808/2/L42.

[186] T. Melson, H.-T. Janka, and A. Marek. Neutrino-driven Supernova of a Low-

mass Iron-core Progenitor Boosted by Three-dimensional Turbule nt Convec-
tion. *ApJ*, 801:L24, Mar. 2015. doi: 10.1088/2041-8205/801/2/L24.

[187] R. L. Minkowski and G. O. Abell. *The National Geographic Society-Palomar
Observatory Sky Survey*, page 481. the University of Chicago Press, 1963.

[188] S. Miyaji, K. Nomoto, K. Yokoi, and D. Sugimoto. Supernova triggered by
electron captures. *PASJ*, 32:303–329, Jan 1980.

[189] S. W. Mochnacki. Accurate integrations of the Roche model. *ApJS*, 55:551–
561, Aug 1984. doi: 10.1086/190967.

[190] B. Müller, A. Heger, D. Liptai, and J. B. Cameron. A simple approach to the
supernova progenitor-explosion connection. *MNRAS*, 460:742–764, July 2016.
doi: 10.1093/mnras/stw1083.

[191] B. Müller, T. Melson, A. Heger, and H.-T. Janka. Supernova simulations from
a 3D progenitor model - Impact of perturbations and evolution of explosion
properties. *MNRAS*, 472:491–513, Nov. 2017. doi: 10.1093/mnras/stx1962.

[192] J. W. Murphy and J. C. Dolence. An Integral Condition for Core-collapse
Supernova Explosions. *ApJ*, 834(2):183, Jan 2017. doi: 10.3847/1538-4357/
834/2/183.

[193] S. Naoz, T. Fragos, A. Geller, A. P. Stephan, and F. A. Rasio. Formation
of Black Hole Low-mass X-Ray Binaries in Hierarchical Triple Systems. *ApJ*,
822(2):L24, May 2016. doi: 10.3847/2041-8205/822/2/L24.

[194] C. J. Neijssel, A. Vigna-Gómez, S. Stevenson, J. W. Barrett, S. M. Gaebel,
F. Broekgaarden, S. E. de Mink, D. Szécsi, S. Vinciguerra, and I. Mandel.
The effect of the metallicity-specific star formation history on double compact
object mergers. *arXiv e-prints*, art. arXiv:1906.08136, Jun 2019.

[195] K. Nomoto. Evolution of 8-10 solar mass stars toward electron capture super-novae. I - Formation of electron-degenerate O + Ne + Mg cores. *ApJ*, 277: 791–805, Feb. 1984. doi: 10.1086/161749.

[196] K. Nomoto. Evolution of 8-10 solar mass stars toward electron capture super-novae. II - Collapse of an O + Ne + Mg core. *ApJ*, 322:206–214, Nov. 1987. doi: 10.1086/165716.

[197] K. Nomoto, C. Kobayashi, and N. Tominaga. Nucleosynthesis in Stars and the Chemical Enrichment of Galaxies. *ARA&A*, 51:457–509, Aug. 2013. doi: 10.1146/annurev-astro-082812-140956.

[198] J. Nordhaus, T. D. Brandt, A. Burrows, E. Livne, and C. D. Ott. Theoretical support for the hydrodynamic mechanism of pulsar kicks. *Phys. Rev. D*, 82 (10):103016, Nov. 2010. doi: 10.1103/PhysRevD.82.103016.

[199] E. O'Connor and C. D. Ott. Black Hole Formation in Failing Core-Collapse Supernovae. *ApJ*, 730(2):70, Apr 2011. doi: 10.1088/0004-637X/730/2/70.

[200] S. T. Ohlmann, F. K. Röpke, R. Pakmor, and V. Springel. Hydrodynamic Moving-mesh Simulations of the Common Envelope Phase in Binary Stellar Systems. *ApJ*, 816:L9, Jan. 2016. doi: 10.3847/2041-8205/816/1/L9.

[201] S. T. Ohlmann, F. K. Röpke, R. Pakmor, and V. Springel. Constructing stable 3D hydrodynamical models of giant stars. *A&A*, 599:A5, Mar. 2017. doi: 10.1051/0004-6361/201629692.

[202] E. Öpik. Statistical Studies of Double Stars: On the Distribution of Relative Luminosities and Distances of Double Stars in the Harvard Revised Photometry North of Declination -31deg. *Publications of the Tartu Astrofizica Observatory*, 25, 1924.

[203] J. R. Oppenheimer and G. M. Volkoff. On Massive Neutron Cores. *Physical Review*, 55:374–381, Feb. 1939. doi: 10.1103/PhysRev.55.374.

[204] R. O'Shaughnessy and C. Kim. Pulsar Binary Birthrates with Spin-opening Angle Correlations. *ApJ*, 715:230–241, May 2010. doi: 10.1088/0004-637X/715/1/230.

[205] R. O'Shaughnessy, C. Kim, T. Fragos, V. Kalogera, and K. Belczynski. Constraining Population Synthesis Models via the Binary Neutron Star Population. *ApJ*, 633:1076–1084, Nov. 2005. doi: 10.1086/468180.

[206] R. O'Shaughnessy, C. Kim, V. Kalogera, and K. Belczynski. Constraining Population Synthesis Models via Empirical Binary Compact Object Merger and Supernova Rates. *ApJ*, 672:479-488, Jan. 2008. doi: 10.1086/523620.

[207] S. Osłowski, T. Bulik, D. Gondek-Rosińska, and K. Belczyński. Population synthesis of double neutron stars. *MNRAS*, 413:461–479, May 2011. doi: 10.1111/j.1365-2966.2010.18147.x.

[208] F. Özel and P. Freire. Masses, Radii, and the Equation of State of Neutron Stars. *ARA&A*, 54:401–440, Sept. 2016. doi: 10.1146/annurev-astro-081915-023322.

[209] F. Özel, D. Psaltis, R. Narayan, and J. E. McClintock. The Black Hole Mass Distribution in the Galaxy. *ApJ*, 725:1918–1927, Dec. 2010. doi: 10.1088/0004-637X/725/2/1918.

[210] B. Paczyński. Evolutionary Processes in Close Binary Systems. *ARA&A*, 9: 183, Jan 1971. doi: 10.1146/annurev.aa.09.090171.001151.

[211] B. Paczynski. Common Envelope Binaries. In P. Eggleton, S. Mitton, and J. Whelan, editors, *Structure and Evolution of Close Binary Systems*, volume 73 of *IAU Symposium*, page 75, 1976.

[212] A. Pasquali, A. Nota, N. Langer, R. E. Schulte-Ladbeck, and M. Clampin. R4 and Its Circumstellar Nebula: Evidence for a Binary Merger? *AJ*, 119: 1352–1358, Mar. 2000. doi: 10.1086/301257.

[213] J.-C. Passy, O. De Marco, C. L. Fryer, F. Herwig, S. Diehl, J. S. Oishi, M.-M. Mac Low, G. L. Bryan, and G. Rockefeller. Simulating the Common Envelope Phase of a Red Giant Using Smoothed-particle Hydrodynamics and Uniform-grid Codes. *ApJ*, 744:52, Jan. 2012. doi: 10.1088/0004-637X/744/1/52.

[214] A. Pastorello, E. Cappellaro, C. Inserra, S. J. Smartt, G. Pignata, S. Benetti, S. Valenti, M. Fraser, K. Takáts, S. Benitez, M. T. Botticella, J. Brimacombe, F. Bufano, F. Cellier-Holzem, M. T. Costado, G. Cupani, I. Curtis, N. Elias-Rosa, M. Ergon, J. P. U. Fynbo, F.-J. Hambsch, M. Hamuy, A. Harutyunyan, K. M. Ivarson, E. Kankare, J. C. Martin, R. Kotak, A. P. LaCluyze, K. Maguire, S. Mattila, J. Maza, M. McCrum, M. Miluzio, H. U. Norgaard-Nielsen, M. C. Nysewander, P. Ochner, Y.-C. Pan, M. L. Pumo, D. E. Reichart, T. G. Tan, S. Taubenberger, L. Tomasella, M. Turatto, and D. Wright. Interacting Supernovae and Supernova Impostors: SN 2009ip, is this the End? *ApJ*, 767:1, Apr. 2013. doi: 10.1088/0004-637X/767/1/1.

[215] K. Pavlovskii, N. Ivanova, K. Belczynski, and K. X. Van. Stability of mass transfer from massive giants: double black hole binary formation and ultraluminous X-ray sources. *MNRAS*, 465:2092–2100, Feb. 2017. doi: 10.1093/mnras/stw2786.

[216] B. Paxton, L. Bildsten, A. Dotter, F. Herwig, P. Lesaffre, and F. Timmes. Modules for experiments in stellar astrophysics (mesa). *The Astrophysical Journal Supplement Series*, 192(1):3, 2010.

[217] B. Paxton, M. Cantiello, P. Arras, L. Bildsten, E. F. Brown, A. Dotter, C. Mankovich, M. Montgomery, D. Stello, F. Timmes, et al. Modules for

experiments in stellar astrophysics (mesa): planets, oscillations, rotation, and massive stars. *The Astrophysical Journal Supplement Series*, 208(1):4, 2013.

[218] B. Paxton, P. Marchant, J. Schwab, E. B. Bauer, L. Bildsten, M. Cantiello, L. Dessart, R. Farmer, H. Hu, N. Langer, et al. Modules for experiments in stellar astrophysics (mesa): binaries, pulsations, and explosions. *The Astrophysical Journal Supplement Series*, 220(1):15, 2015.

[219] B. Paxton, J. Schwab, E. B. Bauer, L. Bildsten, S. Blinnikov, P. Duffell, R. Farmer, J. A. Goldberg, P. Marchant, E. Sorokina, A. Thoul, R. H. D. Townsend, and F. X. Timmes. Modules for Experiments in Stellar Astrophysics (MESA): Convective Boundaries, Element Diffusion, and Massive Star Explosions. *ApJS*, 234:34, Feb. 2018. doi: 10.3847/1538-4365/aaa5a8.

[220] P. C. Peters. Gravitational radiation and the motion of two point masses. *Physical Review*, 136(4B):B1224, 1964.

[221] P. C. Peters and J. Mathews. Gravitational Radiation from Point Masses in a Keplerian Orbit. *Physical Review*, 131(1):435–440, Jul 1963. doi: 10.1103/PhysRev.131.435.

[222] E. Pfahl, S. Rappaport, and P. Podsiadlowski. On the Population of Wind-accreting Neutron Stars in the Galaxy. *ApJ*, 571:L37–L40, May 2002. doi: 10.1086/341197.

[223] E. Pfahl, S. Rappaport, P. Podsiadlowski, and H. Spruit. A New Class of High-Mass X-Ray Binaries: Implications for Core Collapse and Neutron Star Recoil. *ApJ*, 574:364–376, July 2002. doi: 10.1086/340794.

[224] E. S. Phinney. The rate of neutron star binary mergers in the universe-minimal predictions for gravity wave detectors. *The Astrophysical Journal*, 380:L17–L21, 1991.

[225] E. S. Phinney and S. Sigurdsson. Ejection of pulsars and binaries to the outskirts of globular clusters. *Nature*, 349:220–223, Jan. 1991. doi: 10.1038/349220a0.

[226] Planck Collaboration, P. A. R. Ade, N. Aghanim, M. Arnaud, M. Ashdown, J. Aumont, C. Baccigalupi, A. J. Banday, R. B. Barreiro, J. G. Bartlett, and et al. Planck 2015 results. XIII. Cosmological parameters. *A&A*, 594:A13, Sept. 2016. doi: 10.1051/0004-6361/201525830.

[227] P. Podsiadlowski. Massive binary evolution. *New A Rev.*, 54(3-6):39–44, Mar 2010. doi: 10.1016/j.newar.2010.09.023.

[228] P. Podsiadlowski, P. C. Joss, and J. J. L. Hsu. Presupernova evolution in massive interacting binaries. *ApJ*, 391:246–264, May 1992. doi: 10.1086/171341.

[229] P. Podsiadlowski, N. Langer, A. J. T. Poelarends, S. Rappaport, A. Heger, and E. Pfahl. The Effects of Binary Evolution on the Dynamics of Core Collapse and Neutron Star Kicks. *ApJ*, 612:1044–1051, Sept. 2004. doi: 10.1086/421713.

[230] P. Podsiadlowski, N. Ivanova, S. Justham, and S. Rappaport. Explosive common-envelope ejection: implications for gamma-ray bursts and low-mass black-hole binaries. *MNRAS*, 406:840–847, Aug. 2010. doi: 10.1111/j.1365-2966.2010.16751.x.

[231] A. J. T. Poelarends, F. Herwig, N. Langer, and A. Heger. The Supernova Channel of Super-AGB Stars. *ApJ*, 675:614-625, Mar. 2008. doi: 10.1086/520872.

[232] A. J. T. Poelarends, S. Wurtz, J. Tarka, L. Cole Adams, and S. T. Hills. Electron Capture Supernovae from Close Binary Systems. *ApJ*, 850:197, Dec. 2017. doi: 10.3847/1538-4357/aa988a.

[233] O. R. Pols. Case A evolution of massive close binaries: formation of contact systems and possible reversal of the supernova order. *A&A*, 290:119–128, Oct. 1994.

[234] O. R. Pols, K.-P. Schröder, J. R. Hurley, C. A. Tout, and P. P. Eggleton. Stellar evolution models for Z = 0.0001 to 0.03. *MNRAS*, 298:525–536, Aug. 1998. doi: 10.1046/j.1365-8711.1998.01658.x.

[235] S. F. Portegies Zwart and S. L. McMillan. Black hole mergers in the universe. *The Astrophysical Journal Letters*, 528(1):L17, 1999.

[236] S. F. Portegies Zwart and E. P. J. van den Heuvel. A runaway collision in a young star cluster as the origin of the brightest supernova. *Nature*, 450: 388–389, Nov. 2007. doi: 10.1038/nature06276.

[237] S. F. Portegies Zwart and F. Verbunt. Population synthesis of high-mass binaries. *A&A*, 309:179–196, May 1996.

[238] S. F. Portegies Zwart and L. R. Yungelson. Formation and evolution of binary neutron stars. *A&A*, 332:173–188, Apr. 1998.

[239] K. A. Postnov and L. R. Yungelson. The Evolution of Compact Binary Star Systems. *Living Reviews in Relativity*, 17(1):3, May 2014. doi: 10.12942/lrr-2014-3.

[240] J. Puls, J. S. Vink, and F. Najarro. Mass loss from hot massive stars. *A&A Rev.*, 16:209–325, Dec. 2008. doi: 10.1007/s00159-008-0015-8.

[241] G. Rakavy, G. Shaviv, and Z. Zinamon. Carbon and oxygen burning stars and pre-supernova models. *The Astrophysical Journal*, 150:131, 1967.

[242] F. A. Rasio and M. Livio. On the Formation and Evolution of Common Envelope Systems. *ApJ*, 471:366, Nov. 1996. doi: 10.1086/177975.

[243] G. Rauw, M. De Becker, Y. Nazé, P. A. Crowther, E. Gosset, H. Sana, K. A. van der Hucht, J.-M. Vreux, and P. M. Williams. WR 20a: A massive cornerstone binary system comprising two extreme early-type stars. *A&A*, 420: L9–L13, June 2004. doi: 10.1051/0004-6361:20040150.

[244] G. Rauw, P. A. Crowther, M. De Becker, E. Gosset, Y. Nazé, H. Sana, K. A. van der Hucht, J.-M. Vreux, and P. M. Williams. The spectrum of the very massive binary system WR 20a (WN6ha + WN6ha): Fundamental parameters and wind interactions. *A&A*, 432:985–998, Mar. 2005. doi: 10.1051/0004-6361: 20042136.

[245] T. A. Reichardt, O. De Marco, R. Iaconi, C. A. Tout, and D. J. Price. Extending common envelope simulations from Roche lobe overflow to the nebular phase. *MNRAS*, 484(1):631–647, Mar 2019. doi: 10.1093/mnras/sty3485.

[246] M. Renzo, C. D. Ott, S. N. Shore, and S. E. de Mink. Systematic survey of the effects of wind mass loss algorithms on the evolution of single massive stars. *A&A*, 603:A118, Jul 2017. doi: 10.1051/0004-6361/201730698.

[247] P. M. Ricker and R. E. Taam. The Interaction of Stellar Objects within a Common Envelope. *ApJ*, 672:L41, Jan. 2008. doi: 10.1086/526343.

[248] P. M. Ricker and R. E. Taam. An AMR Study of the Common-envelope Phase of Binary Evolution. *ApJ*, 746:74, Feb. 2012. doi: 10.1088/0004-637X/746/1/ 74.

[249] C. L. Rodriguez and F. Antonini. A Triple Origin for the Heavy and Low-spin Binary Black Holes Detected by LIGO/VIRGO. *ApJ*, 863(1):7, Aug 2018. doi: 10.3847/1538-4357/aacea4.

[250] E. E. Salpeter. The Luminosity Function and Stellar Evolution. *ApJ*, 121:161, Jan. 1955. doi: 10.1086/145971.

[251] H. Sana, S. E. de Mink, A. de Koter, N. Langer, C. J. Evans, M. Gieles, E. Gosset, R. G. Izzard, J.-B. Le Bouquin, and F. R. N. Schneider. Binary Interaction Dominates the Evolution of Massive Stars. *Science*, 337:444, July 2012. doi: 10.1126/science.1223344.

[252] H. Sana, J. B. Le Bouquin, S. Lacour, J. P. Berger, G. Duvert, L. Gauchet, B. Norris, J. Olofsson, D. Pickel, G. Zins, O. Absil, A. de Koter, K. Kratter, O. Schnurr, and H. Zinnecker. Southern Massive Stars at High Angular Resolution: Observational Campaign and Companion Detection. *ApJS*, 215(1):15, Nov 2014. doi: 10.1088/0067-0049/215/1/15.

[253] E. L. Sandquist, R. E. Taam, X. Chen, P. Bodenheimer, and A. Burkert. Double Core Evolution. X. Through the Envelope Ejection Phase. *ApJ*, 500: 909–922, June 1998. doi: 10.1086/305778.

[254] L. Scheck, T. Plewa, H.-T. Janka, K. Kifonidis, and E. Müller. Pulsar Recoil by Large-Scale Anisotropies in Supernova Explosions. *Physical Review Letters*, 92(1):011103, Jan. 2004. doi: 10.1103/PhysRevLett.92.011103.

[255] L. Scheck, K. Kifonidis, H.-T. Janka, and E. Müller. Multidimensional supernova simulations with approximative neutrino transport. I. Neutron star kicks and the anisotropy of neutrino-driven explosions in two spatial dimensions. *A&A*, 457:963–986, Oct. 2006. doi: 10.1051/0004-6361:20064855.

[256] J. Schwab, P. Podsiadlowski, and S. Rappaport. Further Evidence for the Bimodal Distribution of Neutron-star Masses. *ApJ*, 719:722–727, Aug. 2010. doi: 10.1088/0004-637X/719/1/722.

[257] K. Schwarzschild. Über das Gravitationsfeld eines Massenpunktes nach der Einsteinschen Theorie. *Sitzungsberichte der Königlich Preußischen Akademie der Wissenschaften (Berlin), 1916, Seite 189-196*, 1916.

[258] J. F. Sepinsky, B. Willems, V. Kalogera, and F. A. Rasio. Interacting Binaries with Eccentric Orbits: Secular Orbital Evolution Due to Conservative Mass Transfer. *ApJ*, 667(2):1170–1184, Oct 2007. doi: 10.1086/520911.

[259] H. L. Shipman. Masses and radii of white-dwarf stars. III - Results for 110 hydrogen-rich and 28 helium-rich stars. *ApJ*, 228:240–256, Feb. 1979. doi: 10.1086/156841.

[260] I. Shivvers, M. Modjaz, W. Zheng, Y. Liu, A. V. Filippenko, J. M. Silverman, T. Matheson, A. Pastorello, O. Graur, R. J. Foley, R. Chornock, N. Smith, J. Leaman, and S. Benetti. Revisiting the Lick Observatory Supernova Search Volume-limited Sample: Updated Classifications and Revised Stripped-envelope Supernova Fractions. *PASP*, 129(5):054201, May 2017. doi: 10.1088/1538-3873/aa54a6.

[261] B. W. Silverman. *Density estimation for statistics and data analysis*. CRC press, 1986.

[262] M. V. v. d. Sluijs. *Formation and evolution of compact binaries*. Utrecht University, 2006.

[263] S. J. Smartt. Observational Constraints on the Progenitors of Core-Collapse Supernovae: The Case for Missing Hi gh-Mass Stars. *PASA*, 32:e016, Apr. 2015. doi: 10.1017/pasa.2015.17.

[264] N. Smith. Mass Loss: Its Effect on the Evolution and Fate of High-Mass Stars. *ARA&A*, 52:487–528, Aug. 2014. doi: 10.1146/annurev-astro-081913-040025.

[265] G. E. Soberman, E. S. Phinney, and E. P. J. van den Heuvel. Stability criteria for mass transfer in binary stellar evolution. *A&A*, 327:620–635, Nov. 1997.

[266] M. Spera and M. Mapelli. Very massive stars, pair-instability supernovae and

intermediate-mass black holes with the sevn code. *MNRAS*, 470:4739–4749, Oct. 2017. doi: 10.1093/mnras/stx1576.

[267] M. Spera, M. Mapelli, and A. Bressan. The mass spectrum of compact remnants from the PARSEC stellar evolution tracks. *MNRAS*, 451(4):4086–4103, Aug 2015. doi: 10.1093/mnras/stv1161.

[268] M. Spera, N. Giacobbo, and M. Mapelli. Shedding light on the black hole mass spectrum. *Mem. Soc. Astron. Italiana*, 87:575, Jan 2016.

[269] M. Spera, M. Mapelli, N. Giacobbo, A. A. Trani, A. Bressan, and G. Costa. Merging black hole binaries with the SEVN code. *MNRAS*, 485(1):889–907, May 2019. doi: 10.1093/mnras/stz359.

[270] S. Stevenson, A. Vigna-Gómez, I. Mandel, J. W. Barrett, C. J. Neijssel, D. Perkins, and S. E. de Mink. Formation of the first three gravitational-wave observations through isolated binary evolution. *Nature Communications*, 8: 14906, Apr. 2017. doi: 10.1038/ncomms14906.

[271] K. Stovall, P. C. C. Freire, S. Chatterjee, P. B. Demorest, D. R. Lorimer, M. A. McLaughlin, N. Pol, J. van Leeuwen, R. S. Wharton, B. Allen, M. Boyce, A. Brazier, K. Caballero, F. Camilo, R. Camuccio, J. M. Cordes, F. Crawford, J. S. Deneva, R. D. Ferdman, J. W. T. Hessels, F. A. Jenet, V. M. Kaspi, B. Knispel, P. Lazarus, R. Lynch, E. Parent, C. Patel, Z. Pleunis, S. M. Ransom, P. Scholz, A. Seymour, X. Siemens, I. H. Stairs, J. Swiggum, and W. W. Zhu. PALFA Discovery of a Highly Relativistic Double Neutron Star Binary. *ApJ*, 854:L22, Feb. 2018. doi: 10.3847/2041-8213/aaad06.

[272] T. Sukhbold and S. E. Woosley. The Compactness of Presupernova Stellar Cores. *ApJ*, 783(1):10, Mar 2014. doi: 10.1088/0004-637X/783/1/10.

[273] W. T. Sullivan. *The early years of radio astronomy: Reflections fifty years after Jansky's discovery.* Cambridge University Press, 2004.

[274] A. Summa, F. Hanke, H.-T. Janka, T. Melson, A. Marek, and . B. Müller. Progenitor-dependent Explosion Dynamics in Self-consistent, Axisymmetric Simulations of Neutrino- driven Core-collapse Supernovae. *ApJ*, 825:6, July 2016. doi: 10.3847/0004-637X/825/1/6.

[275] J. K. Swiggum, R. Rosen, M. A. McLaughlin, D. R. Lorimer, S. Heatherly, R. Lynch, S. Scoles, T. Hockett, E. Filik, J. A. Marlowe, B. N. Barlow, M. Weaver, M. Hilzendeger, S. Ernst, R. Crowley, E. Stone, B. Miller, R. Nunez, G. Trevino, M. Doehler, A. Cramer, D. Yencsik, J. Thorley, R. Andrews, A. Laws, K. Wenger, L. Teter, T. Snyder, A. Dittmann, S. Gray, M. Carter, C. McGough, S. Dydiw, C. Pruett, J. Fink, and A. Vanderhout. PSR J1930-1852: a Pulsar in the Widest Known Orbit around Another Neutron Star. *ApJ*, 805:156, June 2015. doi: 10.1088/0004-637X/805/2/156.

[276] G. A. Tammann, A. Sandage, and B. Reindl. New Period-Luminosity and Period-Color relations of classical Cepheids: I. Cepheids in the Galaxy. *A&A*, 404:423–448, Jun 2003. doi: 10.1051/0004-6361:20030354.

[277] T. M. Tauris and M. Bailes. The origin of millisecond pulsar velocities. *A&A*, 315:432–444, Nov. 1996.

[278] T. M. Tauris and R. J. Takens. Runaway velocities of stellar components originating from disrupted binaries via asymmetric supernova explosions. *A&A*, 330:1047–1059, Feb 1998.

[279] T. M. Tauris and E. P. J. van den Heuvel. *Formation and evolution of compact stellar X-ray sources*, pages 623–665. Cambridge University Press, Apr. 2006.

[280] T. M. Tauris, N. Langer, T. J. Moriya, P. Podsiadlowski, S.-C. Yoon, and S. I. Blinnikov. Ultra-stripped Type Ic Supernovae from Close Binary Evolution. *ApJ*, 778:L23, Dec. 2013. doi: 10.1088/2041-8205/778/2/L23.

[281] T. M. Tauris, N. Langer, and P. Podsiadlowski. Ultra-stripped supernovae: progenitors and fate. *MNRAS*, 451:2123–2144, Aug. 2015. doi: 10.1093/ mnras/stv990.

[282] T. M. Tauris, M. Kramer, P. C. C. Freire, N. Wex, H.-T. Janka, N. Langer, P. Podsiadlowski, E. Bozzo, S. Chaty, M. U. Kruckow, E. P. J. van den Heuvel, J. Antoniadis, R. P. Breton, and D. J. Champion. Formation of Double Neutron Star Systems. *ApJ*, 846:170, Sept. 2017. doi: 10.3847/1538-4357/aa7e89.

[283] J. H. Taylor and J. M. Weisberg. A new test of general relativity - Gravitational radiation and the binary pulsar PSR 1913+16. *ApJ*, 253:908–920, Feb. 1982. doi: 10.1086/159690.

[284] W. D. Taylor, C. J. Evans, H. Sana, N. R. Walborn, S. E. de Mink, V. E. Stroud, A. Alvarez-Candal, R. H. Barbá, J. M. Bestenlehner, A. Z. Bonanos, I. Brott, P. A. Crowther, A. de Koter, K. Friedrich, G. Gräfener, V. Hénault-Brunet, A. Herrero, L. Kaper, N. Langer, D. J. Lennon, J. Maíz Apellániz, N. Markova, N. Morrell, L. Monaco, and J. S. Vink. The VLT-FLAMES Tarantula Survey. II. R139 revealed as a massive binary system. *A&A*, 530: L10, June 2011. doi: 10.1051/0004-6361/201116785.

[285] The LIGO Scientific Collaboration, the Virgo Collaboration, B. P. Abbott, R. Abbott, T. D. Abbott, S. Abraham, F. Acernese, K. Ackley, C. Adams, R. X. Adhikari, V. B. Adya, C. Affeldt, M. Agathos, K. Agatsuma, N. Aggarwal, O. D. Aguiar, L. Aiello, A. Ain, P. Ajith, G. Allen, A. Allocca, M. A. Aloy, P. A. Altin, A. Amato, A. Ananyeva, S. B. Anderson, W. G. Anderson, S. V. Angelova, S. Antier, S. Appert, K. Arai, M. C. Araya, J. S. Areeda, M. Arène, N. Arnaud, K. G. Arun, S. Ascenzi, G. Ashton, S. M. Aston, P. Astone, F. Aubin, P. Aufmuth, K. AultONeal, C. Austin, V. Avendano, A. Avila-Alvarez, S. Babak, and P. Bacon. GWTC-1: A Gravitational-Wave Transient Catalog of Compact Binary Mergers Observed by LIGO and Virgo during the

First and Second Observing Runs. *arXiv e-prints*, art. arXiv:1811.12907, Nov 2018.

[286] K. S. Thorne and A. N. Zytkow. Stars with degenerate neutron cores. I - Structure of equilibrium models. *ApJ*, 212:832–858, Mar. 1977. doi: 10.1086/155109.

[287] F. X. Timmes, S. E. Woosley, and T. A. Weaver. The Neutron Star and Black Hole Initial Mass Function. *ApJ*, 457:834, Feb 1996. doi: 10.1086/176778.

[288] R. C. Tolman. Static Solutions of Einstein's Field Equations for Spheres of Fluid. *Physical Review*, 55:364–373, Feb. 1939. doi: 10.1103/PhysRev.55.364.

[289] S. Toonen, G. Nelemans, and S. Portegies Zwart. Supernova Type Ia progenitors from merging double white dwarfs. Using a new population synthesis model. *A&A*, 546:A70, Oct. 2012. doi: 10.1051/0004-6361/201218966.

[290] A. V. Tutukov and L. R. Yungel'son. Formation of neutron stars in binary systems. *AZh*, 70:812, Aug. 1993.

[291] E. P. J. van den Heuvel. Late Stages of Close Binary Systems. In P. Eggleton, S. Mitton, and J. Whelan, editors, *Structure and Evolution of Close Binary Systems*, volume 73 of *IAU Symposium*, page 35, 1976.

[292] E. P. J. van den Heuvel. Evolutionary Processes in X-Ray Binaries and Their Progenitor Systems. In M. D. Papagiannis, editor, *Eighth Texas Symposium on Relativistic Astrophysics*, volume 302, page 14, Jan 1977. doi: 10.1111/j.1749-6632.1977.tb37034.x.

[293] E. P. J. van den Heuvel and C. De Loore. The nature of X-ray binaries III. Evolution of massive close binaries with one collapsed component - with a possible application to Cygnus X-3. *A&A*, 25:387, Jun 1973.

[294] D. Vanbeveren. The evolution of massive close binaries revised. *A&A*, 252: 159, Dec 1991.

[295] F. Verbunt and E. Cator. A New Look at Distances and Velocities of Neutron Stars. *Journal of Astrophysics and Astronomy*, 38:40, Sept. 2017. doi: 10. 1007/s12036-017-9474-5.

[296] F. Verbunt, A. Igoshev, and E. Cator. The observed velocity distribution of young pulsars. *A&A*, 608:A57, Dec. 2017. doi: 10.1051/0004-6361/201731518.

[297] A. Vigna-Gómez. Simulations from: On the formation history of galactic double neutron stars [data set]. `http://doi.org/10.5281/zenodo.3358304`, 2019.

[298] A. Vigna-Gómez. Inlists for paper: Massive stellar mergers as precursors of hydrogen-rich pulsational pair instability supernovae (version 1.0). `http://doi.org/10.5281/zenodo.2644593`, 2019.

[299] A. Vigna-Gómez, C. J. Neijssel, S. Stevenson, J. W. Barrett, K. Belczynski, S. Justham, S. E. de Mink, B. Müller, P. Podsiadlowski, M. Renzo, D. Szécsi, and I. Mandel. On the formation history of Galactic double neutron stars. *MNRAS*, 481:4009–4029, Dec. 2018. doi: 10.1093/mnras/sty2463.

[300] A. Vigna-Gómez, S. Justham, I. Mandel, S. E. de Mink, and P. Podsiadlowski. Massive Stellar Mergers as Precursors of Hydrogen-rich Pulsational Pair In-stability Supernovae. *ApJ*, 876(2):L29, May 2019. doi: 10.3847/2041-8213/ ab1bdf.

[301] J. S. Vink, A. de Koter, and H. J. G. L. M. Lamers. Mass-loss predictions for O and B stars as a function of metallicity. *A&A*, 369:574–588, Apr. 2001. doi: 10.1051/0004-6361:20010127.

[302] R. Voss and T. M. Tauris. Galactic distribution of merging neutron stars and black holes - prospects for short gamma-ray burst progenitors and LIGO/VIRGO. *MNRAS*, 342:1169–1184, July 2003. doi: 10.1046/j.1365-8711. 2003.06616.x.

[303] S. Wanajo, H.-T. Janka, and B. Müller. Electron-capture Supernovae as The Origin of Elements Beyond Iron. *ApJ*, 726:L15, Jan. 2011. doi: 10.1088/ 2041-8205/726/2/L15.

[304] T. A. Weaver, G. B. Zimmerman, and S. E. Woosley. Presupernova evolution of massive stars. *ApJ*, 225:1021–1029, Nov 1978. doi: 10.1086/156569.

[305] R. F. Webbink. Double white dwarfs as progenitors of R Coronae Borealis stars and Type I supernovae. *ApJ*, 277:355–360, Feb. 1984. doi: 10.1086/161701.

[306] J. A. Wheeler. Superdense Stars. *ARA&A*, 4:393, Jan 1966. doi: 10.1146/ annurev.aa.04.090166.002141.

[307] A. Wongwathanarat, H.-T. Janka, and E. Müller. Three-dimensional neutrino-driven supernovae: Neutron star kicks, spins, and asymmetric ejection  of nucleosynthesis products. *A&A*, 552:A126, Apr. 2013. doi: 10.1051/0004-6361/ 201220636.

[308] S. E. Woosley. Pulsational Pair-instability Supernovae. *ApJ*, 836:244, Feb. 2017. doi: 10.3847/1538-4357/836/2/244.

[309] S. E. Woosley. Models for the Unusual Supernova iPTF14hls. *ApJ*, 863:105, Aug. 2018. doi: 10.3847/1538-4357/aad044.

[310] S. E. Woosley, S. Blinnikov, and A. Heger. Pulsational pair instability as an explanation for the most luminous supernovae. *Nature*, 450:390–392, Nov. 2007. doi: 10.1038/nature06333.

[311] Ł. Wyrzykowski, Z. Kostrzewa-Rutkowska, J. Skowron, K. A. Rybicki, P. Mróz, S. Kozłowski, A. Udalski, M. K. Szymański, G. Pietrzyński, I. Soszyński, K. Ulaczyk, P. Pietrukowicz, R. Poleski, M. Pawlak, K. Iłkiewicz, and N. J. Rattenbury. Black hole, neutron star and white dwarf candidates from microlensing with OGLE-III. *MNRAS*, 458:3012–3026, May 2016. doi: 10.1093/mnras/stw426.

[312] X.-J. Xu and X.-D. Li. On the Binding Energy Parameter $\lambda$ of Common Envelope Evolution. *ApJ*, 716:114–121, June 2010. doi: 10.1088/0004-637X/716/1/114.

[313] S. C. Yoon and N. Langer. Evolution of rapidly rotating metal-poor massive stars towards gamma-ray bursts. *A&A*, 443(2):643–648, Nov 2005. doi: 10.1051/0004-6361:20054030.

[314] S. C. Yoon, A. Dierks, and N. Langer. Evolution of massive Population III stars with rotation and magnetic fields. *A&A*, 542:A113, Jun 2012. doi: 10.1051/0004-6361/201117769.

[315] J.-P. Zahn. The dynamical tide in close binaries. *A&A*, 41:329–344, July 1975.

[316] J.-P. Zahn. Tidal friction in close binary stars. *A&A*, 57:383–394, May 1977.

[317] J. P. Zahn. Tidal dissipation in binary systems. In M. J. Goupil and J. P. Zahn, editors, *EAS Publications Series*, volume 29 of *EAS Publications Series*, pages 67–90, Jan 2008. doi: 10.1051/eas:0829002.

[318] E. Zapartas, S. E. de Mink, R. G. Izzard, S.-C. Yoon, C. Badenes, Y. Götberg, A. de Koter, C. J. Neijssel, M. Renzo, A. Schootemeijer, and T. S. Shrotriya. Delay-time distribution of core-collapse supernovae with late events resulting from binary interaction. *A&A*, 601:A29, May 2017. doi: 10.1051/0004-6361/201629685.